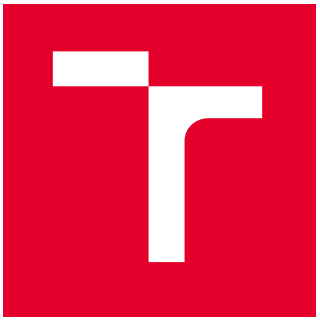

BRNO UNIVERSITY OF TECHNOLOGY

VYSOKÉ UČENÍ TECHNICKÉ V BRNĚ

FACULTY OF MECHANICAL ENGINEERING

FAKULTA STROJNÍHO INŽENÝRSTVÍ

INSTITUTE OF PRODUCTION MACHINES, SYSTEMS AND ROBOTICS

ÚSTAV VÝROBNÍCH STROJŮ, SYSTÉMŮ A ROBOTIKY

EFFECTS OF NON-LINEAR STIFFNESS ON TURN PROCESS STABILITY IN HORIZONTAL TURNING MACHINES

VLIV NELINEÁRNÍ TUHOSTI NA STABILITU ŘEZNÉHO PROCESU U STROJŮ S VODOROVNOU OSOU SOUSTRUŽENÍ

DOCTORAL THESIS

DIZERTAČNÍ PRÁCE

AUTHOR — **Ing. Petr Hadraba**

AUTOR PRÁCE

SUPERVISOR — **doc. Ing. Zdeněk Hadaš, Ph.D.**

ŠKOLITEL

BRNO 2023

Abstract

Nonlinear stiffness affects the dynamics of modern machine tools. An important parameter of machine tool productivity is self-excited vibration, which limits the performance of the machine tool. This work was motivated by an industrial case where the behaviour of a machine tool cannot be predicted by traditional methods and the machine exhibits a significant change in dynamic behaviour. This work presents a step-by-step analysis that was focused on the simulation of self-excited vibrations and the effect of nonlinear stiffness on the resulting vibration stability. As the complexity of the model increases, a linearisation approach has been introduced that allows faster analysis of the machining stability. For better mapping and creation of a stability lobe diagram for a nonlinear structure, an algorithm for the synthesis of linearised solutions at the working point is presented. The linearisation approach was combined with nonlinear static simulation considering the nonlinear behaviour model of the linear ball guide and used to predict vibration behaviour. The nonlinear static model uses a dynamic cosimulation and substructuring method to incorporate the effects of structural deformation into the analysis. The experimental machining test made it possible to compare the analysis results and demonstrated good agreement with the maximum frequency deviations in the 3 Hz band.

Keywords

Chatter, Nonlinear dynamics, Linear ball guideway, Lathe

Abstrakt

Nelineární tuhost ovlivňuje dynamiku moderních obráběcícho strojů. Důležitým parametrem produktivity obráběcího stroje jsou samobuzené vibrace, které omezuje výkon obráběcího stroje. Tato práce byla motivována průmyslovým případem, kdy chování obráběcího stroje nelze předvídat tradičními metodami a stroj vykazuje významnou změnou dynamického chování. Tato práce krok za krokem představuje analýzu, která byla zaměřena na simulaci samobuzených vibrací a vlivu nelineární tuhosti na výslednou stabilitu chvění. Se zvyšující se složitostí modelu byl představen linearizační přístup, který umožňuje rychlejší analýzu stability obrábění. Pro lepší mapování a tvorbu stabilitního lobe diagramu pro nelineární strukturu je uveden algoritmus syntézy linearizovaných řešení v pracovním bodě. Linearizační přístup byl kombinován s nelineární statickou simulací s ohledem na model nelineárního chování lineárního kuličkového vedení a použit pro predikci chování chvění. Nelineární statický model využívá metodu dynamické kosimulace a substrukturování, aby do analýzy začlenil účinky strukturální deformace. Experimentální zkouška obrábění umožňila porovnat výsledky analýzy a prokázala dobrou shodu s maximálními frekvenčními odchylkami v pásmu 3 Hz.

Klíčová slova

Samobuzené vibrace při obrábění, Nelineární dynamika , Lineární kuličkové vedení, Soustruh

Bibliographic Citation

HADRABA, Petr. Effects of Non-Linear Stiffness on Turn Process Stability in Horizontal Turning Machines. Brno, 2023. Available also at: https://www.vutbr.cz/studenti/zav-prace/detail/146598. Doctoral Thesis. Brno University of Technology, Faculty of Mechanical Engineering, Institute of Production Machines, Systems, and Robotics. Supervisor Zdenek Hadas.

Declaration

I declare that I am a dissertation on 'Effects of Non-Linear Stiffness on Turn Process Stability in Horizontal Turning Machines' elaborated independently with the use of professional literature and sources, listed in the list of resources attached to this work.

In Brno, 26. 4. 2023

Petr Hadraba

Acknowledgments

I want to take this opportunity to thank my supervisor Zdenek Hadas for his valuable advice and long-term support for my work. I also thank Professor Junz Jiunn-jyh Wang for his valuable advice in my research. I also thank the company Tajmac-ZPS for valuable practical experience, the inspiration for my work, and the implementation of the experiment. Lastly, I would like to thank my family and friends for their constant support and trust in me.

Contents

1
Introduction

The machine tool industry is facing productivity saturation and lags behind other fast-developing industrial fields. The reason is that the investment horizon of new machine tools is quite long. It is not unusual to see working machines built several decades ago. Moreover, traditional cam-based machine tools could even exceed the productivity of modern CNC machines. Therefore, there is not much space for new progressive development. Despite this fact, there is a significant obstacle in the machining industry, the lack of skilled machinists, which brings a new challenge in this century, how to decrease the number of human labour needs in machining. Industry 4.0 should be an answer to this issue. Digitalisation and the Internet of Things should optimise the workflow in factories and enable production with minimal needs for human workers. In contrast to a problem with a self-driving car, machine tools work in a controlled manner. However, the machine man still needs long-term experience and good knowledge of the machine for the best results. One of the signs of mastering machine tools is to use maximal productivity of the cutting process without vibration. Without a well-defined limit of chatter stability, it is impossible to achieve high productivity without an experienced operator.

The chatter phenomenon is familiar to anyone who operates machine tools. Most operators can easily recognise an unstable cut by sound during machining and the quality of the workpiece surface. Although chatter theory has been well known for a long time, many types of uncertainty complicate its application. Most processes are based on machinist senses and experience rather than chatter analysis.

Many parameters cause uncertainties: the inconsistency of the workpiece's material property, knife wear, changeable behaviour of the machine tool dynamic due to its dependence on tool position, machining parameters dependency of specific cutting force on the machining conditions, changeable behaviour of the machine's dynamic which dependence on tool position, the process damping during machining or nonlinearities of the structure – all these factors influence the stability of machining. All these factors limit the use of a simple lobe diagram to a specific case. However, with the decreasing number of highly skilled workers who could adjust the process based on their experience and the increasing effort to replace human labour, the importance of reliable stability prediction increases significantly.

This thesis tries to find an answer to one of these aspects which complicates the reliability of the stability diagram, the effect of nonlinear stiffness on the machine tool stability. The motivation for this work was the author's experience with stability prediction, which often differs from measured experimental machining. The most suspicious was the frequency shift of the excited chatter vibration, where a change in stiffness must be the cause. Therefore, it is necessary to find methods to predict this kind of behaviour.

2
Aims of PhD. Thesis

Although nonlinearities are a natural part of machines, they are caused by many different: structural, contact, or otherwise causes; they are often not considered in the design and operation of machines. This work aims at a description of stability prediction and defines a methodology for chatter stability prediction, which could enable better machine tool design and improve the targeting of active chatter suppression.

- Analysis of the influence of nonlinearity of bonds on the stability of the cutting process
- Methodology for the construction of machine tools in terms of increasing stability of self-excited vibrations
- Analysis of the possibilities of nonstructural increase of cutting stability of machine tools

3
General System Theory

3.1 System

The common situation in research is to work with problems with unknown causes. During the process, seems to be extremely complicated; however, after the solving seems to be trivial. The process of understanding and general thinking has a long history that started with ancient Greek philosophers. which established the boundary of modern science. On this basis, the whole world of philosophy as a start of the modern history of system theory could be considered Hegel' s 'The Science of logic' [1] where Hegel defined the nature of systems by the following statements:

- The whole is more than the sum of parts.
- The whole defines the nature of the parts.
- Parts cannot be understood by studying the whole.
- Parts are dynamically interrelated or interdependent.

Von Bertalanffy studied the connections between nonmaterial and material phenomenon [2], he observed that the concept of several well-known models from technical fields could be applied to biological material and nonmaterial phenomenon. Figure 3.1 shows the feedback detection system model that could describe biological structure and technical concept.

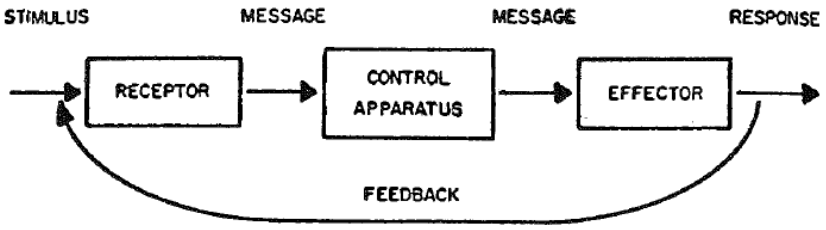

Figure 3.1: Simple scheme of feedback system [2]

Klir [3] provides simple definition of system *The term 'system' stands, in general, for a set of some things and a relation among the things.* This could be represented by mathematical formula where S stands for a system, T for set of things and R for relations:

$$S = (T, R). \tag{3.1}$$

Figure 3.2 shows a graphical representation of this little bit 'vague' description; where it is obvious that the system is the set of thins connected by relations.

Better definition has been given by Ackoff [5], where system is a set of two or more elements which satisfy folowing conditions:

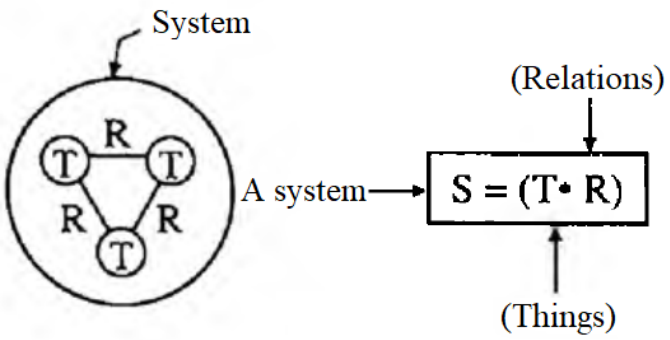

Figure 3.2: Klir's mathematical definition of system and its visualisation [4]

- The behaviour of each element has an effect on the behaviour of the whole.
- The behaviour of the elements and their effects on the whole are interdependent.
- However subgroups of the elements are formed, all have an effect on the behaviour of the whole but none has an independent effect on it.

The goal of general system theory is to enable the transfer of knowledge from one scientific field to another to enable the application of the computational method developed in one single field to apply in whole sets of potential fields. With a little exaggeration, we can say that general system theory lays the basis for multidiscipline collaboration in science.

3.2 Problem of Complexity

Weaver describes the problem of complexity in the original paper [6], on case of billiard table with ball on the table, where with the increasing number on the table the complexity of the problem increases. Figure 3.3 shows the type of problems divided into three regions where the extremes are represented by organized simplicity representing simple problems and disorganised complexity, which could be assumed as chaotic region. The important region, is the organised complexity region which can be described by a combination of statistical method and advanced computation. There are two axes where on one rove is randomness and on the other is a complexity, the randomness expressing an unknown relation which is dot easily describe the complexity on the other hand describes the situation where the problem could be described but the solving demand increases gradually. The deterministic chaos causes the boundary between organized complexity and disorganized complexity where even a simple model could be affected by the deterministic chaos.

It is important to realise what type of example is being solved. Because different cases need a special approach-orientated. Sometimes the problem can be simplified and transposed to an easier problem-solving area or due to its chaotic behaviour cannot be solved at all. Therefore, the first analysis of the problem must focus on the character of the problem.

3.3 Method for General Problem Solving

Janicek proposed system methodology algorithm [7], providing formalised step-by-step operation for effective systems solving. This methodology is not limited only to technical

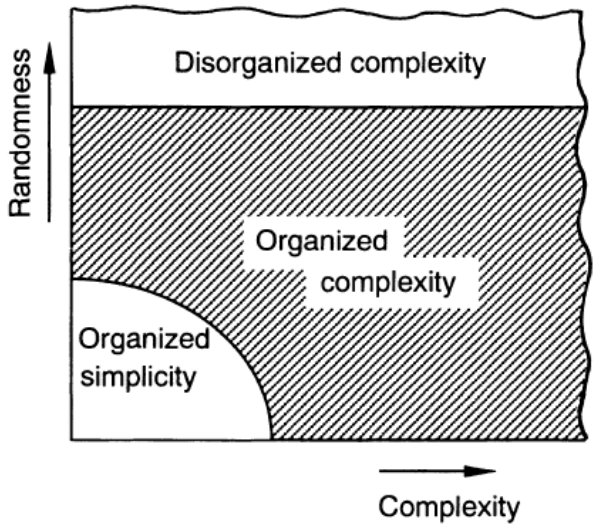

Figure 3.3: Classes according to Weaver[6] of systems and associated problems that require distinct mathematical tools

fields-orientated but could be generalised for any system. This general system-orientated methodology enables application in any fields and its purpose is to guide analysis in an optimal way. This methodology uses forms of attributes to sort out the nature of the systems. The basic and necessary condition is to consider humans as erring creatures, and even they are following the best formalised methodology, it highly produces fatal errors simplifying and overlooks the necessary assumptions. Correct analyses are possible only if we realise our own error.

4

Chatter – Self-exited Vibration in Machining Process

4.1 Theory of Chatter Source

In the theory of self-excited oscillations, there are two basic models that describe stability during machining:

- Mode coupling effect
- Regenerative chatter.

Tlusty describes the principle of positional coupling, which enables to describe some of the occurrence of vibrations during machining of a material that is not corrugated from the previous operation (e.g., linear planing) [8]. The model is based on a system with two different perpendicular stiffness. Therefore, the basis is an oscillation model with two degrees of freedom and a different natural frequency for each direction. The tool performs an elliptical movement during machining. If we consider the system from Fig. 4.1 and the movement in a clockwise direction, when moving from A to B, the width of the depth of cut decreases, so the force is less than when cutting from B to A. Assuming that the energy supplied in this way is greater than the energy wasted by damping, the system increases its oscillation.

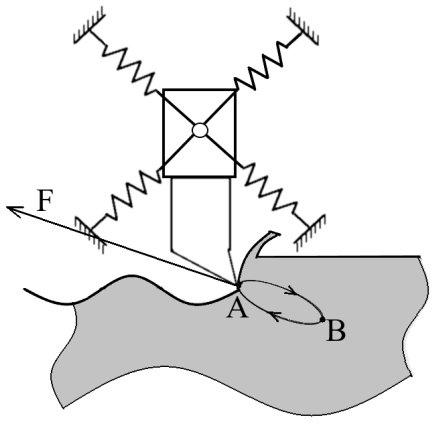

Figure 4.1: Mode coupling effect scheme

The regenerative chatter principle is based on the interaction between surfaces that happen in the previous turn and the actual blade deflection of the knife. Fig. 4.2 shows a simplified model with an example of the dependence of the stability on the phase shift between the actual and previous cut. A stable cut occurs when the phase shift is small, the

cutting force is therefore almost constant even during the initial undulation of the surface; the cut will gradually calm down in this case, as this system will not be supplied with new energy. The opposite case occurs when the phase changes π and then the minimum and maximum cuts alternate, which excites the system with a variable cutting force.

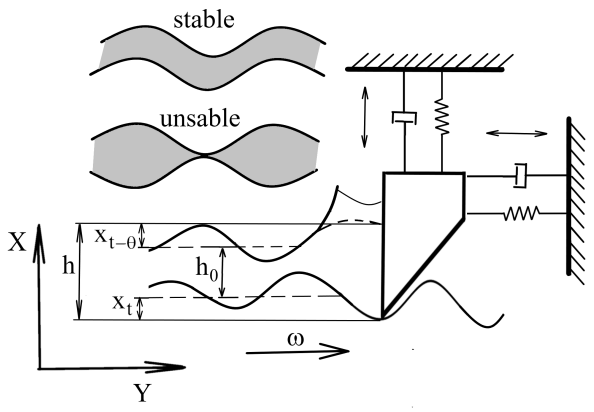

Figure 4.2: Regenerative chatter scheme

Both of these models require a range of simplifying assumptions, such as the independence of the cutting resistance from the depth of the cut, a constant angle of the cutting force vector to the surface, etc. All these simplifications are essential in most cases, but there are cases where neglect of some effects is very significant.

4.2 Chatter Stability Estimation in Turning Process

The key is to define conditions when the system will be stable and unstable; Tlusty defined it by a chip limit width b_{lim} as a fraction where the cutting force K_s and the real negative part of the transfer function of the system $G(u)$ are in the denominator:

$$b_{lim} = \frac{-1}{2K_s G(u)}. \tag{4.1}$$

If we consider a minimum of negative real functions $min(G(u))$, then we obtain the criteria for the whole spindle speed stability. However, this criterion is too strict, so the next step in classical analysis is to define the faze shift ϵ, which is the inverse tangent of the fraction of the real and imaginary part of the transfer function:

$$\epsilon = atan\left(\frac{real(G(u))}{imagG(u)}\right). \tag{4.2}$$

The last step before building the lobe diagram is to calculate the reaction frequency f_{r_i} for each harmonic lobe.

$$f_{r_i} = \frac{f_s}{i - \frac{\epsilon}{\pi}}; \quad i = 1, 2, 3...n. \tag{4.3}$$

Combining the reaction frequency width criterion to limit the stable chip width, we get a stability lobe diagram; this diagram draws the boundary between stable and unusable conditions, the typical diagram can be seen in Fig. 4.3 [8, 9].

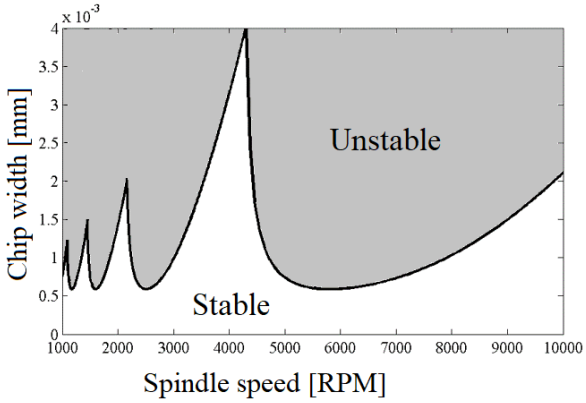

Figure 4.3: Lobe diagram divides machining condition on stabile and unstable

4.3 Current Research in Field of Self-Excited Vibrations

Today's trend is, above all, a better description of the machining process and the connection of individual influences on the stability of the cutting process. These are the parameters of the cutting process, where the friction between the tool back and the chip, the shear stress in the chip and the angle of inclination of the cutting edge affect the direction of the force result. It should be noted that these properties are also related to chip temperature.

Jiang focuses on experimental verification of lathe stability estimation, which assumes a flexible workpiece and considers nonlinear cutting resistance [10], its proposed model compares with the results using the method presented by Altintas [11]. Altintas addresses, among other things, the difference between numerical simulation and analytical solution. Where Altintas addresses, among other things, the difference between numerical simulation and analytical solution. Furthermore, this work deals with the FEM simulation of the cutting process. Ayed using FEM compares the properties of cutting parameters depending on the grain structure of the titanium alloy [12].

Most works assume cutting resistance coefficients obtained from measurements of a stable machining process. Turkes uses a piezo actuator-driven cutting process to obtain dynamic cutting forces and, at the same time, focuses on the effect of material damping on machining stability[13]. Several works deal with process damping. Due to process damping at a low spindle speed, the machine stability increases significantly. However, the process damping depends on a large number of parameters, especially on the degree of cutting edge wear, so its estimation is not a simple task. Due to the complexity of this problem, many works are devoted to it, e.g. [14, 15, 16].

One part of the research direction of self-excited vibrations focuses on thin-walled components machining when the rigidity of the workpiece significantly influence the overall stability of the system. Rubeo deals with this issue and presents time simulations, which he validates by measurement [17].

4.4 Chatter Suppression

As was mentioned before, the structure's dynamic defines chatter stability. Therefore, lowering the mode amplitudes leads to chatter stability increasing. There are several ways which could be called passive, these implement: increasing stiffness, damping, or designing mass damper, the passive also mean that does not need any systems feedback. On the other hand, there could be an active strategy that focuses on actively controlling the process based on data from the cutting process. These could work on cutting parameter modification or the active force vibration suppression.

Zhu presents the classification in Fig. 4.4, mainly the active division according to actuator seems too detailed in contrast with putting all possible design modification into the single category of changing systems behaviour [18]. Yuan, in contrast, classified adjusting process parameters as a passive strategy [19], this difference is due to different evaluation criteria also due to different examples; Yuan presents the tuning the machining condition to a most stable situation as passive. Zhu presents the sinusoidal spindle speed variation SSV as an example of this category, which could be both passive and active depending on the criterion because it does not need direct feedback from the cutting process. However, there is no dilemma from an energetic point of view, and it is active without any doubt.

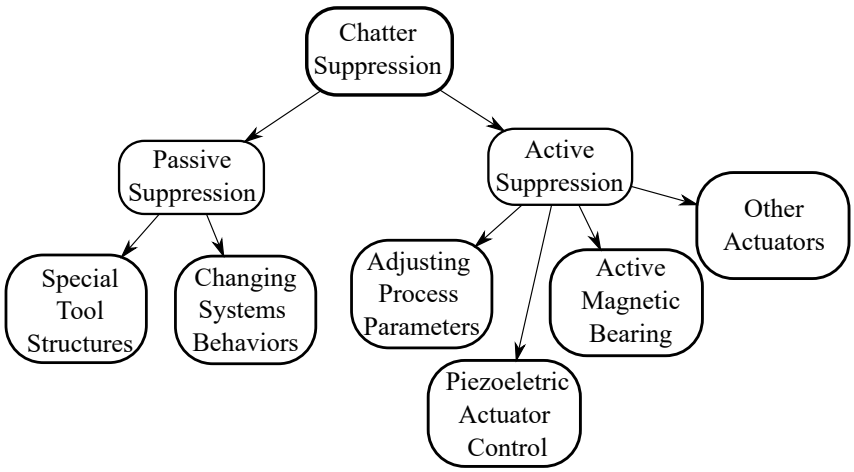

Figure 4.4: The diagram of chatter suppression classification

Kamal also presents the category of the semi-active method gives an example magnetorheological or electrorheological fluid-controlled damped boring bar [20]. Obviously, there are many different divisions of approaches, and there is not a single definable taxonomy, but ultimately it is a matter of modifying the vibration modes, changing the phase shift and increasing the damping.

4.4.1 Passive Chatter Suppression

As was mentioned before, the dynamic is the key factor for chatter stability, simply put, increasing stability is possible by reducing weight or increasing stiffness and damping. This could be achieved by material choice or by topological optimization. Ashby provides a comparison of dynamic behaviour, which can be seen in Fig. 4.5 [21], where the Y-axis represents an inverse value of damping, the X-value represents the ratio between density and stiffness. The trade-off surface (the shaded band) represents the subset of material

with good performances in both metrics. However, the dynamic parameter for a machine tool is not the only requirement for the machine tool behaviour. Möhring summarises all the aspects of material choice for machine design structure including both thermal and mechanical aspects [22].

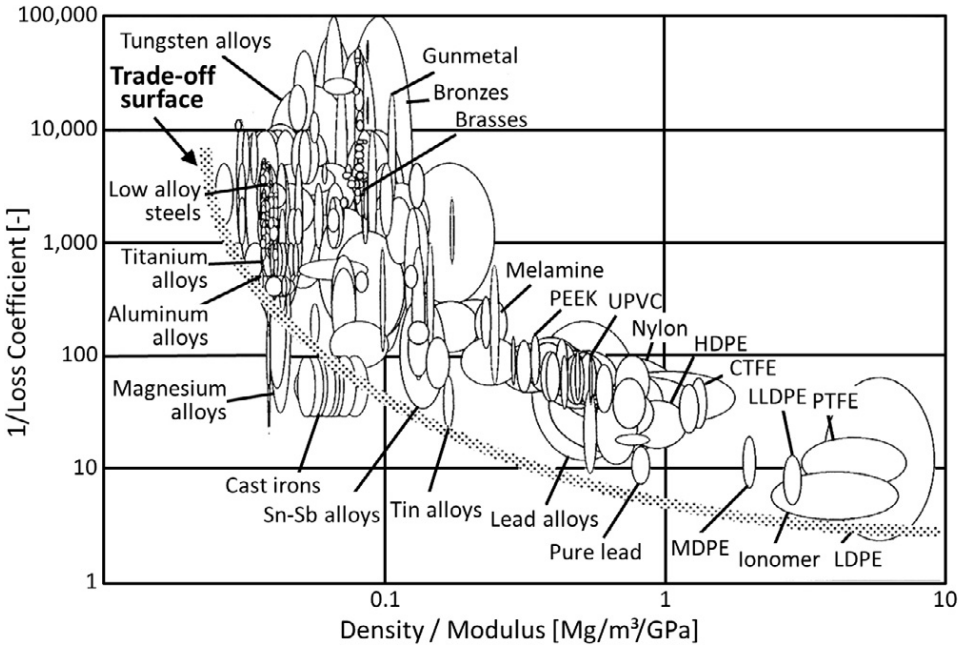

Figure 4.5: Performance metrics for density-stiffness ratio and damping where the shaded band shows theoptimum trade-off surface

Increasing the stiffness and eliminating oscillations during oscillations requires a demanding analysis of the system. The basic requirement is knowledge of the loading structure. Knowing how the structure will be loaded makes it possible to use topological optimization methods to design structures that maximize rigidity and minimize system weight.

Topological optimization methods are often based on the imitation of natural processes, whether it is the reinforcement of bones or tree trunks. An example is the fractal leaf vein structure, which supports the shell/plane structure. Li tries to imitate this kind of structure with his topological optimization algorithm[23]. An example of topological optimization of machine tools is presented by Shen, which uses adaptive growth methods to design machine reinforcements, and optimize the connector layout, which leads to increasing of highest mode displacement on 50 % of the original amplitude and shifting most of the modes to the higher frequencies [24].

The problem of topological optimization is often the restriction to certain constant input conditions, partly static; this shortcoming tries to eliminate Weule, which extends the optimization by motion, using multi-body simulation; the structure then compares the differently formed structures [25]. Shen applied an adaptive growth method for optimizing the supporting 3D structure of attached tuned mass dampers (tuned mass dampers) under harmonic excitation [26].

tuned mass dampers are devices used to reduce the resonant amplitude and eliminate unwanted vibrations. The basic principle of a passive dynamic damper is to tune to the same natural frequency as the damped system, leading to the decay of the natural frequency peak into two with a smaller amplitude. tuned mass dampers are often used

in high-rise buildings where they stabilize the structure against external influences [27]. By reducing the resonant amplitude, the minimum of the real negative response of the system is also reduced, thereby increasing the stability of the system against self-excited vibrations. The option is to place a damper on the machine structure as Yang presents [28], or to integrate it directly into the tool holder [29, 30]. One of the main disadvantages is that the weight requirement for mass dampers is too limiting for most systems.

A common problem with self-excited vibrations is the lack of damping, which also affects the usability of tuned mass damper. This issue could solve an alternative to tuned mass damper can be a particle tuned damper. The main advantage is the increase in energy dissipation by the chaotic interaction of particles [31, 32, 33]. However, it depends on the acceleration, and at small values, the effect does not appear, which significantly limits the use as a prevention of chatter. Yang introduced another way to improve damping during machining - eddy current damping, where a movement of a permanent magnet induces eddy current and dissipate the vibration energy. Yang used it for a thin wall milling where he achieved 40 % improvement of chatter stability [34]. The main disadvantage of this type of damper is that its effectiveness is frequency-dependent (rising with the frequency). To achieve a reasonable damping effect at low vibration frequency requires a large magnetic field, which makes it impossible to apply in most cases.

4.4.2 Active Chatter Suppression

An alternative to the tuned mass dampers are active dampers. This type of dynamic damper extends the dynamic damper by a force that has the opposite phase to that of the original vibration. The device therefore works on the principle that, based on the sensed vibration, it evaluates the action and acts against the vibration by means of a servomechanism. Here it is clear that this is a relatively expensive investment. The advantage is that this device can operate in a relatively wide area of the frequency spectrum - the main limitation is the maximum acceleration of the drive and the speed of processing the measured data. Zuperl presents usage of neural networks for quick evaluation of action interventions [35].

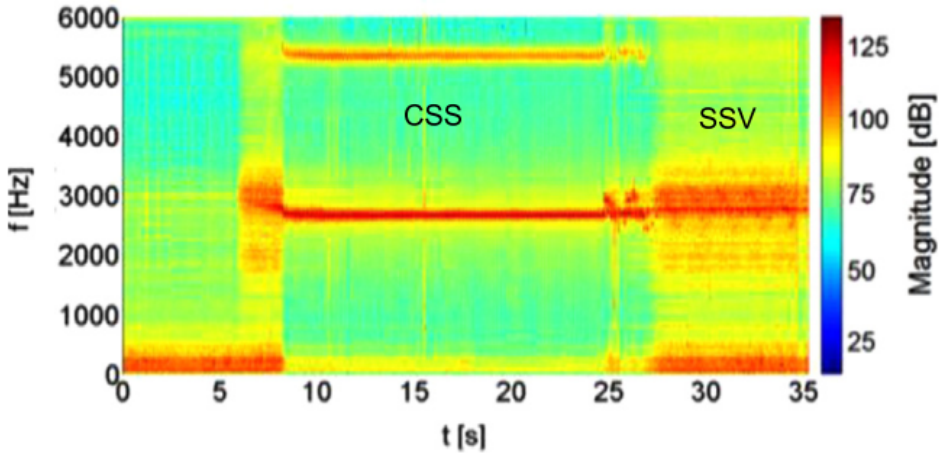

Figure 4.6: Spectrogram from experimental verification of the use of sinusoidal modulation of spindle speed SSV in comparison with the constant spindle speed CSS [36]

The basis of most methods is an effort to reduce the regenerative principle. Simply

put, it tries to compensate for the phase shift between the corrugation from the previous cut and the current blade deflection so that the chip thickness is as even as possible, and the pulsations that cause self-excited oscillations do not occur. Several methods based primarily on sinusoidal spindle speed modulation are presented for turning. Insperger deals with modelling the effect of modulation on a system with one degree of freedom [37]. Urbikain focuses mainly on experimental verification of suitable parameters for modulation settings [36],the results of the experimental verification are visible on the spectrogram Fig. 4.6, which shows a significant difference between the application of spindle speed variation and constant spindle speed machining.A noticeable surface improvement during machining with SSV is observable in Fig. 4.7.

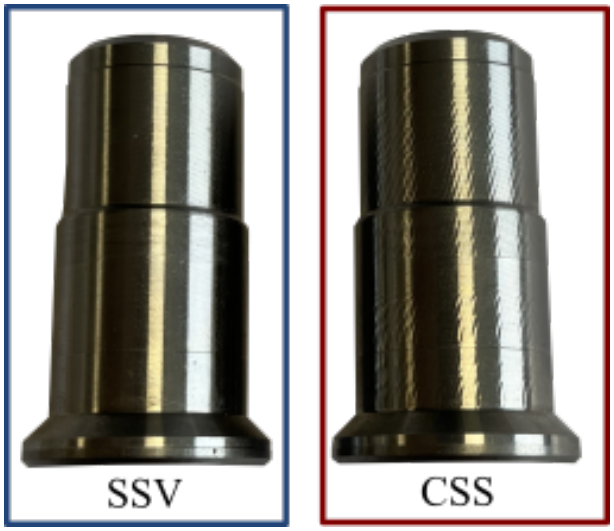

Figure 4.7: Workpieces surface using sinusoidal modulation of SSV spindle speed in comparison with the constant spindle speed CSS

Milling offers more possibilities from the essence of technology, but the principle remains the same. In addition to the ability to control self-excited oscillations at variable speeds, it is also possible to use a milling cutter with variable cutting edge spacing, this combination presents [38]. An algorithm for estimating sinus variation parameters, presented by Yamato [39].Simple sinusoidal, rectangular and triangulation modulations are not suitable for high-speed machining because they do not include the effect of phase on milling stability. The solution is provided by multi-harmonic modulation [40].

There is a whole range of methods for adaptive control, but the essential requirement for their correct functionality is knowledge of the behaviour of the controlled system. Again, we come to the question of which system we control. The increased instability may be significant for some applications and hardly observable for others.

5
Approach Based on Modal Reduction Model

5.1 Machine Tool Vibration Analysis

The problem for the analysis of dynamic properties is the fact that the dynamic properties of the machine change significantly with the stroke in the individual axes. Theoretically, there should be a separate analysis for each stroke combination. This procedure is completely unrealistic, especially if we take into account the fact that the dynamics of the machine will often be significantly affected by the accessories of a particular customer. in modelling such systems, an approach based on decomposition into subsystems that are connected by constraints prevails, such as the model presented by Kšica [41], and extends this model to estimate the stability of machine tool[42].

The constraints are mainly influenced by the linear lines, the 40 to 60 % stiffness of the machine and 90 % damping [43] [44], but these numbers need to be taken with considerable margin, as it depends crucially on the type of system. For multi-spindle automats (small compact assemblies), the effect of linear guides on the total stiffness is up to over 80 %. Considering this fact and previous information about the nonlinearity of linear lines, we come to the problem of modelling systems with nonlinear components.

Wang [45] describes by modelling a table with linear guidance, which is replaced by nonlinear bonds. Experimental measurements verify this model, and, for example, the phasor plane is used for the presentation. This model describes a part of the machine tool, so the question is how it is possible to extend this model to a more complex structure. Zhang deals with the synthesis of individual parts [46], which uses models of machine parts, which a nonlinear model of connections interconnects. A similar calculation structure is offered by the multi-body software approach where the machine is a machine modelled as a system of interacting systems [47].

5.2 Modal Reduction

FEM models usually have hundreds of thousands, sometimes millions of degrees of DOF freedom, which is inadequate to address dynamic behaviour. Therefore, it is necessary to reduce the DOF value to a minimum value that will maintain the behaviour in the required spectrum and at the same time allow a solution in a reasonable time. There are several reduction methods; we give the example of two methods used in computer software – Guyan reduction and Graig-Bampton reduction.

5.2.1 Guyan Reduction

Guyan method, also known as a static condensation [48], sorts the DOF on master – m and slave – s, where the number of master DOF is lower than slave $m << s$. The slave can not be loaded, analyzed or describe as dominant mass. The method is based on a

simple static equation:

$$\mathbf{Ku} = \mathbf{f}. \tag{5.1}$$

The stiffness matrix K is than transform into form there the the elements are sorted out:

$$\begin{bmatrix} \mathbf{K_{mm}} & \mathbf{K_{ms}} \\ \mathbf{K_{sm}} & \mathbf{K_{ss}} \end{bmatrix} \left\{ \begin{array}{c} u_m \\ u_s \end{array} \right\} = \left\{ \begin{array}{c} f_m \\ 0 \end{array} \right\}. \tag{5.2}$$

Using the second equation and assuming the regularity of the matrix K_ss, we can express $\mathbf{u_s}$:

$$\mathbf{K_{sm}u_m} + \mathbf{K_{ss}u_s} = \mathbf{0}. \tag{5.3}$$

$$\mathbf{u_s} = \mathbf{K_{ss}^{-1}K_{sm}u_m}. \tag{5.4}$$

This relationship allows the connection of reduced and original coordinates and defines $\mathbf{T_G}$ the Guyan reduction transformation matrix:

$$\mathbf{T_G} = \begin{bmatrix} \mathbf{I} \\ -\mathbf{K_{ss}K_{sm}} \end{bmatrix}. \tag{5.5}$$

Reduced system $\tilde{\mathbf{X}}$ would be given using transfer matrix $\mathbf{T_G}$ to the original structure, where $\mathbf{X}$ could represent the original mass, stiffness or damping matrix:

$$\tilde{\mathbf{X}} = \mathbf{T_G^T X T_G}, \mathbf{X} = \mathbf{M}, \mathbf{B}, \mathbf{K}. \tag{5.6}$$

In the case of stiffness, the reduction leads to simplest therm:

$$\tilde{\mathbf{K}} = \mathbf{K_{mm}} - \mathbf{K_{ss}^{-1}K_{sm}}. \tag{5.7}$$

5.2.2 Craig-Bampton Component Mode Synthesis

A frequently used method for dynamic substructuring the Component Mode Synthesis CMS. Craig and Bampton developed the method to enable solving large scale numeric models with time dependent force [49].

Gordon introduces the method as follows [50], unlike Guyan reduction, Craig-Bampton synthesis reduces mass and stiffness at the same time using standard dynamic equation:

$$[\mathbf{M_{AA}}] \{\ddot{u}_A\} + [\mathbf{K_{AA}}] \{u_A\} = \{\mathbf{F(t)}\}. \tag{5.8}$$

Where the method sorts original nodes u_A into boundary u_b and internal (leftover) u_L, which could be represented by rigid body vector $\boldsymbol{\phi_R}$ and fixed boundary normal modes $\boldsymbol{\phi_L}$ asamled in transform matrix $\boldsymbol{\phi_{cb}}$:

$$\{u_A\} = \left\{ \begin{array}{c} u_b \\ u_L \end{array} \right\} = \begin{bmatrix} \boldsymbol{I} & \mathbf{0} \\ \boldsymbol{\phi_R} & \boldsymbol{\phi_L} \end{bmatrix} \left\{ \begin{array}{c} u_b \\ q \end{array} \right\}, \tag{5.9}$$

$$\boldsymbol{\phi_{cb}} = \begin{bmatrix} \boldsymbol{I} & \mathbf{0} \\ \boldsymbol{\phi_R} & \boldsymbol{\phi_L} \end{bmatrix}. \tag{5.10}$$

Applying the transform matrix in the first matrix we will get the following equation:

$$\boldsymbol{\phi_{cb}^T} [\boldsymbol{M_{AA}}] \boldsymbol{\phi_{cb}} \left\{ \begin{array}{c} \ddot{u}_b \\ \ddot{q} \end{array} \right\} + \boldsymbol{\phi_{cb}^T} [\boldsymbol{K_{AA}}] \boldsymbol{\phi_{cb}} \left\{ \begin{array}{c} u_b \\ q \end{array} \right\} = \boldsymbol{\phi_{cb}^T} \left\{ \begin{array}{c} F_b \\ F_L \end{array} \right\}. \tag{5.11}$$

The transformed mass $\boldsymbol{M_{cb}}$ and stiffness $\boldsymbol{K_{cb}}$ matrices will be defined as follows:

$$[\boldsymbol{M_{cb}}] = \boldsymbol{\phi_{cb}^T}[\boldsymbol{M_{AA}}]\boldsymbol{\phi_{cb}} = \begin{bmatrix} \boldsymbol{M_{bb}} & \boldsymbol{M_{bq}} \\ \boldsymbol{M_{qb}} & \boldsymbol{M_{qq}} \end{bmatrix}, \tag{5.12}$$

$$[\boldsymbol{K_{cb}}] = \boldsymbol{\phi_{cb}^T}[\boldsymbol{K_{AA}}]\boldsymbol{\phi_{cb}} = \begin{bmatrix} \boldsymbol{K_{bb}} & \boldsymbol{0} \\ \boldsymbol{0} & \boldsymbol{K_{qq}} \end{bmatrix}. \tag{5.13}$$

In the next step the matrices $\boldsymbol{M_{cb}}$ and $\boldsymbol{K_{cb}}$ are substituted in equation 5.11, the method assumes that load is applied to the boundary nodes so the force vector F_L could be neglected:

$$\begin{bmatrix} \boldsymbol{M_{bb}} & \boldsymbol{M_{bq}} \\ \boldsymbol{M_{qb}} & \boldsymbol{M_{qq}} \end{bmatrix} \begin{Bmatrix} \ddot{u}_b \\ \ddot{q} \end{Bmatrix} + \begin{bmatrix} \boldsymbol{K_{bb}} & \boldsymbol{0} \\ \boldsymbol{0} & \boldsymbol{K_{qq}} \end{bmatrix} \begin{Bmatrix} u_b \\ q \end{Bmatrix} = \begin{Bmatrix} \boldsymbol{F_b} \\ \boldsymbol{0} \end{Bmatrix}. \tag{5.14}$$

Where the dynamic equation is extended by modal damping $\boldsymbol{2\xi\omega}$:

$$\begin{bmatrix} \boldsymbol{M_{bb}} & \boldsymbol{M_{bq}} \\ \boldsymbol{M_{qb}} & \boldsymbol{I} \end{bmatrix} \begin{Bmatrix} \ddot{u}_b \\ \ddot{q} \end{Bmatrix} + \begin{bmatrix} \boldsymbol{0} & \boldsymbol{0} \\ \boldsymbol{0} & \boldsymbol{2\xi\omega} \end{bmatrix} \begin{Bmatrix} \dot{u}_b \\ \dot{q} \end{Bmatrix} + \begin{bmatrix} \boldsymbol{K_{bb}} & \boldsymbol{0} \\ \boldsymbol{0} & \boldsymbol{\omega^2} \end{bmatrix} \begin{Bmatrix} u_b \\ q \end{Bmatrix} = \begin{Bmatrix} \boldsymbol{F_b} \\ \boldsymbol{0} \end{Bmatrix}. \tag{5.15}$$

This method is used in many software tools, such as ANSYS, which allows exporting a reduced substructure. This possibility was used for creating the nonlinear model in Chapter 11.

6

Problem of Unpredictable Vibration During Machining Process

6.1 Problem Analysis

Unexpected vibrations occur with the newly developed multi-spindle lathe support (see Fig. 6.1). In the part of the speed spectrum, the machine behaves following the theory of regenerative self-excited vibrations during machining.

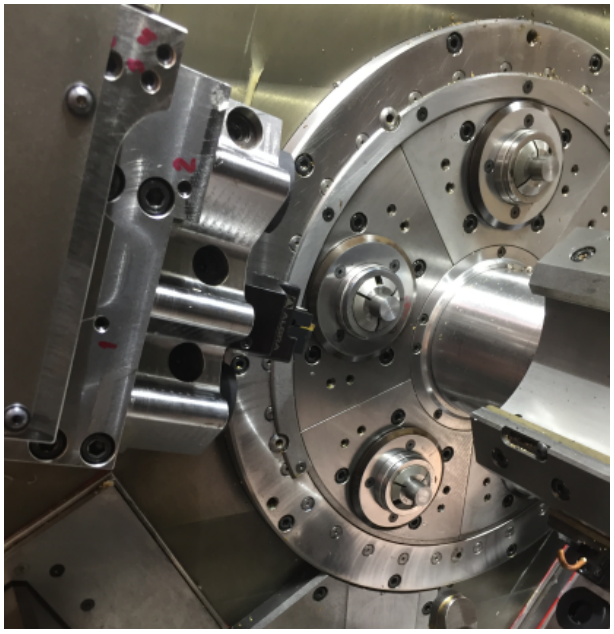

Figure 6.1: Measured dynamic compliance of the new slide

Fig. 6.2 measured dynamic compliance in three directions XYZ as a response to hammer hit in these directions. It shows that the highest amplitudes are in the first mode approximately on 48 Hz; this mode is dominant in the plane Y-Z. The second mode (71 Hz) is dominant in the X direction with the second-highest amplitudes, with the increasing frequency amplitudes hights decrease rapidly.

Using standard chatter theory (described in the previous chapter) could be easily created lobe diagram and chatter frequency diagram Fig. 6.4. These two figures show an apparent match between frequency measurement and the prediction for spindle speed 3000 and 3300 rpm; despite stable cut prediction, the measurement follows the predicted trend where higher spindle speed increase stability. The inaccurate position of the lobe can be explained by the change of the specific cutting force.

In contrast, at 3600 rpm accurses unpredicted behaviour, which has no basis in the chatter theory, in the theoretically stable condition, destructive chatter accrues, with the

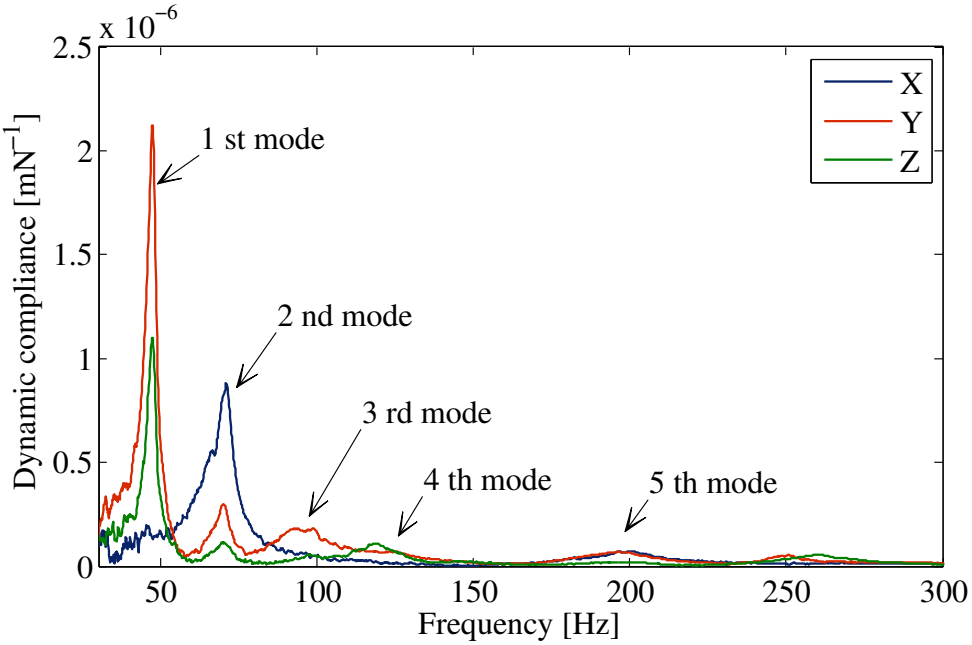

Figure 6.2: Measured dynamic compliance of the new slide

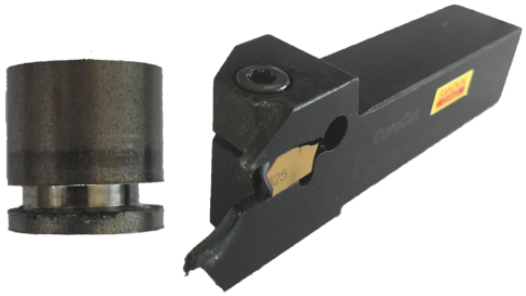

Figure 6.3: Knife destructed by chatter vibration and off-center groove

lower frequency that is for the chatter dominant second mode. As can be seen in the reconstructed knife phasor – Fig. 6.5 , the growth of vibration is exponential and stopped by knife destruction. The slowness of the onset of vibrations indicates a small frequency shift and thus the proximity of its own frequency, which is the cause. However, the excited frequency of 58 Hz is near the local minimum of the systems frequency response.

The Poincaré map – Fig. 6.6 only confirms the instability of the system – logarithmic spiral indicates increasing vibrations of the system without significant discontinuities in the cut, so it is a continuous section with grading vibrations.

Based on the frequency shift between the spindle speed and the excited chatter frequency, it can be concluded that the frequency of the natural frequency, which is the cause of the vibration, should be in the band around 54 Hz, which, however, has no support in the measurement.This fact leads to the hypothesis that the system's frequency response has to change. To rule out that the cause is the first mode of vibration that is closest. Therefore, the effect of the first mode must be ruled out. One way to achieve this is to design a tuned mass damper.

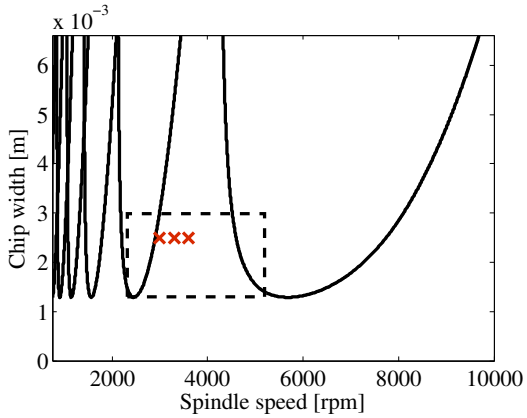

(a) Full scale diagram

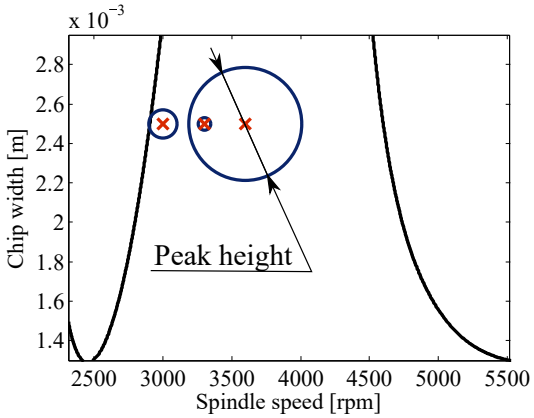

(b) Detail with signal strength representations

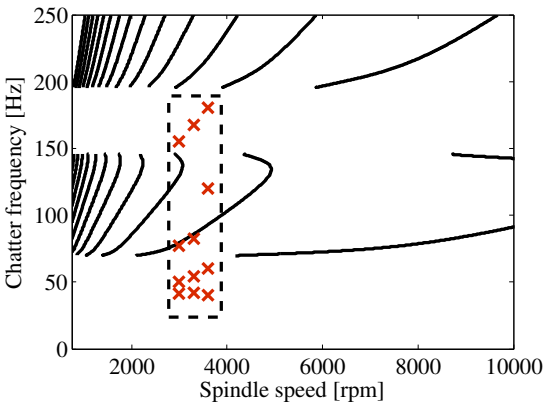

(c) Full scale diagram

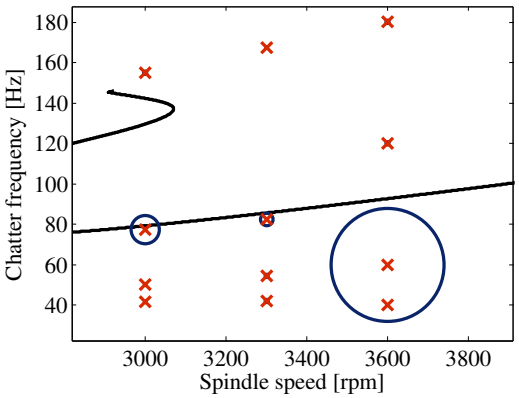

(d) Detail with signal strength representations

Figure 6.4: Predicted lobe diagram compared with measured machining conditions

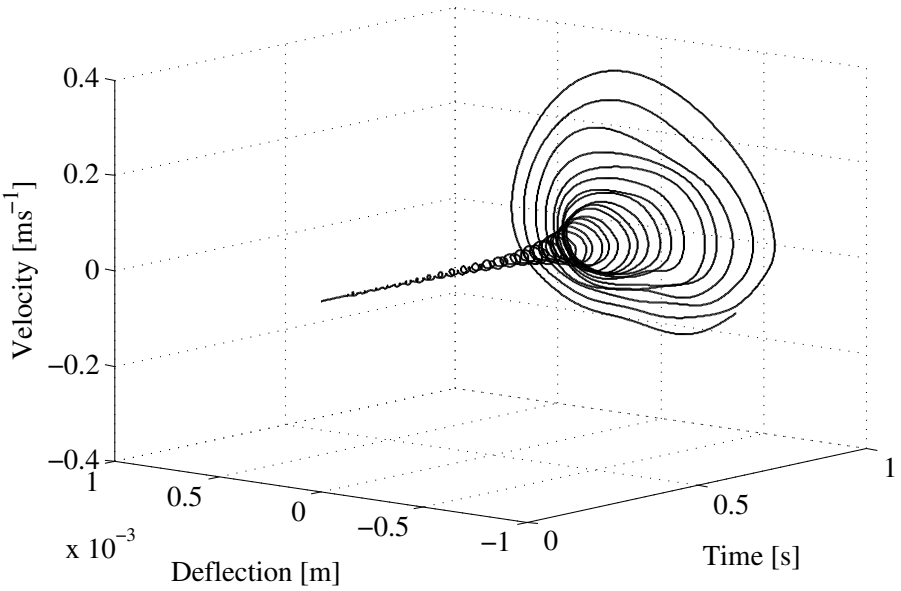

Figure 6.5: Phasor image of machining at 3600 rpm showing the gradual oscillation of the support until the destruction of the knife

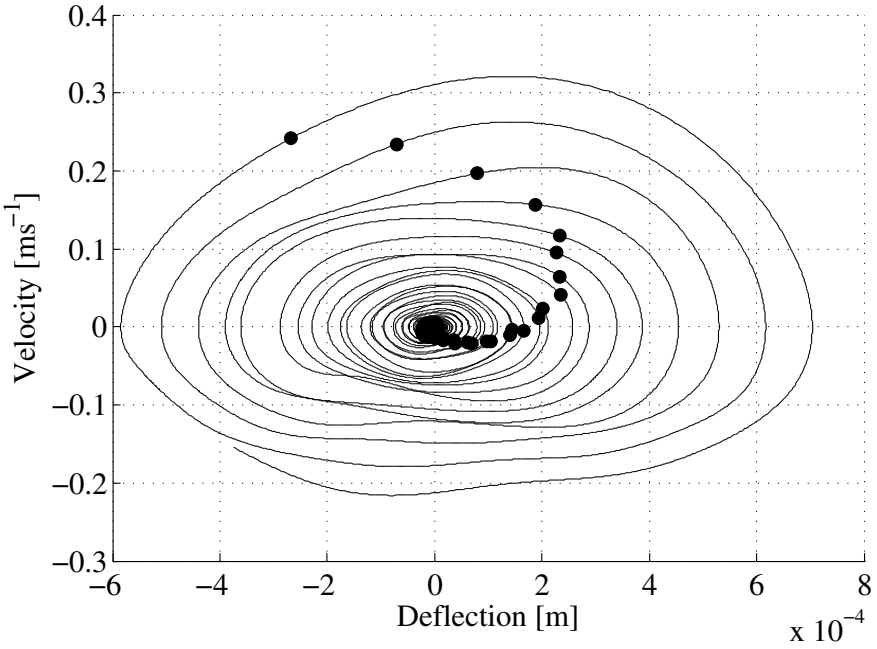

Figure 6.6: Poincaré map for machining at 3600 rpm resembling a logarithmic spiral shows high instability of the system

6.2 Effect of Tuned Mass Damper

The tuned mass damper was designed to minimise the amplitude of the first mode. According to the analysis, the first mode should not have an impact on machine tool stability; this is due to a low reaction in the X direction, however, during the machining measurement, where the frequency is observed corresponding to the first mode vibration – probably the reaction of secondary excited vibration by noncontinuous cut.

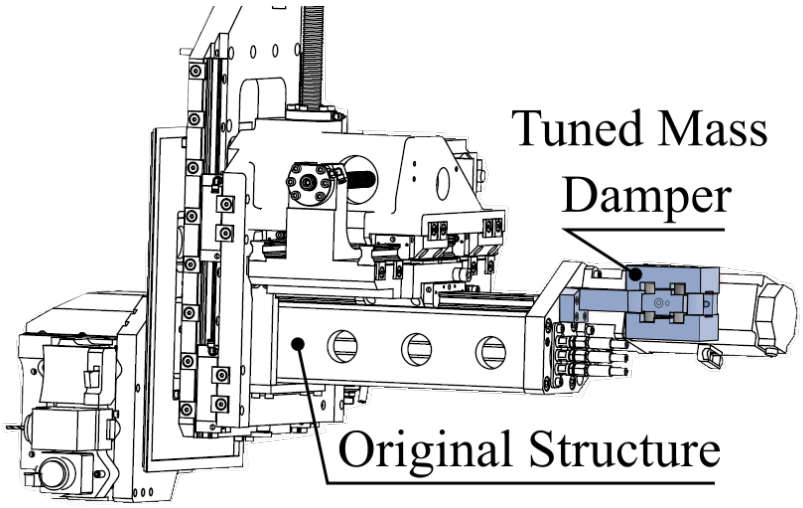

Figure 6.7: Mass damper placement on the structure

Figure 6.7 shows the damper design placed in the area with high amplitudes on the end of the central beam, the opposite side of the cut. The main parts are beams with a slider that enables tuning the structure's frequencies by changing the active length of the beam. On this slider are connected rubber isolators with steal mass provides the main compliance and the mass – see Fig. 6.8.

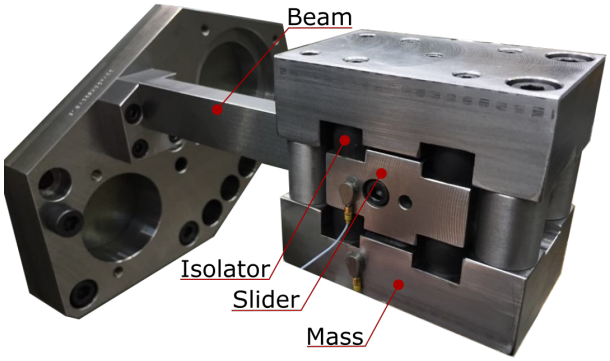

Figure 6.8: Photo of mass damper during testing

The tuned mass damper was tuned to minimise the amplitude of the first mode. According to the analysis, the first mode should not have an impact on machine tool stability; it is due to a low reaction in the X direction, however, during the machining measurement, where the frequency is observed corresponding to the first mode vibration – probably the reaction of secondary excited vibration by noncontinuous cut. Fig. 6.9 compares the dynamic compliance of the original structure and the one with the damper;

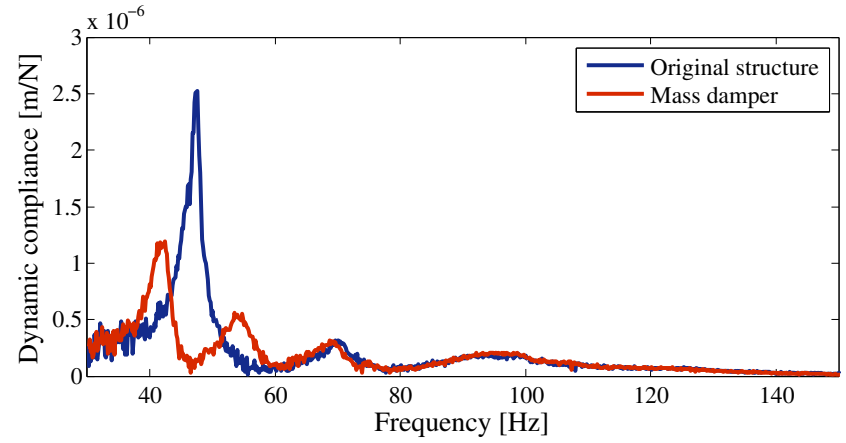

(a) Absolute value

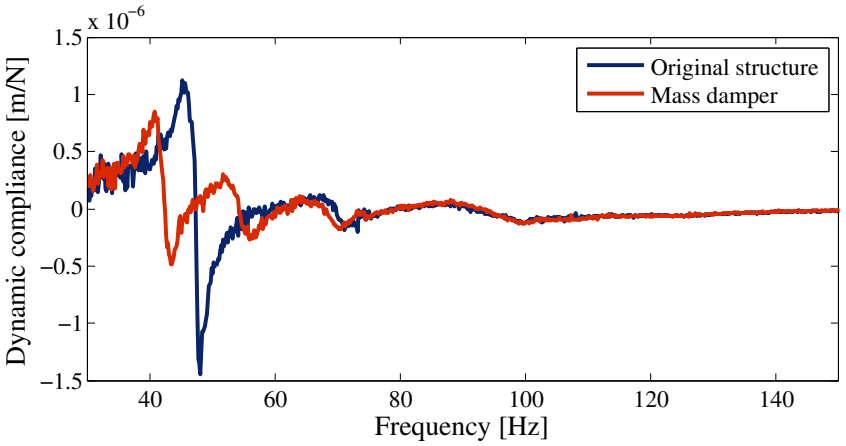

(b) Real component

Figure 6.9: Predicted lobe diagram compared with measured machining conditions

both absolute and real spectrum peak of the first mode decreases for the structure with the damper to less than 40 % of the original structure.

Fig. 6.10 shows a comparison of structure with and without mass damper for the same machining conditions – 2.5mm grooving for 3000 rpm. The tuned mass damper suppresses excitation of vibration peak at 44 Hz; also, its harmonics at 88 Hz disappear and the higher frequency compounds. However, the structure with the mass damper keeps the chatter frequency at 77.5 Hz with its harmonics. The qualitative change is noticeable in knife trajectory reconstruction – Fig. 6.12 where the secondarily excited vibration disappears, but for both signals there is a significant chatter frequency, which matches the predicted frequency.

Despite the removal of the first mode, there is no significant change at 3600 rpm; the knife breaks again without any frequency change. The only difference is the slowing down of the instability, which could be caused by increasing the total weight of the original structure. It follows that, regardless of the change in the first shape of the oscillation, the cause of the instability has not changed, and it is necessary to focus attention on another cause.

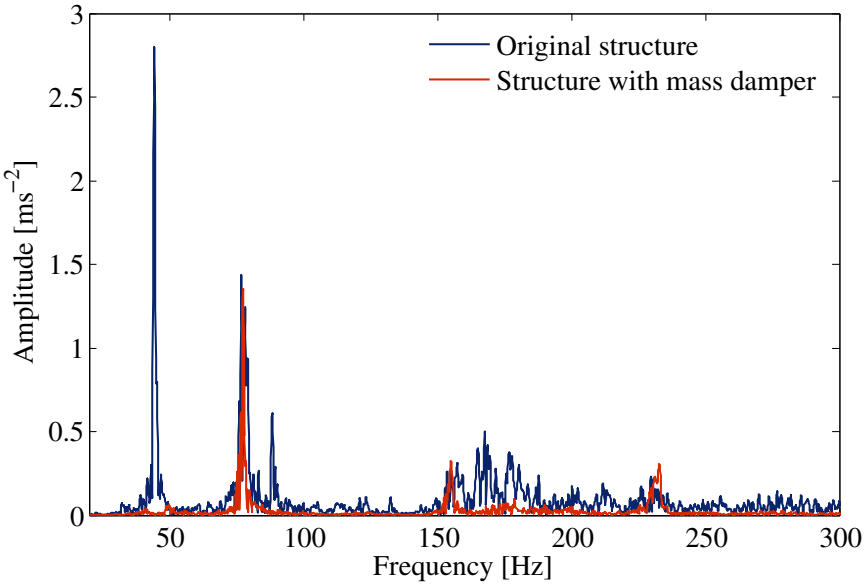

Figure 6.10: Comparison of frequency spectra during machining without and with the use of a dynamic damper reaction in Y-direction during 3000 rpm turning

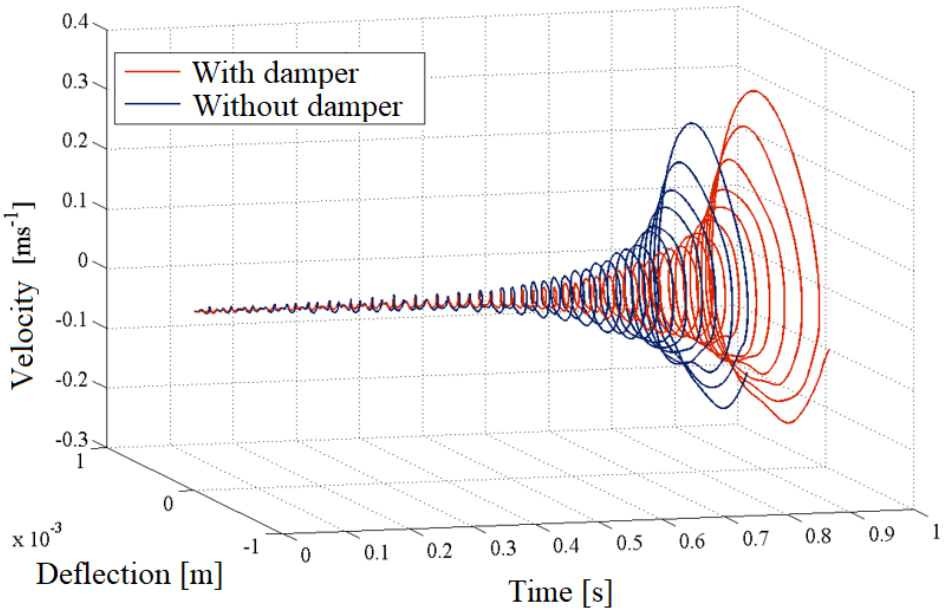

Figure 6.11: Reconstructed phasors of structure with and without the tuned mass damper tuned on the first mode during grooving with spindle speed 3600 rpm

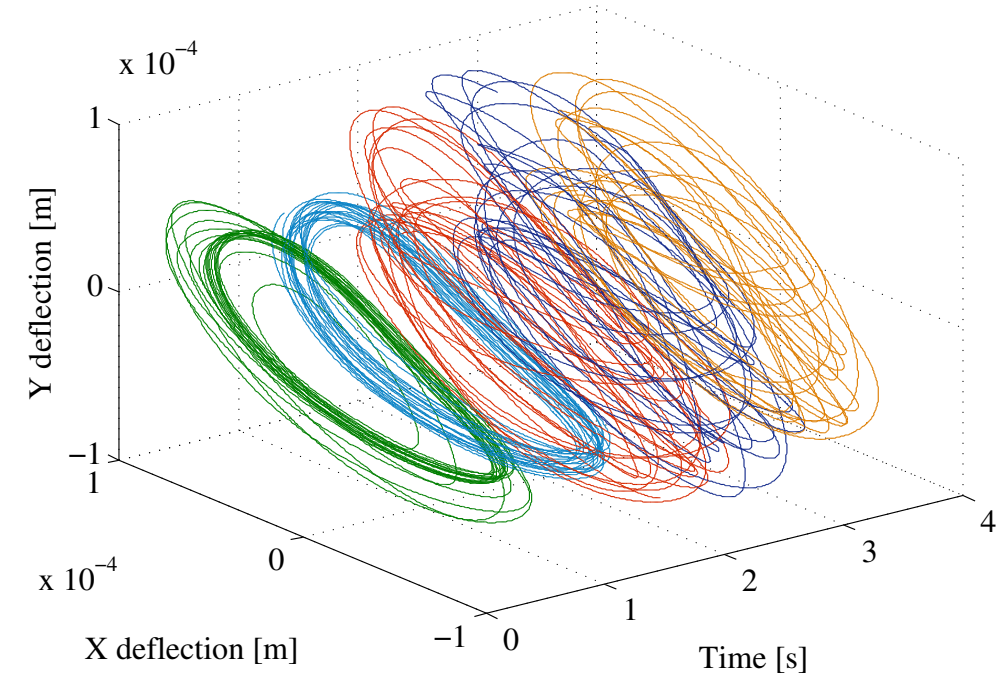

(a) Without damper

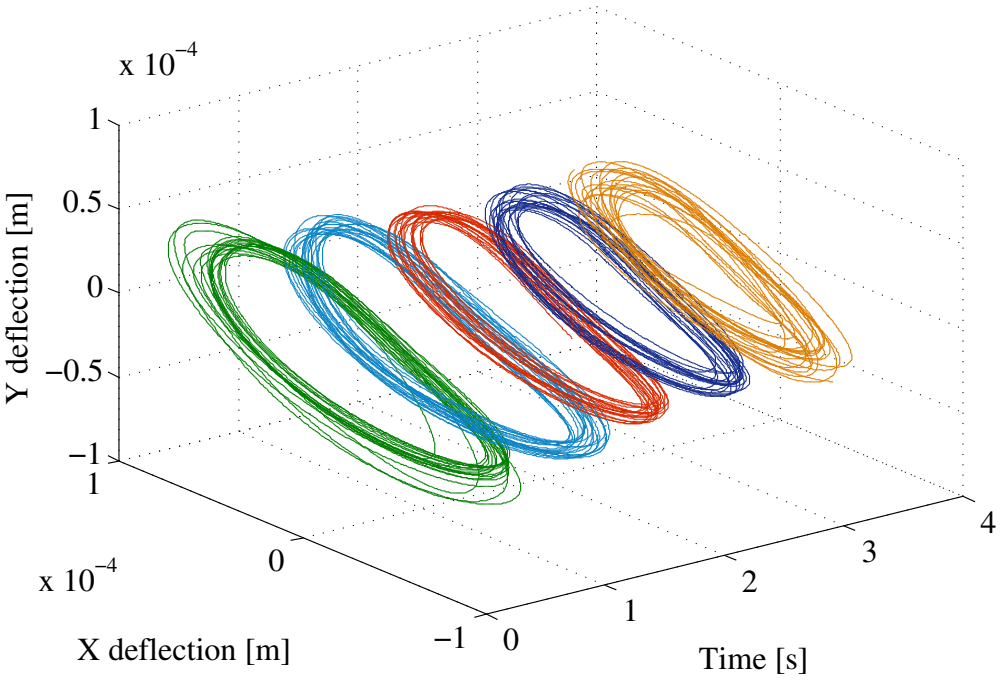

(b) With damper

Figure 6.12: Comparison of knife trajectory for structure with and without mass damper during 3000 rpm turning

7

Time-domain Regenerative Chatter Analysis of Non-linear Stiffness System

7.1 Time-domain Simulation for Chatter Analysis

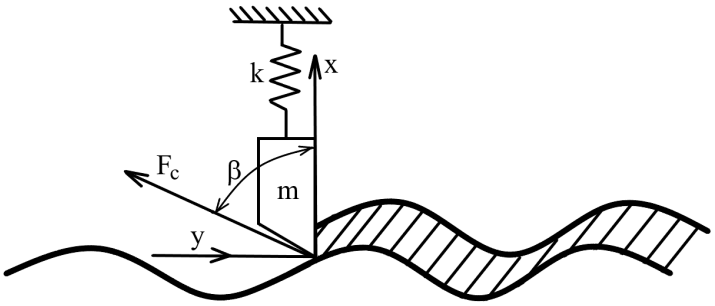

Figure 7.1: Scheme of machining with chatter vibrations

Figure 7.1 depicts a simple scheme of chatter vibration model, which is the base for time-domain simulation. The time-domain simulation is a possible way to analyse nonlinear systems. However, it is also quite time-consuming. Fig. 7.2 shows the main

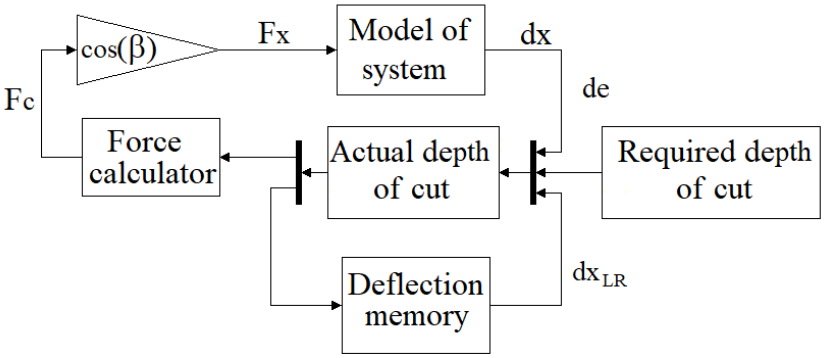

Figure 7.2: Scheme of regenerative chatter simulation model

parts of the simulation: the key part is the dynamic model of the nonlinear structure with force inputs and deflection outputs, the deflection output flows into the block, which sums actual knife deflection required deep cut and previous turns deflection. The result is an actual deep of the cut that flows into a force calculator that calculates chips cross-section and according to a specific cutting force that calculates cutting force. The specific cutting force could be a constant or function of machining conditions – the significant role has the chip depth dependency. Then is force according to the knife geometry split

into the direction, which is then inputs for the dynamic model of the structure. The final analysis is done on the deflection signals which compound the information about the stability and maximal deflection and about the chatter vibration frequency.

7.2 Simplified Nonlinear Stiffness Model

The static deflection measurement shows the nonlinear trend. Therefore the measurement points on the force-deflection diagram were fitted by three models using regression. The simplest model is a linear model, which is used as a control model; its equation is:

$$F = k_1 \cdot x \tag{7.1}$$

Nonlinear models are cubic and quadratic equations; to keep a negative value in the quadratic model, was used absolute value. The equations for cubic and quadratic are, respectively:

$$F = k_1 \cdot x^3 + k_2 \cdot x \tag{7.2}$$

$$F = k_1 \cdot x \cdot |x| + k_2 \cdot x \tag{7.3}$$

Fig. 7.3 and Table 7.1 show the results. All models represent the data according to the results of P-value; the best match has the quadratic model, which fits the data the most smoothly and has the lowest mean square error MSE. The quadratic model is slightly worse but still fits the data trend, although the hypothesis that the linear model does not depreciate cannot be rejected. Based on the trend of the measured data, it is obvious that the system is nonlinear and that the number of measure points influences the P-value.

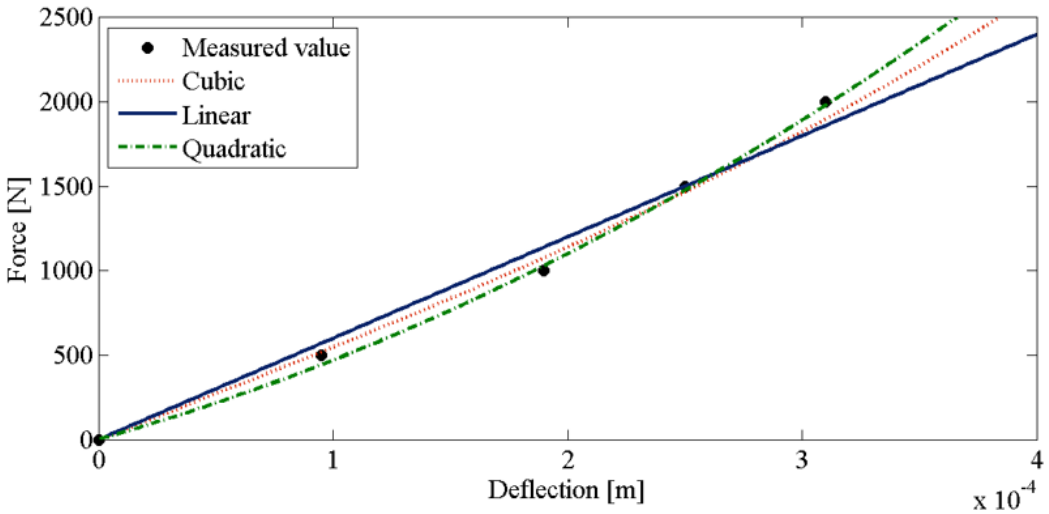

Figure 7.3: The comparison between measured values and regression models

7.3 Lobe Diagram Time-Domain Simulation and Simulated Impact Hammer Response

The impact hammer modal testing is the standard method for measuring dynamic behaviour; therefore, the simulation of this system enables us to compare the response of

Table 7.1: Regression results for three models

	k_1	k_2	P-value	R-square	MSE
Linear	5.98e+06	-	3.31e-05	0.989	67.6
Quadratic	3.79e+09	4.95e+06	1.26 e-04	0.999	21.8
Cubic	7.58e+12	5.39e+06	2.47 e-04	0.999	30.5

models from the previous section and tune the systems to have similar frequency and damping to match the real measurement of the system parameter. For all three models, the second mode is linear and is identified from the measurement. The simulation is time-domain, so there is no problem with the nonlinearity.

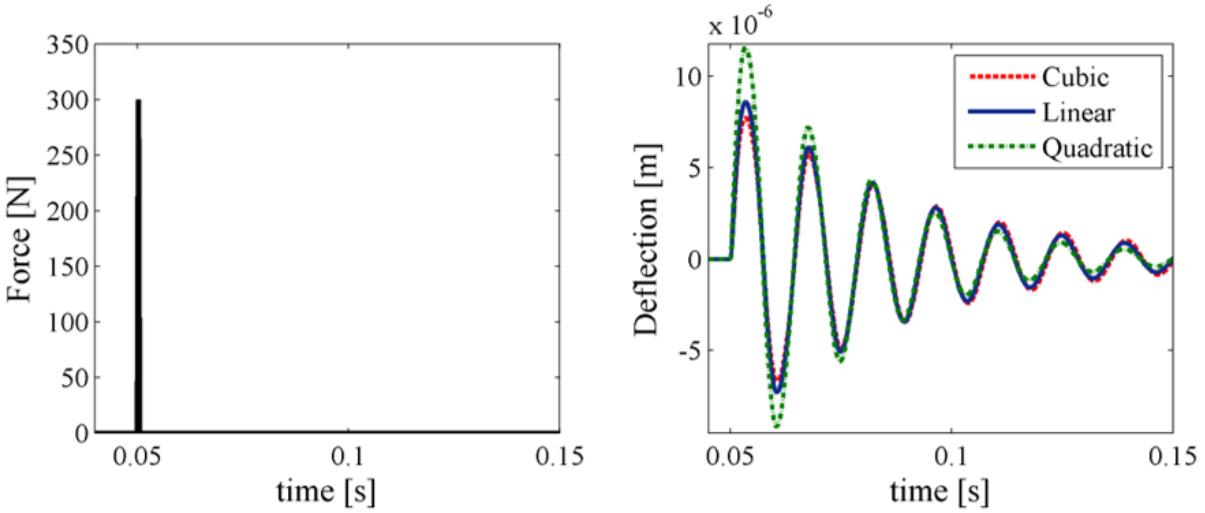

Figure 7.4: Modal hammer simulation impulse – force and reaction

Figure 7.4 shows the results in the time domain, the force impulse, and the system deflection response, the linear and cubic model has an almost identical response, the quadratic model has a lower stiffness, which is also noticeable from dynamic compliance – Fig. 7.5. In all three systems, the negative real part minimum is tuned to a similar value, therefore applying chatter theory, the minimal chip width should be similar. Figure 7.6 shows the estimated lobe diagrams; naturally, the lobe diagram follows the trend of the negative real part, so the cubic and linear models are in good agreement with the slight spindle speed change and slightly lower stability of the cubic model. The stability decrease mainly for higher chip width is more significant for the quadratic model. However, the central positions of the lobes are similar, in contrast to the results of time-domain simulations – Fig. 7.7: where the quadratic model has a significant lobe shift to a higher spindle speed. All models have the same minimum chip width boundary, which is in accordance with the estimation. The linear model reached the highest amplitudes during the simulation, which is not unexpected due to the character of the nonlinear system vibration. The area of maximal amplitudes (highly unstable regions) differs in position, in the linear systems, are located in the front side of the lobe – the steep left side, which corresponds to the system area between -90° to -180°, but in nonlinear systems, the maximal instability regions move to the right, wherein cubic systems are located in the middle of the lobe, and in the quadratic model are shift further to the right side. This behaviour corresponds to a type of nonlinearity – where both systems have hardening characteristics. All of these

findings highlight the main problem of estimation lobe diagrams based on the response to the impulse hammer.

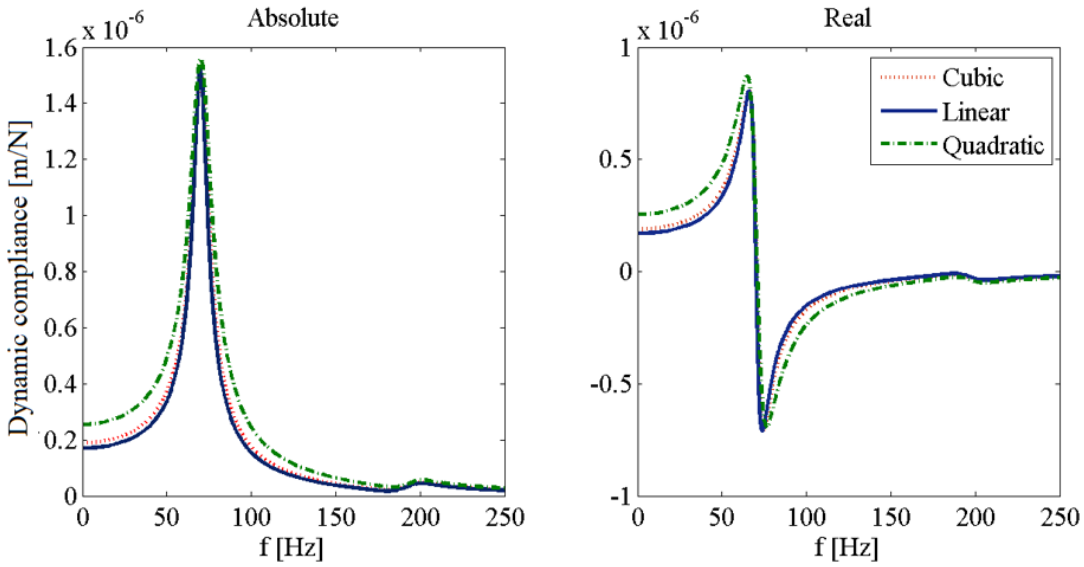

Figure 7.5: The absolute and real frequency response for simulated impulse

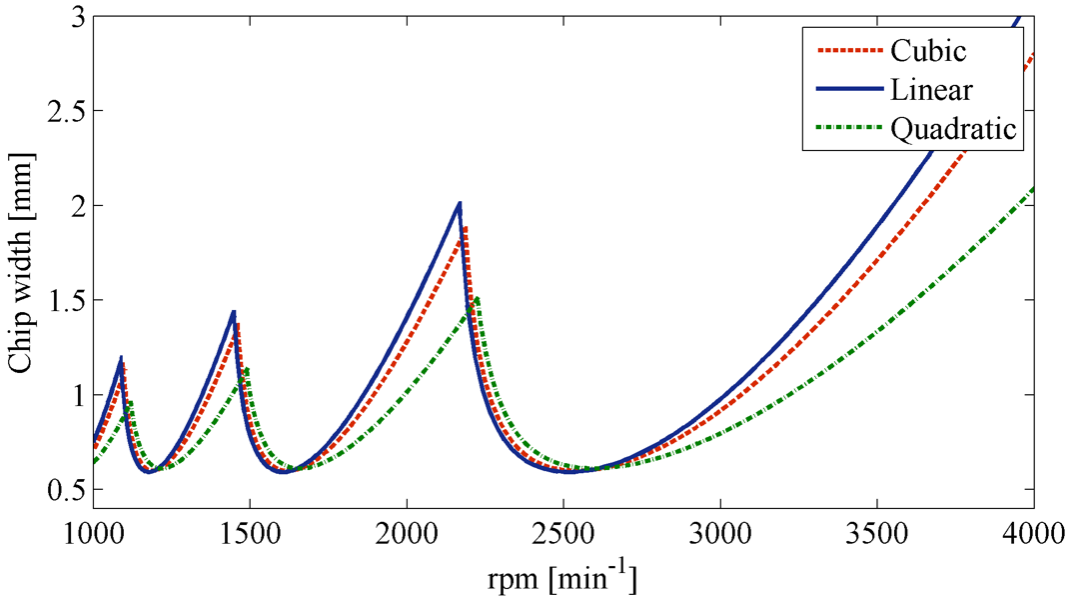

Figure 7.6: Estimated lobe diagram based on simulated impact hammer reaction

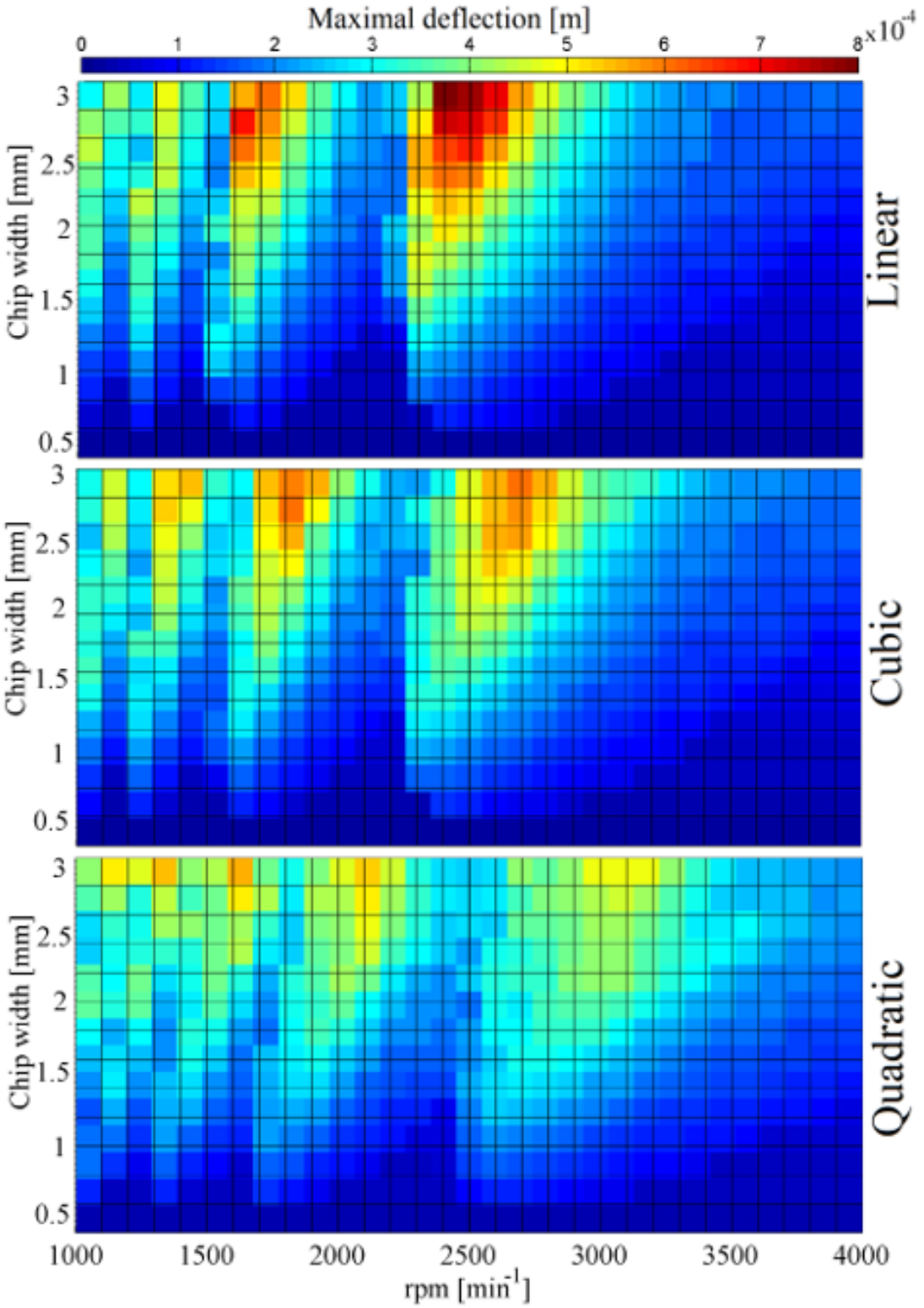

Figure 7.7: The maximum deflection of time-domain simulations of grooving operation for three models of stiffness projected into spindle speed, chip width dependency

8

Simplified 2D Analysis and Linearisation at Operating Point Synthesis Algorithm

The simulation model is inspired by an engineering problem – tool damage caused by regenerative chatter in a theoretically stable area. The stability was estimated by an FEM (finite element model), a modal hammer measurement, and the experimental machining validated estimation. The result shows a good match in unstable regions; the chatter frequencies match the predicted ones. However, the chatter arised in the theoretically stable region and its frequency do not correspond to the chatter frequency with a higher chip width. This behaviour leads to the hypothesis that it is the consequence of contact nonlinearity.

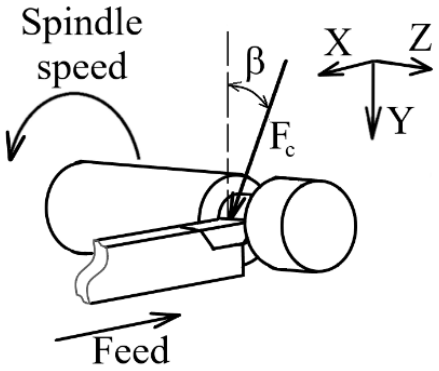

Figure 8.1: Grooving scheme

The analysis was done on the example of a grooving operation. Fig. 8.1 shows a scheme of the grooving process with the cutting force orientation; the cutting force lies in the plain XY where also lies the feed direction, which is oriented in the X direction. Due to this operation, the structure could be simplified as a two-dimensional problem, a beam with a two-spring support. This model describes mainly the first mode responsible for the chatter. However, the model has freedom in the Y direction; we consider movement only in the X direction and rotation in the Z axis. The scheme of the model could be seen in Fig. 8.2. The model is a rigid body represented by its mass and momentum of inertia in the center of gravity. This part connects the basis by two springs and dampers. In this case, the influence of the machine part stiffness is marginal, comparing the contact stiffness, so it is neglected.

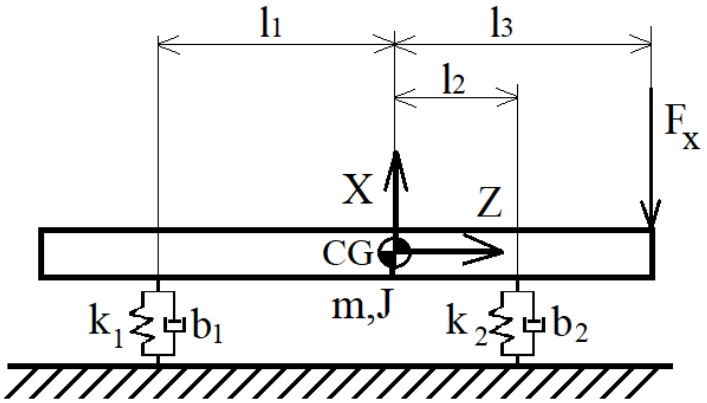

Figure 8.2: Scheme of parallel spring system

8.1 Linear Model

Regarding the previous assumptions, the model is represented by its momentum of inertia by two differential equations. The first represents the centre of gravity's displacement in the X-direction, and the second describes its rotation displacement.

$$m\ddot{x}, = k_1(x - l_1\theta) - k_2(x - l_2\theta) - b_1(\dot{x} + l_1\dot{\theta}) - b_2(\dot{x} + l_2\dot{\theta}) + F \tag{8.1}$$

$$J\ddot{\theta}, = k_1(x - l_1\theta)l_1 - k_2(x - l_2\theta)l_2 - b_1(\dot{x} + l_1\dot{\theta})l_1 - b_2(\dot{x} + l_2\dot{\theta})l_2 + Fl_3 \tag{8.2}$$

By transforming equations 8.1 and 8.2 to the matrix form, we get metrics **M**, **K**, **B**, and force vector **F**:

$$\mathbf{M} = \begin{bmatrix} m & 0 \\ 0 & J \end{bmatrix} \tag{8.3}$$

$$\mathbf{K} = \begin{bmatrix} k_1 - k_2 & -k_1 l_1 + k_2 l_2 \\ -k_1 l_1 + k_2 l_2 & -k_1 l_1^2 + k_2 l_2^2 \end{bmatrix} \tag{8.4}$$

$$\mathbf{B} = \begin{bmatrix} b_1 - b_2 & -b_1 l_1 + b_2 l_2 \\ -b_1 l_1 + b_2 l_2 & -b_1 l_1^2 + b_2 l_2^2 \end{bmatrix} \tag{8.5}$$

$$\mathbf{F} = \begin{pmatrix} 1 \\ l_3 \end{pmatrix} \tag{8.6}$$

Equation 8.7 provides the solution to the deflection and rotation in centre of gravity $x_C G$, which depends on the angular speed of the harmonic force vector:

$$x_{CG}(\omega) = (\mathbf{K} - \omega^2\mathbf{M} + i\omega\mathbf{B})^{-1}F \tag{8.7}$$

For a stability analysis, it is necessary to get a solution under the force. The total deflection is a combination of rotation and translation of the centre of gravity:

$$x_F(\omega) = (1, l_3)x_{CG}(\omega) \tag{8.8}$$

Damping values b_1, b_2 are represented by a simple linear model. The value of the damping coefficient was chosen to reach approximately 3 % of the critical damping for both modes for the linear structure. However, due to the nonlinear stiffness, the proportion of damping is changing. The damping coefficient and the rest of the parameters except stiffness are in Tab. 8.1 The stiffness of the springs is defined by the nonlinear model described below.

Table 8.1: Parameters of parallel spring system

Mass	m	$85\,kg$
Moment of inertia	J	$6\,kgm^2$
	l_1	$20\,mm$
Dimensions	l_2	$38\,mm$
	l_5	$293\,mm$
Damping Coefficient	b_1, b_2	$6 \cdot 10^3\,Nm^{-1}s$

8.2 Nonlinear Stiffness Model of Linear Ball Guideway with Preload

Due to the combination of preload and nonlinear stiffness, the whole linear ball guideway system's nonlinearity is relatively high and causes changes in chatter stability. The behavior can be easily described by the Hertzian contact between a ball and a groove contact. The simplest model is usually represented by a two-ball groove contact with a preload. Sun and Kong present this kind of model and use experimental validation to prove its behavior [51], [52]. In the following work, Kong extends and presents a polynomial approximation of linear ball guideway stiffness [53]. These more advanced models also consider the angular relations in the linear ball guideway. However, these models are too complicated, and the primary behavior matches the simple Hertzian contact model. The equation describes the basic Hertz's contact model of the linear ball guideway stiffness:

$$F(x) = \begin{cases} k \cdot ((x_0 + x)^{3/2} - (x_0 - x)^{3/2}) & \mid x \mid < x_0 \\ k \cdot (x_0 + x)^{3/2} & x > x_0 \\ -k \cdot (x - x_0)^{3/2} & x < -x_0. \end{cases} \tag{8.9}$$

Where F is the reaction force of the contact, x_0 the displacement caused by preload, k is the stiffness coefficient, and x is a deflection from the guideway's equilibrium position. The stiffness dramatically changes around the boundary of the preload loss. If we consider that the loss of preload happens when one row of the ball-groove contact has a double preload deflection and the other is without any deflection, then we can define the contact loss load F_l as the proportion of preload force F_p:

$$F_p = k \cdot x_0^{3/2}, \tag{8.10}$$

$$F_l = F_p \cdot \frac{(2x_0)^{3/2}}{x_0^{3/2}} = F_p \cdot 2^{3/2}. \tag{8.11}$$

Manufacturers usually declare a load of lost preload to be $2.8 \cdot F_p$. The parameters are preload force $F_p = 140\,N$ and nonlinear stiffness coefficient $k = 7.55e9N/m^{3/2}$. For these conditions, we get the resulting dependence of stiffness on deflection in Fig: 8.3, where there is a noticeable region with stiffness decreasing by 30 %.

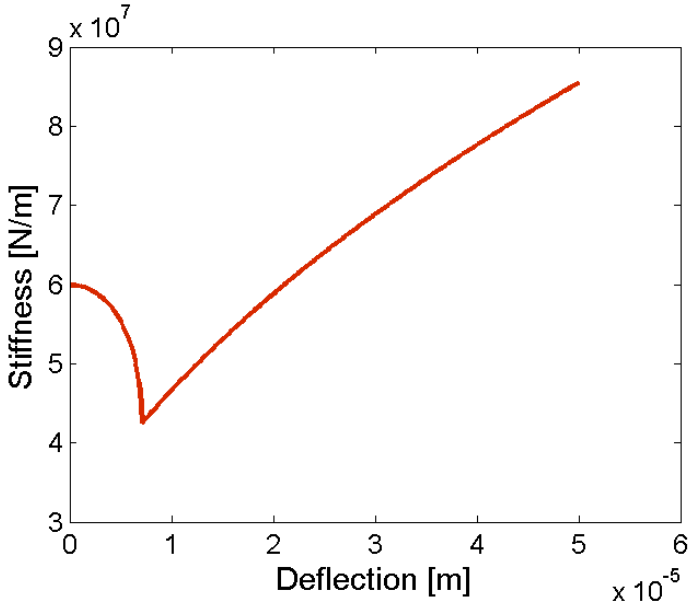

Figure 8.3: Stiffness dependency of models on the deflection

8.3 Static Equilibrium of Structure

In the future, for the chatter estimation it is necessary to analyze a static solution first. It is because we assume that the chatter starts from the smooth surface. The presented system is statically definite, so we can use momentum and force equilibrium equations to define the force in each boundary and depend on the load.

$$F_1 = F \cdot \frac{l_3 - l_2}{l_1 + l_2} \doteq 0.522 \cdot F \tag{8.12}$$

$$F_2 = -F \cdot \left(1 + \frac{l_3 - l_2}{l_1 + l_2}\right) \doteq -1.522 \cdot F \tag{8.13}$$

From the values above, it is evident that the force in the second spring k_2 is almost three times higher than in the first spring k_1. This fact means that the reaction of k_2 has a crucial role in chatter stability. With the assumption of small angles, the total deformation of the system under a load can be defined by the equation:

$$x = \left(\frac{f_{k_1}(F_1) + f_{k_2}(F_2)}{l_1 + l_2}\right) \cdot (l_3 - l_2) + f_{k_3}(F_2) \tag{8.14}$$

8.4 Dynamic Response of Simulated Modal Hammer Impulse

As we showed in the motivation part, some irregularities could occur during the modal hammer measurement - different hit peaks cause changes in the system response. Structural nonlinearities could cause this behaviour. Therefore, the time-domain simulation of the modal hammer measurement was applied to the presented nonlinear structure to verify this behaviour. The input signals that follow the force signals in Fig. 7.42 were

applied to the analysed structure. The resulting deflection was then transformed by the Fast Fourier transform (FFT) to frequency domain dynamic compliance in Fig. 8.4. The results show that the system response depends on the modal hammer hit property, the maximal peak frequency, and the changes in shape. Hence, the model presented could represent the frequency shift and the change in the peak shape.

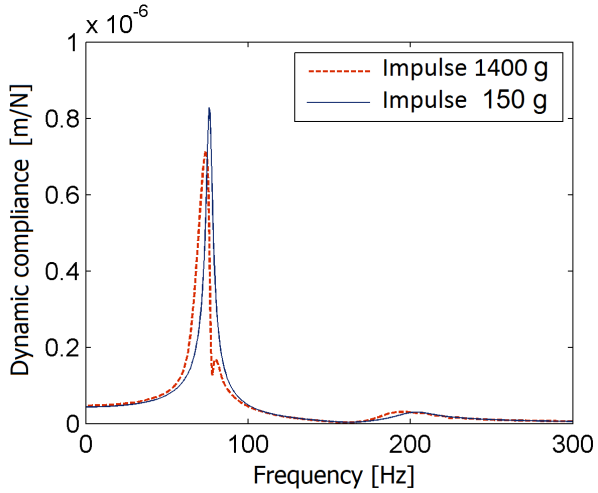

Figure 8.4: Simulated impact response

8.5 Proposed Synthesis of Linearisation in Operating Points Algorithm for Chatter Analysis of Structure With Nonlinear Stiffness

The main idea of the synthesis of linearisation in operating points algorithm (SLOP) is that the nonlinear structure under different loads has a unique set of linearised stiffness. Hence, it would also have a different stability lobe diagram (stability lobe diagram).

Figure 8.5 shows the case of three different loads corresponding to different chip widths (each stability lobe diagram is valid only for a specific chip width) the figure shows these areas as blue-stable and gray-unstable stripes. The final stability lobe diagram is composed of many of these local solutions; the total number depends on the required accuracy and the stability lobe diagram range. The assumption for the local linearization synthesis is that the chatter starts from a smooth surface with no other interruptions. According to this, the start of instability depends on the local behavior of the system. This is the reason why we can split the task of the lobe diagram into several subanalyses, and then the results of the local stability prediction are combined into one lobe diagram.

This algorithm aims at a fast detection of possible instability in the structure with height structural stiffness nonlinearity. The principle is to decompose the stability assumption problem into several subproblems. The diagram see Fig 8.6 describes the algorithm; the first step is to define a range of stability analysis and evaluate the cutting force applied during the stable machining process according equations: 4.1 – 4.3. After that, the nonlinear static analyses are applied to each of these loads. This analysis's required outputs are the stiffnesses of each connector, which is a linearization of each of these solutions.

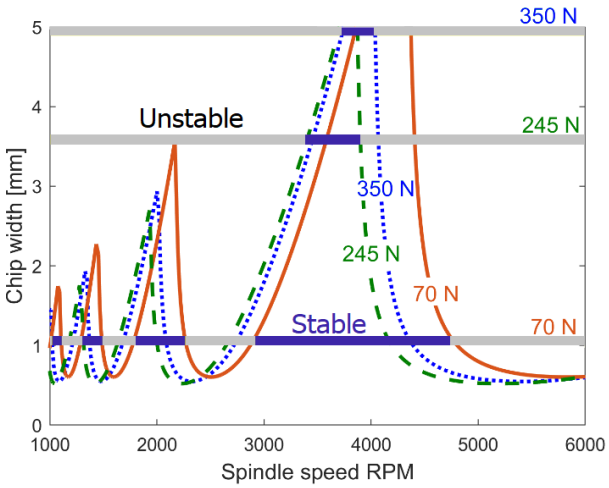

Figure 8.5: An example of the operation of an SLOP: three linearised stability lobe diagrams for different load segments corresponding to the chip width form the final stability lobe diagram

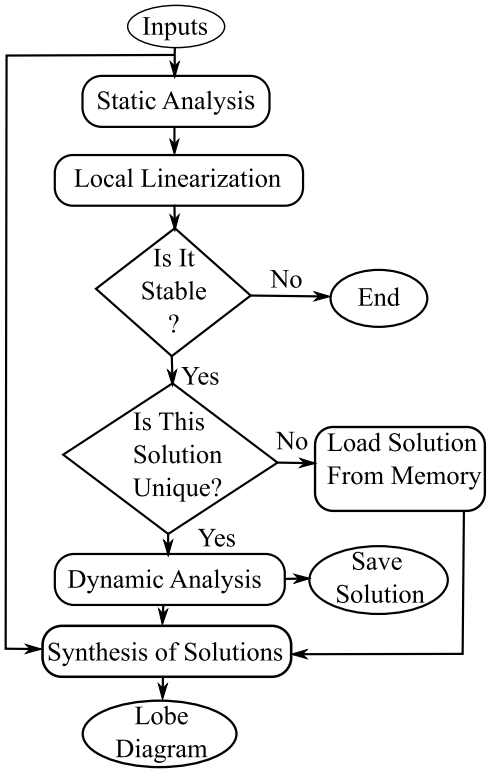

Figure 8.6: Scheme of the proposed SLOP algorithm

Before evaluating the system's general stability, the unstable solutions are excluded due to their transient behavior. Then, the unique sets of linearized stiffness combinations are used to create matrix K (equation 8.4) and compute a linear solution following equations 8.7 and 8.9.

This solution is used for a classical chatter analysis. The algorithm assumes that bifurcations can exist in the structure, so there could be more than one stable solution for some loading conditions, and all these unique solutions must be analyzed. In the final step is the synthesis of all these solutions, all possible solutions are compounded into a general lobe diagram.

8.6 Comparison of SLOP Lobe Diagram with Time-domain Simulation

Figure 8.7 shows the results of time-domain simulation 3D graph of the maximal knife amplitude. The results resemble a steep cliff from the front edge of the instability (lobe edge which is defined by the system's range from natural frequency to min real part range) and sloping down to the back edge of instability (lobe edge which is defined by the spectrum above min real part range). Below the 2 mm chip width, the highest amplitude

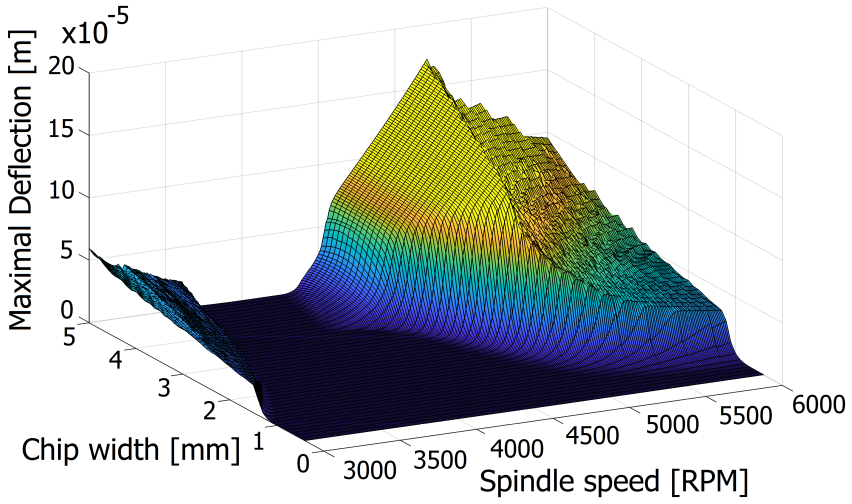

Figure 8.7: Time-domain simulation detection of maximal deflection depending on the chip width and spindle speed

ridge follows the edge of the stable system; above it bends towards lower speeds where at its minimum point it changes the trend, and with higher chip width it grows towards higher speeds.

The projection of the stable and unstable region and comparison with the SLOP results is in Fig. 8.8. The results of both SLOP and time-domain simulations show that even the system based on the Hertzian contact theory causes noticeable changes in the chatter stability. In both results, we can notice the front side's deformation approximately in the lobes, mainly in the area from 3 mm to 4 mm chip width where the stability drops to the lower spindle speed; above this area, the trend changes, and the lobe's edge is deformed following the higher speed. However, the SLOP solution provides a more conservative

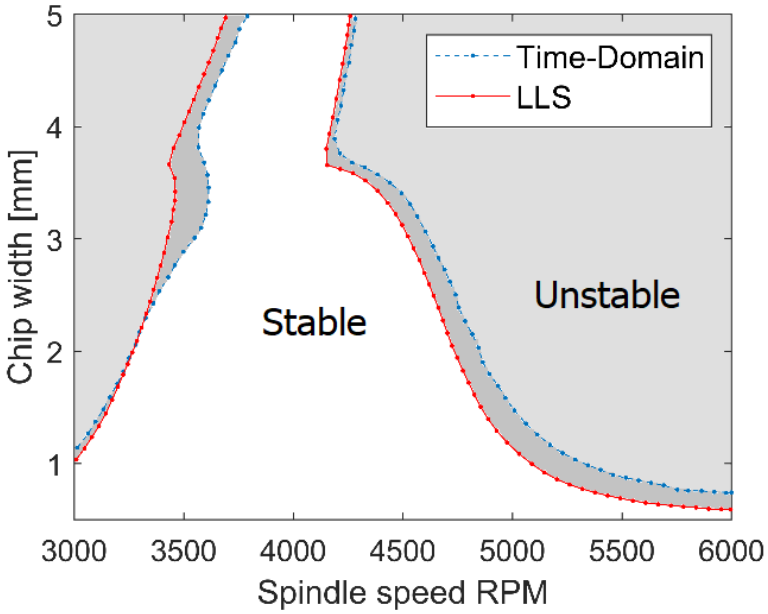

Figure 8.8: Time-domain simulation detection of maximal deflection depending on the chip width and spindle speed

stability estimation. The backside of the lobe provides different results, wherein the results above 2.5 mm chip width time-domain simulation offer better results.

The chatter frequency maps in Fig. 8.9 show that frequencies match well only on the edge of stability. Due to high instability inside the lobe body, the linearization does not match the simulation. The main reason is that these regions do not satisfy the quasi-static deflection assumption; hence their instantaneous stiffness value cannot be generally linearized. This fact is the reason for the resulting deviation in the predicted frequency map.

Table 8.2: Comparison of SLOP time dependence and time simulations with different solvers

SLOP	Time Domain Simulations		
	Ode14x	Ode8	Ode5
5857 s	$2.432 \cdot 10^6$ s	$1.1578 \cdot 10^6$ s	$5.4923 \cdot 10^5$ s

An important parameter is the time required for the analysis. Tab. 8.2 presents the time spent on SLOP and the simulation in the time domain with three different solvers. The resolution (speed step 12 RPM, chip width 0.05 mm) and the space analysed are the same, which corresponds to Fig. 8.8.

The time domain simulation without the ode14x, ode8, and ode5 solvers takes, respectively, one month, two weeks, and one week. In contrast to this, SLOP takes 90 minutes, which means that SLOP is significantly more time-effective, mainly for large-scale evaluation. The possible way to speed up a TDS is to stop the simulation after the chatter is detected, which reduces the time spent by 60 %. Another possible way to decrease the time spent is to use a heuristic algorithm orientated to the detection of edges of instability. However, this reduces the information in the system. The highest SLOP time

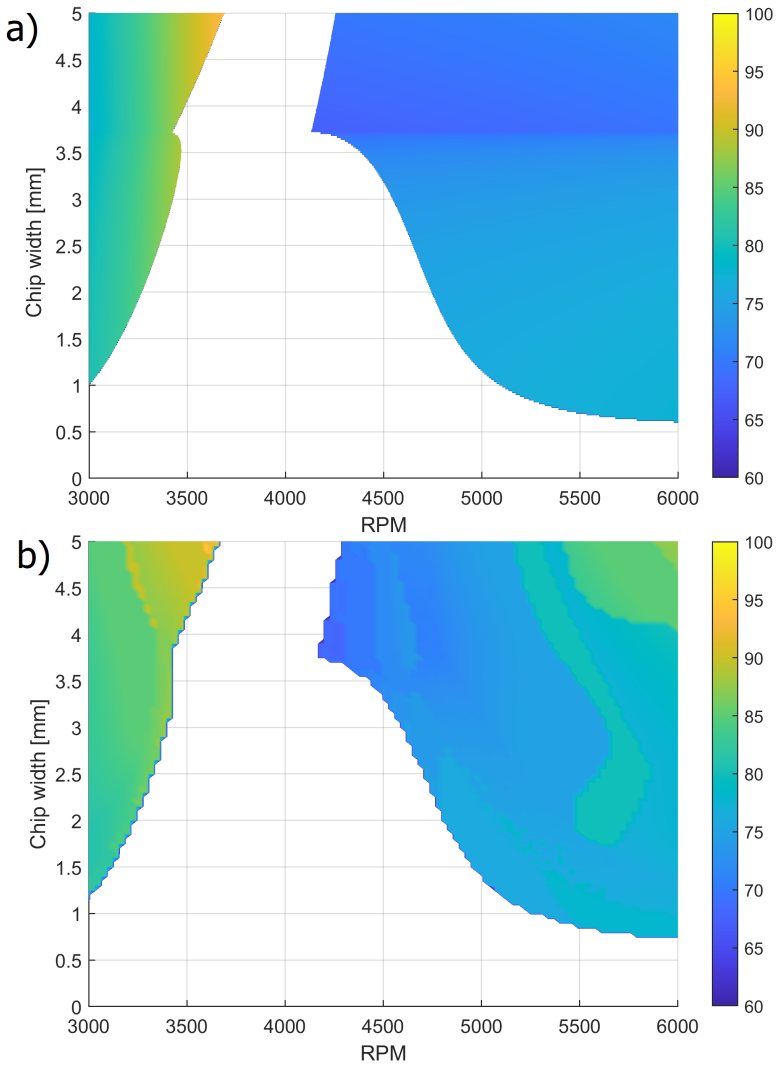

Figure 8.9: Comparison of frequency maps estimated by SLOP algorithm (a) and TDS (b)

spent (above 95 %) is the final step of the algorithm, processing of the lobe boundaries: resampling and identifying stability and instability.

8.7 Feed Dependent Stability Lobe Diagram

The feed is usually a neglected parameter in the chatter stability analysis. However, if the stiffness depends on the load, the feed becomes an important parameter with a significant influence on the stability lobe diagram. Figure 8.11 shows the stability lobe diagram on the cutting force. Two waves caused by the drop in stiffness in each spring, which bends the maximal stability to the w shape, are significant. This diagram is the basis of the SLOP where three individual sections are presented in Fig. 8.5.

The advantage of SLOP is that one linearised data set can be used for another stability lobe diagram with different feed parameters; this makes the whole process quite effective. The set of linearisation space has to be only extended if the required load exceeds the current maximum of the linearised set. Four different feed stability lobe diagrams created by SLOP are presented in Fig. 8.11. It is noticeable that the edge of the lobe follows the

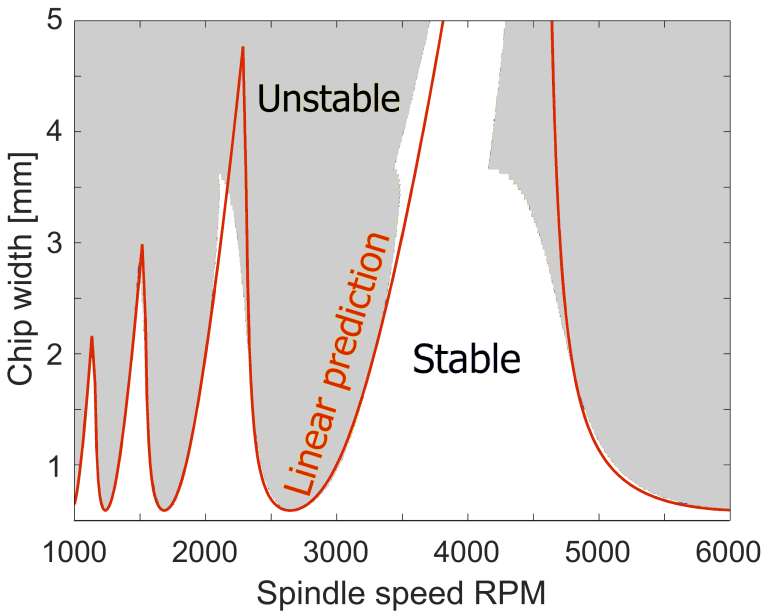

Figure 8.10: Comparison of stability lobe diagram estimated by SLOP algorithm and linear system stability lobe diagram in the wider speed range

trend from Fig. 8.12; in the highest load feed of 0.16 mm / rev, we could see a complete deformed W-shaped on the edge. The trend is obvious – higher feed causes instability lobe diagram W-deformation to the lower chip width, in contrast to the low load, which moves it to the higher chip width. The 0.02 mm / rev feed looks almost like a linear stability lobe diagram; however, it is caused by the shift of the deformed area above the observed area. Broadening the view of the matter will provide us with Fig. 8.10 which shows a comparison of the SLOP stability lobe diagram (for 0.04 mm/rev) with a linear alternative (red line). It shows a good match in the low-speed area where the neighbouring lobes meet before significant deformation occurs. Therefore, the spindle speed range and the stiffness drop should be considered before analysis.

The presented results of SLOP match well with the time-domain simulation. However, this example is simplified and many parameters were neglected. Often, the values of coefficients vary depending on the unknown parameters. Due to this fact, it is necessary to approach the chatter stability problem as a stochastic system. Furthermore, the application of the SLOP to actual machine tool systems with experimental measurements is highly required for future development.

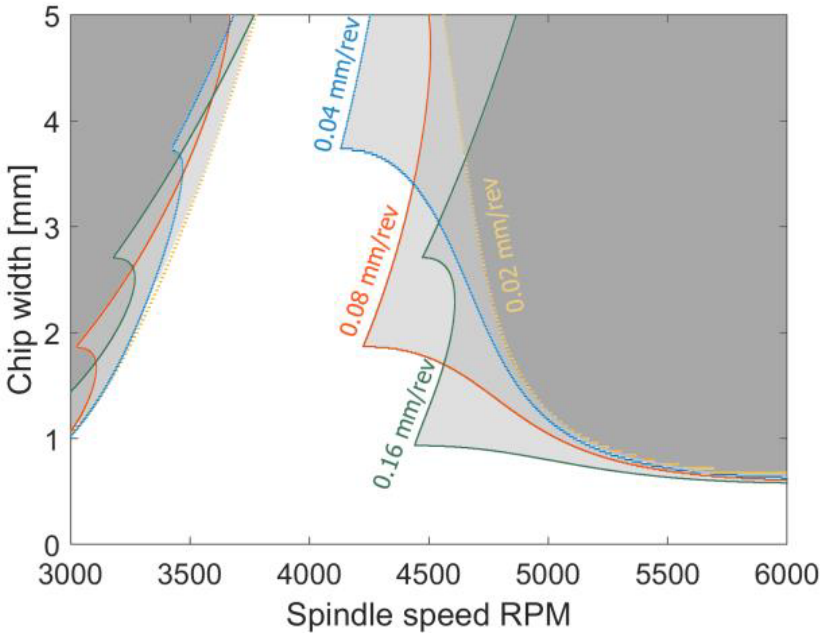

Figure 8.11: Comparison of stability lobe diagram estimated by SLOP algorithm for different feed

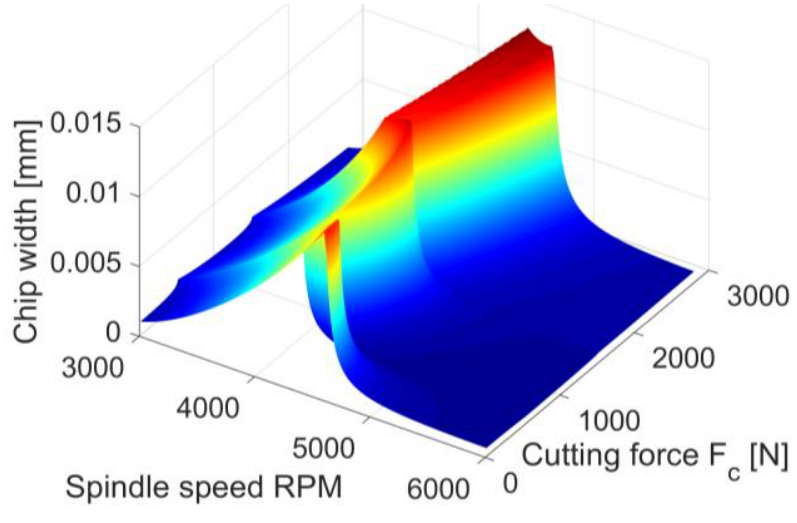

Figure 8.12: Surface created by individual linearised stability lobe diagrams dependent on spindle speed and cutting force

9

Linear Ball Guideway Model Based on Hertz Contact Theory

9.1 Ball Groove Contact

The basis for the behaviour of linear lines is the contact ball groove; From this elementary element we derive the overall rigidity of the line as well as the resulting nonlinear behaviour, and therefore it is necessary to pay attention to it. According to the Hertzian contact theory [54], we can estimate the contact behaviour.

The basic contact force of the ball is defined by the equivalent radius and the equivalent Young modulus. These two parameters define the nonlinear stiffness coefficient. The circular contact area can be described by the following equation:

$$F = \frac{4}{3}\sqrt{R}E^* \cdot x^{3/2} \tag{9.1}$$

Meanwhile, the equivalent elastic modulus, E^*, can be expressed in terms of the elastic modulus, E, and Poisson ratio, ν , of each contact body as

$$\frac{1}{E^*} = \frac{1-\nu_1^2}{E_1} + \frac{1-\nu_2^2}{E_2} \tag{9.2}$$

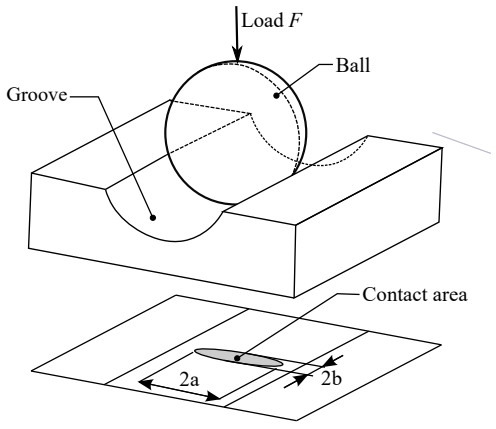

Figure 9.1: Ball – groove contact model

However, for the LBG problem considered in the present study, the ball-groove contact has an elliptical rather than circular geometry, as shown in Fig. 9.1. Hence, Eq. (9.1) should be rewritten as

$$F = \frac{4}{3}\frac{\sqrt{R_e}E^*}{\mu(e)^{3/2}} \cdot x^{3/2}, \tag{9.3}$$

where μ varies as a function of the eccentricity of the contact ellipse, e, which is defined in terms of two constants, A and B, as follows:

$$e = \left(\frac{B}{A}\right)^{1/2} \tag{9.4}$$

These elliptical constants are also used to define the relative radius R_e:

$$R_e = \frac{1}{2}(AB)^{-1/2} \tag{9.5}$$

All parameters of equations 9.2 independent of deformation can be rewritten as the non-linear stiffness parameter k_n; this form resembles Hook's well-known law:

$$F = k_n \cdot x^{3/2} \tag{9.6}$$

This analysis considers only a single point of contact between the groove and the ball (see Fig. 9.1). However, in practise, the rail and carriage in the LBG are connected through two contact points at the top and bottom of each ball, respectively. For the case of an LBG with two rows of balls on either side of the carriage (see Fig. 9.2), the stiffness of each row should therefore be expressed as

$$k_A = \frac{1}{2} \cdot k_n \cdot n_b. \tag{9.7}$$

where k_n is the stiffness of contact between each ball and the groove and n_b is the number of balls in contact in the row. For simplicity, it is assumed that individual rows have identical stiffness behaviour, that is, $k_A = k_B = k_C = k_D$. Each row (A, B, C, D) can then be described by the reaction force F_A which depends on the local reaction x_A, four of these equations then describe the behaviour of LGB as:

$$F_A = k_A \cdot x_A^{3/2}. \tag{9.8}$$

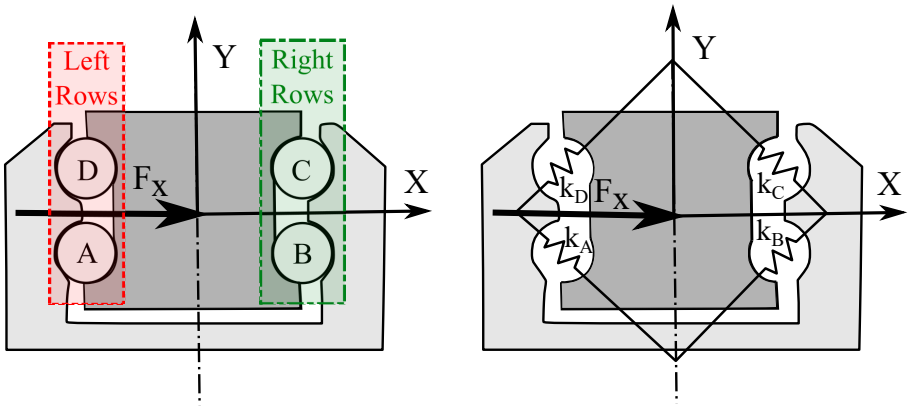

Figure 9.2: Schematic of linear rolling guideway with two rows of balls (left) and replacement of balls by individual row stiffness (right).

Table 9.1: Parameters of the Commercial Linear Ball Guideway

Size	25
The number of balls in each contact row n_b	15
Ball diameter	4.71 mm
Groove radius	2.45 mm
Dynamic load capacity C	36200 N
Preloading force F_{pr}	580 N
Young's modulus E	205 GPa
Poission ratio ν	0.3

9.2 Static Model of Preloaded Linear Guideway

As shown in Fig. 9.2, the individual contacts in the LBG are assumed to form a perfect square. Substituting the parameters given in Table 9.1 for a commercial R1671-212-20 LBG in the equations. (9.1)–(9.7) yields the nonlinear stiffness of row k_A in Fig. 9.2 as 1.51e11, N / $m^{2/3}$. Meanwhile, the preload force, F_p, acting on each row of balls in the LBG can be calculated from the total preload, F_{pr}, declared by the manufacturer as

$$F_p = \frac{\sqrt{2}}{2} \cdot F_{pr} \tag{9.9}$$

The initial contact deformation, x_p, of each ball in row k_A can then be determined as

$$x_p = \left(\frac{F_p}{k_A}\right)^{2/3} \tag{9.10}$$

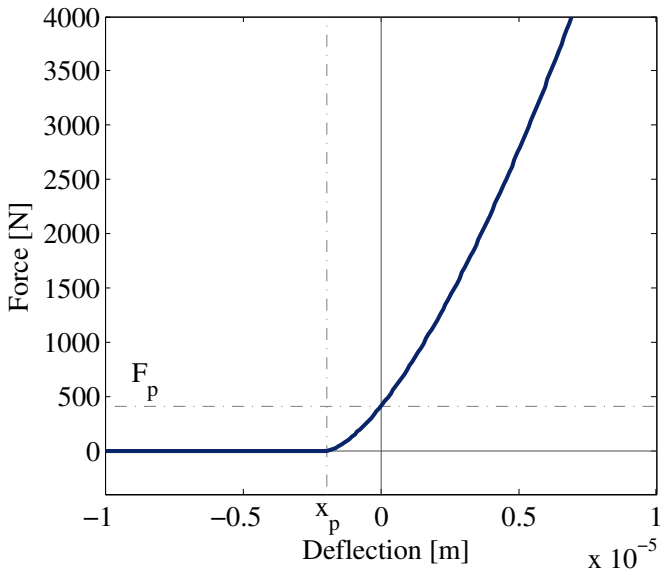

Figure 9.3: Variation of reaction force with contact deflection for single row of preloaded balls in LBG

Substituting the total preload force of 580 N in Table 1 into Eq. 9.9, the preload force acting on row k_A is found to be 410.1 N. The contact deformation, x_p, is then obtained

as 1.95 μm. Figure 9.3 shows the force-deflection characteristic of each row of balls in the considered LBG. A clear nonlinearity in the stiffness is observed, where the border between the two stiffness regimes corresponds to the value of the preload deformation (x_p). At deflection values lower than x_p, contact between the balls and grooves is lost, and hence the load is not transferred between them.

9.3 Single Direction Loading Model

The nonlinear behaviour of LBGs is usually evaluated for the case of single-direction loading [55]. Such an approach has the advantage of simplicity and enables the loading characteristics provided by the manufacturer to be employed directly. However, the model is unable to reflect the typical loading conditions encountered in real-world machining operations, in which the guideway is subjected to a combination of directional loads and torques.

The static model described in Section9.2 considers the case where the guideway is subject to combined two-directional loading and torque. For the case of single-directional loading, the model can be simplified as follows:

$$F(x) = \begin{cases} k_A \cdot ((x_0 + x)^{3/2} - (x_0 - x)^{3/2}) & \mid x \mid \leq x_0 \\ k_A \cdot (x_0 + x)^{3/2} & x > x_0 \\ -k_A \cdot (x - x_0)^{3/2} & x < -x_0. \end{cases} \tag{9.11}$$

The LBG has geometric symmetry, and therefore the nonlinear stiffness can be arbitrarily represented by k_A. Furthermore, x_0 is the initial deflection of the guideway in the x-axis direction under the effects of the preload force and x is the deflection of the guideway in the x-axis direction during the subsequent machining process. The preload force, F_{pr}, can be defined as

$$F_{pr} = k_A \cdot x_0^{3/2}. \tag{9.12}$$

The preload effect is lost when the deflection is equal to twice the value of that produced under the initial preload force. The lost preload force, F_l, the loading force at which the preload effect is lost, can then be defined simply as

$$F_l = F_{pr} \frac{(2x_0)^{3/2}}{x_0^{3/2}} = F_{pr} \cdot 2^{3/2} \tag{9.13}$$

Figure 9.4 shows that the relationship between LGB's deflection and loading force, the preload area, and the area with loss of contact is not very distinguishable. It does not seem that this nonlinearity has a crucial role; however, it does. Figure 9.5 shows that the total stiffness of the system is reduced by around 20% when the loading force reaches the point where the preload effect is lost. Furthermore, a distinct difference in the stiffness behaviours of the different rows of balls is observed. In particular, the stiffness of rows A and D is reduced, whereas that of rows B and C increases. As shown in Table 9.1, the R1671-212-20 guideway considered has a preload force, F_p, of 580 N. The preload lost force is thus calculated from Eq. (9.13) to be 1641 N, as shown in Fig. 9.5.

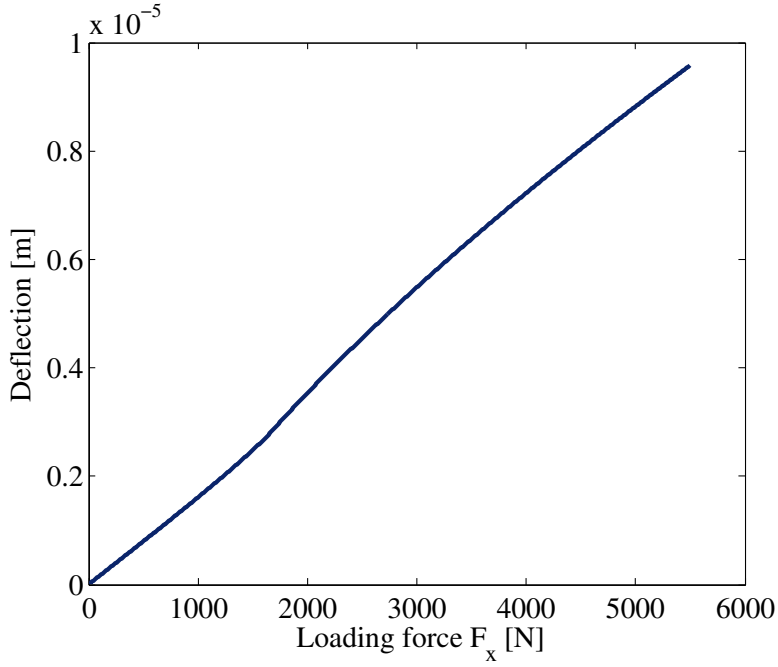

Figure 9.4: Total deflection of the system under directional load

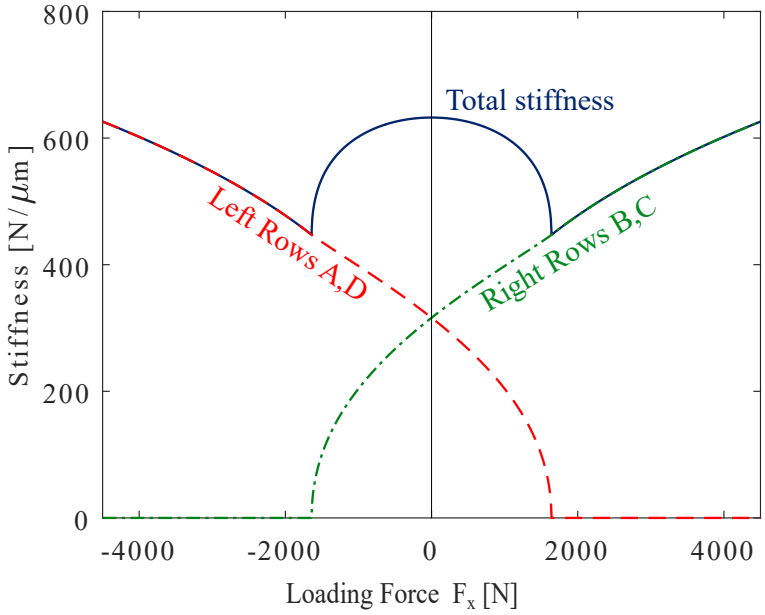

Figure 9.5: Dependence of stiffness on the overall load and the course of stiffness in individual LBG rows

10

Nonlinear Analysis Based on Simplify Static Model

Figure 10.1 shows the machine tool slide structure considered in the present study consisting of a central rectangular beam and two wide LBGs (see Table 9.1) for the related parameters). To facilitate the analysis, the structure is simplified to a single axis in order to reduce the number of unknown parameters and highlight the behaviour of the LBG. In particular, the analysis considers the central beam to have a fixed position in the z-axis direction (i.e., the servo brake is activated).

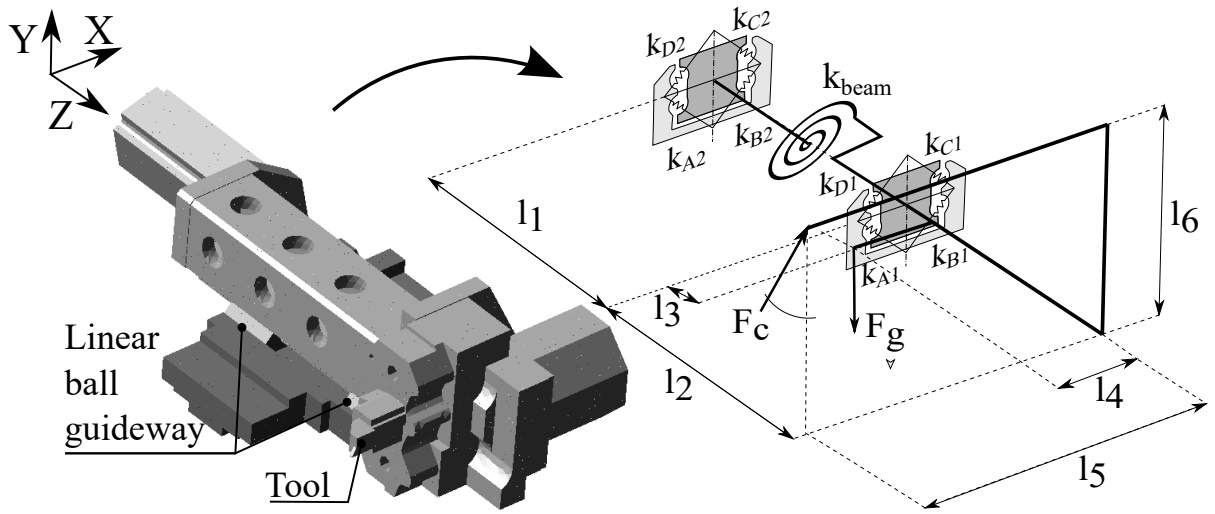

Figure 10.1: Experimental structure and simplified scheme for static analysis

10.1 Structure Under Static Cutting Load

In developing the simplified static solution for the considered problem, it is first necessary to define the boundary conditions and external loads. For simplicity, the radial reaction in the ball screw mechanism of the guideway and the deflection of the guideway in the z-axis direction are both ignored. Furthermore, all of the guideway components (with the exception of the central beam) are assumed to be perfectly rigid. Two loading forces are considered, namely the weight, F_g, and the cutting force, F_c

According to the static scheme shown in Fig. 10.1, the force reactions in each LBG can be described by Eqs. (10.1)-(10.5), while the torque reaction between the two LBGs is given by Eq. (10.6). These equations define the load of both LBGs, using the model in Fig.9.2, the force reactions LBG's rows are numerically solved. Note that the model

parameters for the static analysis are listed in Table 10.1.

$$F_x: \quad F_{k1x} + F_{k2x} = F_c \cdot sin(\beta) \tag{10.1}$$

$$F_y: \quad F_{k1y} + F_{k2y} = F_c \cdot cos(\beta) - F_g \tag{10.2}$$

$$M_x: \quad -F_{k1x} \cdot l_1 = F_c \cdot sin(\beta) \cdot l_2 \tag{10.3}$$

$$M_y: \quad F_{k1y} \cdot l_1 = F_c \cdot cos(\beta) \cdot l_2 - F_g \cdot l_3 \tag{10.4}$$

$$M_z: T_{k1z} + T_{k2z} = F_c \cdot sin(\beta) \cdot l_6 - F_c \cdot cos(\beta) \cdot l_5 + F_g \cdot l_4 \tag{10.5}$$

$$T_{k1z} = (\varphi_{k1z} - \varphi_{k2z}) \cdot k_{beam} \tag{10.6}$$

Table 10.1: Parameters of simplified static model

Dimensions	l_1	$228\,mm$
	l_2	$230\,mm$
	l_3	$20\,mm$
	l_4	$38\,mm$
	l_5	$293\,mm$
	l_6	$161\,mm$
Cutting angle	β	$30\,deg$
Torsional stiffness	k_{beam}	$2.2e9\,Nm/rad$
Weight	F_g	$804.4\,N$
Cutting force	F_c	$0 - 2000\,N$

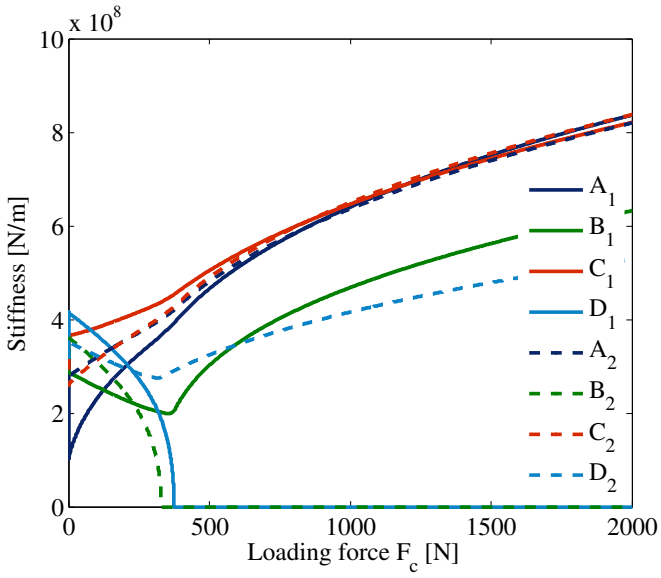

Figure 10.2: Linearised stiffness of all rows in the structure under gravity and cutting load

The results obtained for each eight ball grove contact reaction (A_1-D_2) are then transformed into a linearised stiffness model. Figure 10.2 shows the linearised stiffness results

obtained for each row of balls as a function of the cutting force, F_c. The front LBG contacts have suffixes 1 and the rear 2. Note that under a force of $F_c = 0$ N, the structure is loaded only by the weight, F_g. For the rows subject to a tensile load (D_1, B_2), the stiffness reduces as the cutting force increases due to the loss of contact between the balls and grooves. On the contrary, for rows under compressive stress (A_1, B_1, C_1, A_2, C_2, D_2), the contact area between the balls and grooves increases, and hence the stiffness also increases. The minimal stiffness of the system coincides with the point at which contact is lost between the balls and grooves, i.e., $F_c = 380$ N.

10.2 Modal Analysis and Frequency Response

Having defined the boundary conditions and external loads, the model for modal analysis then assumes all the structural components to be flexible and replaces the ball rows with linear springs. Note that the spring stiffness parameters are taken as the linearised stiffness parameters (A_1-D_2) obtained from the previous nonlinear static model. A modal analysis is then performed to determine the linearised natural frequencies of the experimental structure (see Fig. 10.1).

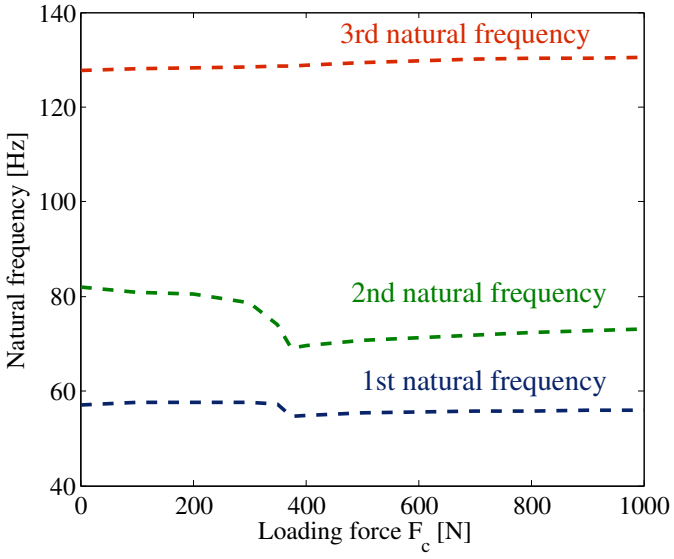

Figure 10.3: Dependence of first free natural frequencies on cutting force F_c

Finally, the modal shapes are determined under different static loads. Figure 10.4 shows the variation of the first three natural frequencies of the experimental structure with the cutting force, F_c. The results show that the second mode experiences a high frequency drop of around 10 Hz under a load of 350 N. The first mode also exhibits a frequency drop at around the same value of the loading force. However, in this case, the frequency drop is relatively small ($\sim$ 2 Hz). The frequency of the third mode, by contrast, shows no obvious drop and increases progressively by around 2 Hz as the cutting force increases. Overall, the results suggest that the chatter stability of the guideway is dominated by the second natural frequency of the guideway structure.

Figure 10.4 shows the first three modes of the linearised guideway structures under the effects of the gravity load and the combined gravity and cutting load, respectively. The first and third modes show no obvious change in shape under the effects of the cutting

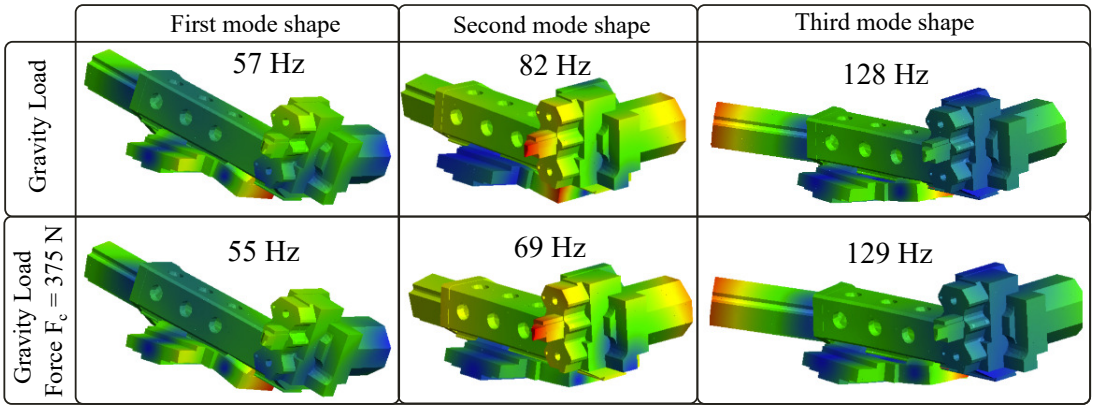

Figure 10.4: Comparison of first three mode shapes of guideway structure under gravity load only (upper) and combined gravity load and static load of F_c 0 and 375N (lower)

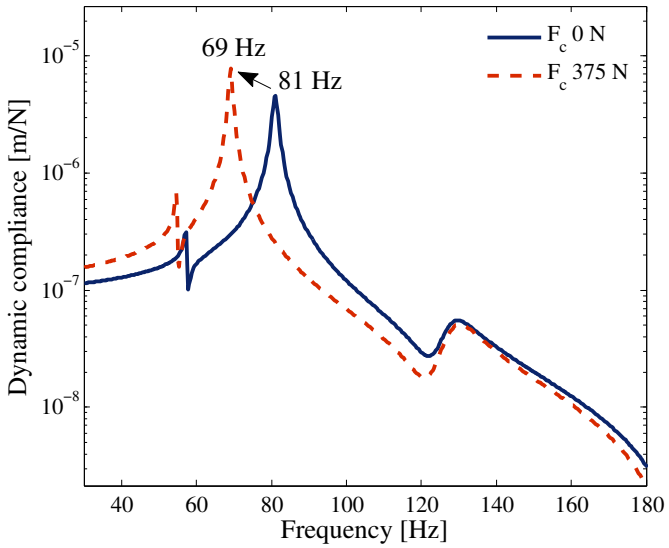

Figure 10.5: Dynamic compliance of tool tip under gravity force and combined gravity force and cutting load

load, although a slight change in frequency is observed. However, the second mode shows a more significant change in shape as a result of the loss of contact between the balls and grooves, and hence a greater reduction in the frequency occurs.

In performing the harmonic analysis, a unit force was applied to the tool tip of the experimental structure in the x-direction and the corresponding tool deflection was evaluated. Figure 10.5 shows the results obtained for the dynamic compliance of the tool tip in the x-axis direction given a gravity loading force only and a combined gravity force and the cutting force of Fc = 375 N, respectively. The results show that the natural frequency reduces, while the amplitude increases, under the effects of the cutting force.

11

Nonlinear Analysis Using Substructuring Approach

The analysis in Section 10.1 ignores the flexibility of the guideway structure components on the contact stiffness. To obtain a more accurate prediction of the stiffness behaviour of the guideway, it is necessary to integrate an FEM model with the nonlinear model of the LBG. However, most FEM packages support nonlinear elements only without preload, and hence it is impossible to apply such models directly to the considered problem, in which the LBG is subject to a preload force before the machining process commences.

Accordingly, in the second model proposed in this study, the guideway system is divided into a linear part and a nonlinear part, respectively. For the linear part, modal reduction is applied, which reduces the number of modes of the linear structure, whilst preserving the static behaviour of the defined contact nodes. Meanwhile, in the nonlinear part, is represented by eight nonlinear equations for each contact row (see Eq 9.8). The nonlinear and linear are then joined in the Simulink environment using force - deflection relations in contact nodes.

The base of this nonlinear analysis is to substitute the mesh with linear behaviour by reducing the transfer function which interacts with nonlinear connections. The analysis is done in MSC Adams and MATLAB Simulink. The combination of these tools enables a width range of analysis based on time-domain simulations.

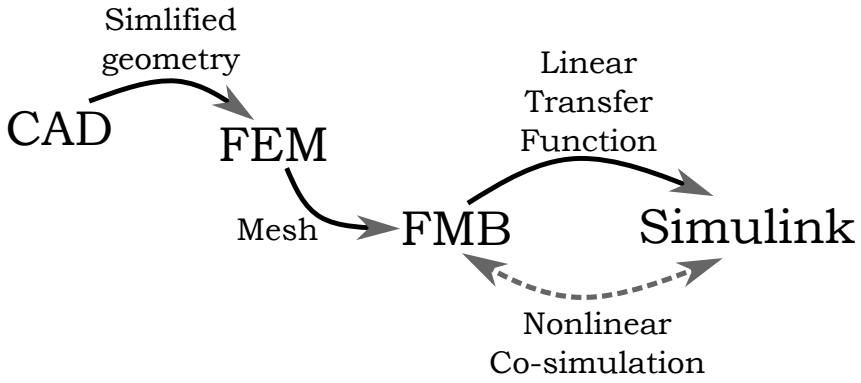

Figure 11.1: Scheme of Multi-body based nonlinear analysis

The base of this nonlinear analysis is to substitute the mesh with linear behaviour by reducing the transfer function, which interacts with nonlinear connections. The analysis is done in MSC Adams and MATLAB Simulink. The combination of these tools enables a wide range of analysis based on time-domain simulations.

The first step is to the simplified CAD model and the creation of reducing the modal structure of all linear parts of the structure at the same time is necessary to define the connection points on the mesh, which will be future inputs and outputs, in this case, force and deflection outputs, which will represent nonlinear connections and force input.

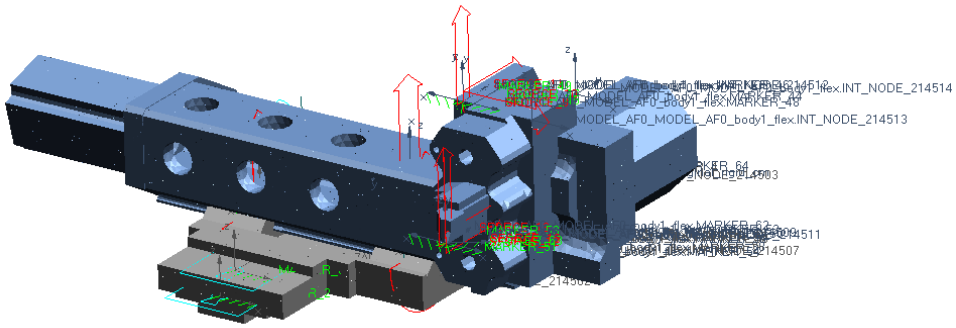

Figure 11.2: Adams model with boundary conditions and defined input and output connections

A modal neutral file is used to import the reduced modal body into MSC Adams, a modal neutral file is used, which defines the body, the topology of the mesh, stiffness, mass, the moment of inertia of elements, and defines the connection points.

This file can then be opened in MSC Adams, where the connections between bodies and the surrounding space can be extended and defined as input and output. In the case of a linear structure, it is easy to add connections between bodies. Although MSC Adams and most FEM tools enable nonlinear spring connection definition, it also has limitations and is ineffective in linear ball bearing cases. Figure 11.2 shows the flexible model with defined force inputs and observed reaction points.

The possible way is to transfer this model to MATLAB Simulink, where the nonlinear connections could be easily represented. Simulink also enables the simulation of regenerative chatter during the cutting process. To transfer the model into Simulink, there are two possibilities of exporting from Adams a linear state-space representation of the model or exporting a nonlinear model, which works as a bridge between Adams and Simulink; however, it requires the cooperation of both programmes at the same time. During the model exporting, algebraic loops should be considered, which could happen due to the direct flow of the feedback loop into the state-space model. It is advantageous to use variables of higher order of derivation, velocity, or acceleration, rather than position, to avoid this problem. If we consider that a linear behaviour can represent our model's main structure, it is better to export a linear state-space model and simulate it simulated without MSC Adams. This set of transfer functions usually has high-frequency compounds that interact with the numeric solver, leading to many problems, for instance, numeric instability or the requirement of minimal computational step size. The reduction of the model could be applied to suppress the high-frequency modes of the system to avoid these problems. Reduced values also increase the computation speed. Due to the modal reduction in previous steps, these responses are not valid and accurate; secondly, they are irrelevant for cutting stability or nonlinear connection analysis. In Simulink, the reduced state-space model can be easily connected to the model of a linear ball guideway. This model could be used to simulate forced vibration, hammer impact, or stability during machining.

11.1 Reaction in LBG Analysed by Multibody Static Load Reaction Analysis

The key advantage of this cosimulation model is that it enables the substitution of different types of analysis using the same model. Static load analysis represents a two-step load, where the first represents the gravity load and the second the cutting force. Due to the dynamic character of the model, it is necessary to simulate the model until the steady condition.

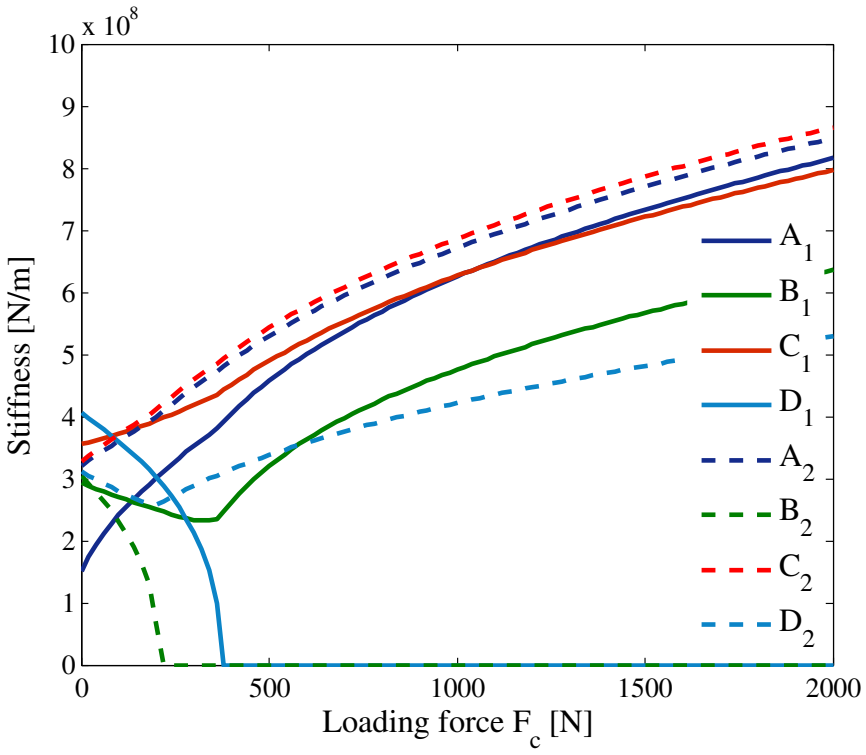

Figure 11.3: Variation of stiffness with loading force for individual ball rows in LBG structure.

The static load simulated follows the trends from the previous analysis with minor differences. Fig. 11.3 shows how the rows depend on the force of the knife's load during the grooving operation. The difference between this analysis and the results of the previous model is a significant change in the decrease in the stiffness of B_2. The leading cause is the flexibility of the structure under the front bound (A_1-D_1) that limits the torque loading capacity. Due to this behaviour, the rear contact has a higher reaction force and a decrease in stiffness.

The analysis of stiffness behaviour in contact is essential for future dynamic research. The stiffness values could be used in the modal analysis to estimate linearised mode shapes. However, the most important role is to identify regions with a significant change of behaviour. In the presented case, the area is 200 – 500 N, where a slight change in the loading force significantly changes the dynamic behaviour of the system.

11.2 Frequency Responses and Impact Simulation

As shown in Fig. 11.4, the first two frequency modes of the guideway, both show a two-step drop in frequency as the loading force increases as a result of the compliance of the structure below LBG. Compared to results of the simplified static analysis 4.1 the minimum frequency drop moves to the higher frequency to 73 Hz this is caused by that the minimal stiffness of both LBG do not meet in the same load. The third frequency mode changes to the higher frequency – 160 Hz; however, it does not have a significant trend in load dependency; therefore, Fig. 11.4 shows only the first two modes, which differ from Figure 10.3. It is noted that the minimum frequency occurs at the same load as in the simplified system (350 N).

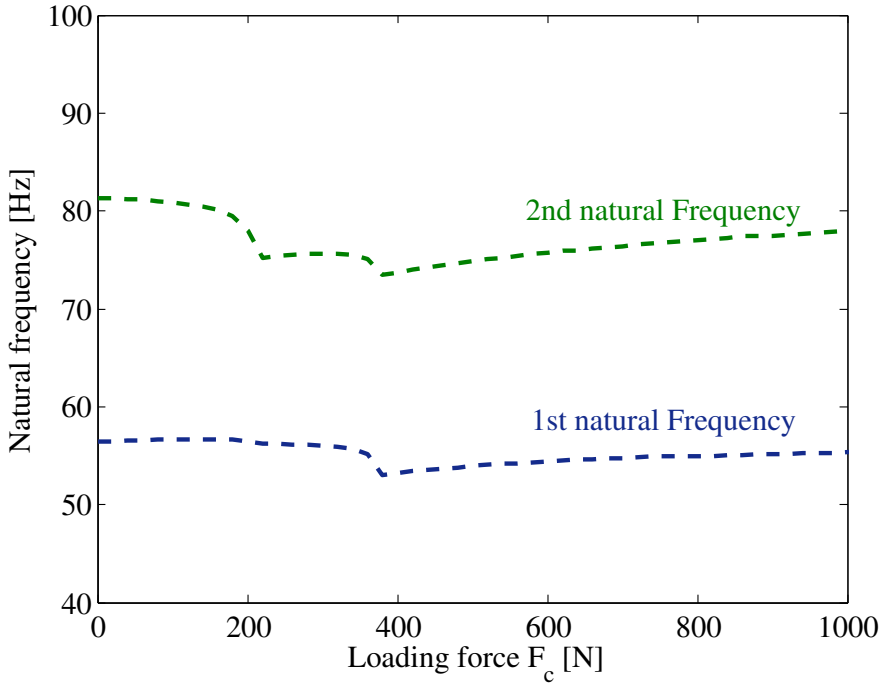

Figure 11.4: Dependence of first two natural frequencies of guideway on cutting force F_c.

Even a simplified solution can define the most problematic load in this case. However, the main benefits of the cosimulation model are the more reliable prediction of dynamic compliance. The substructuring results of dynamic compliance are presented in Fig. 11.5. The compliance for zero cutting load differs from the simplified model (see Fig. 10.5) mainly by the third mode position. Significant changes are for loads of 240 N and 380 N; the compliance of the first mode increases dramatically and becomes more significant for the behaviour. Unlike in the simplified model, the second mode decreases its compliance. Above 380 N load, the trends change, and the first mode decreases and the second mode increases. Since static substructuring analysis considers the guideway structure to provide a more reliable load distribution, it will be used for the following prediction of chatter. However, the simplified model provides only a rough estimation; it identifies the most problematic load and the main trend.

Even a simplified solution can define the most problematic load in this case. However, the main benefits of the cosimulation model are the more reliable prediction of dynamic compliance. The results of dynamic substructuring are presented in Fig. 11.5.

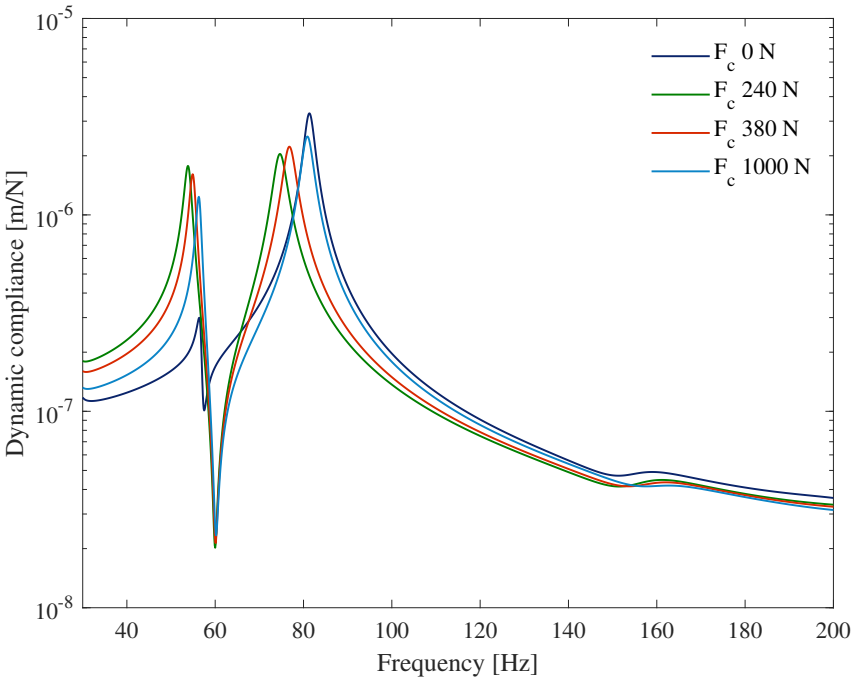

Figure 11.5: Dynamic compliance of tool tip under gravity force and combined gravity force and three cutting loads F_c.

The compliance for zero cutting load differs from the simplified model (see Fig. 10.5) mainly by the third mode position. Significant changes are for loads of 240 N and 380 N; the compliance of the first mode increases dramatically and becomes more significant for the behaviour. Unlike the simplified model, the second mode decreases its compliance. Above the load of 380 N, the trends change and the first mode decreases and the second mode increases. Since static substructuring analysis considers the guideway structure to provide a more reliable load distribution, it will be used for the following prediction of the chatter. However, the simplified model provides only a rough estimation; it identifies the most problematic load and the main trend.

Due to the nonlinear nature of the system, the response of the system is crucially dependent on the nature of the excitation. Fig.11.6 shows three different reactions to harmonic unit force excitation, red and green with different frequency change rates and blue with different directions of frequency change. Both the maximal amplitudes and their frequency position differ.

The key method for dynamic structure response analysis is modal hammer measurement. The cosimulation model enables time-domain analysis, so it is possible to use the signal from the measurement, apply it in the same place on the simulated structure and analyse the response. This applied pulse simulated the 125 g hammer impulse. Figure 11.7 compares the simulated modal hammer with linearised at the same point and linearised at the tool edge. The linearised and simulated signals are identical; different positions of the simulated measurement point cause the difference between the measurement point and a knife tip. The reason for another location is purely practical to enable comparison with real measurements.

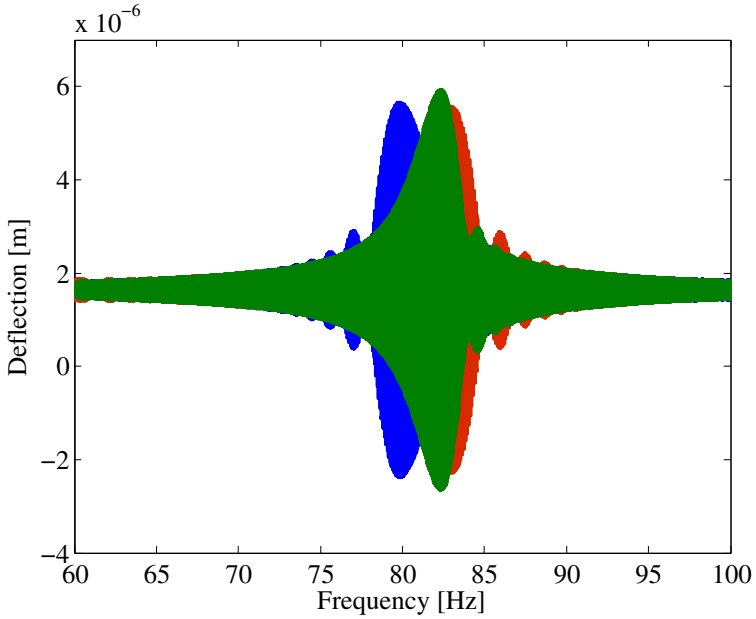

Figure 11.6: Dependence of the system response on different directions and speeds of harmonic excitation

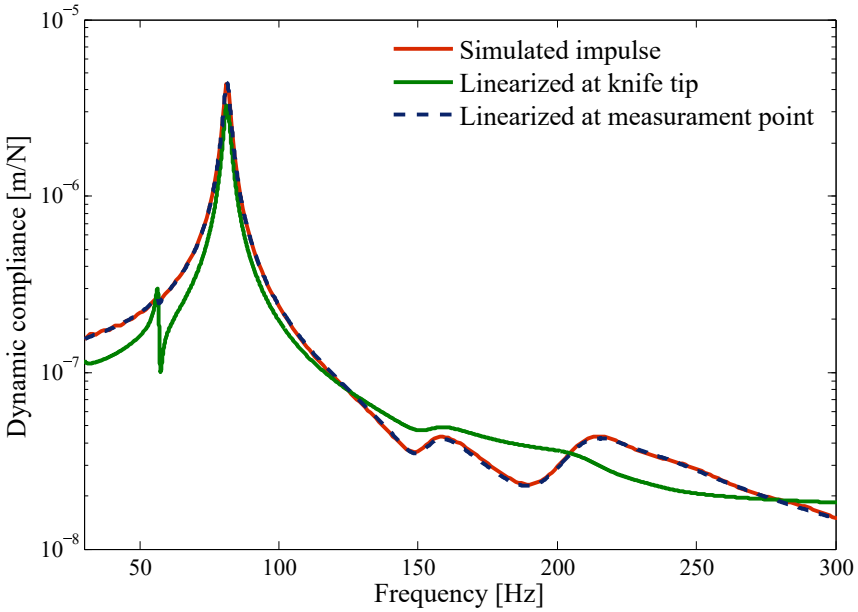

Figure 11.7: Comparison of simulated modal hammer impulse response with linearised dynamic response at the measurement point and with linearisation at the knife tip

12

Chatter Stability and Frequency Estimation Application of SLOP Algorithm

As mentioned above, chatter stability is an essential property of machine tools. However, it is difficult to predict the chatter behaviour of structures with nonlinear joint stiffness since the dynamic compliance of the overall system is load dependent. To solve this problem, the SLOP algorithm was proposed. Using the SLOP algorithm, it is possible to estimate the bode stability diagram for a nonlinear system. The following chapter presents an application of the SLOP algorithm to the cosimulation static model and estimates the response of the chatter frequency. This step enables future experimental validation.

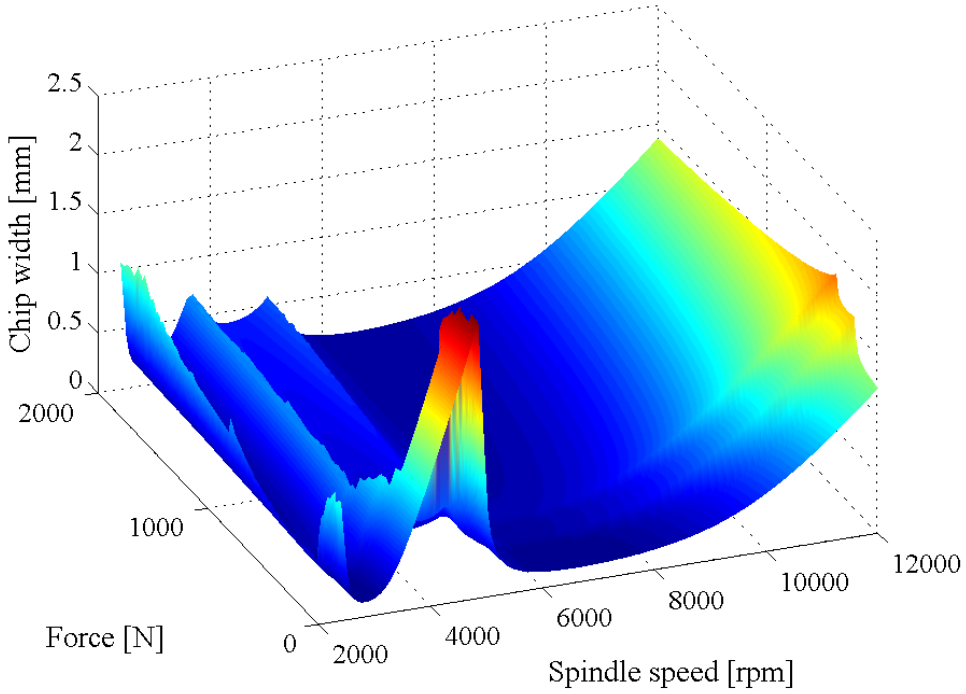

Figure 12.1: Estimated linearised chatter stability lobe diagram of LBG structure as function of static load.

Linearised systems are applied to equations 4.1-4.3; the solution of these equations gives the stability limits for the LBG under different cutting loads (see Fig. 12.1). In other words, for each static load that acts on the tool, there exists a particular linearised dynamic characteristic of the system and a unique stability diagram exists for the load of each static system. Figure 12.1 shows a significant discontinuity in stability in the minimum system of $F_c = 375$ N. However, a more minor discontinuity is also observed at $F_c = 218$ N, corresponding to the loss of contact at B_2.

The cross sections of the surface in Fig. 12.1 represent the stability lobes for different

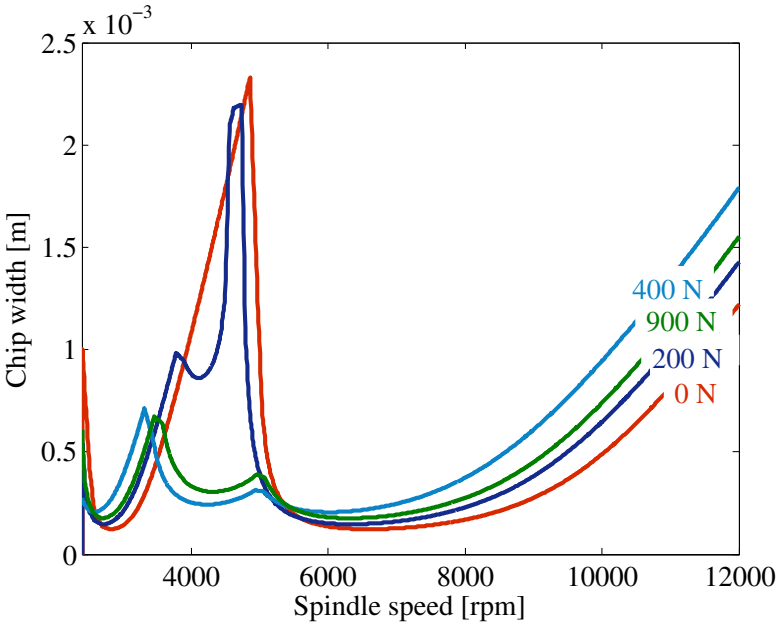

Figure 12.2: Illustrative stability lobe diagrams for structures linearised under different loads.

cutting forces. Figure 12.2 shows four illustrative cross sections corresponding to loads of 0, 200, 400, and 900 N, respectively. Note that the force of 0 N corresponds to the case where the structure is loaded only by gravity and is an important value, since the boundary thus corresponds to that obtained in impulse hammer measurements when the structure is unloaded.

It is noted that in this condition, the stability prediction based on the measurement of the impulse hammer is likely to be highly unreliable for the higher load; with increasing load, the stable area between the two lobes is filled with new instability and the stable area for the unloaded system becomes highly unstable after loading. Paradoxically, the highest criterion of the unconditional stability band has a load in the case of minimum rigidity, and with the lower system compliance the lobe shifts to a lower spindle speed. As the load increases, the area between the two lobes decreases slightly and the lobes move toward higher spindle speeds (as evidenced by the curves for 400 N and 900 N, respectively).

In the lathe machining process, the cutting load depends on the width of the chip, the feed, etc. Therefore, for each loaf variable would be a different stability diagram which could be compiled using linearisation synthesis. The method used to create such a synthesis is described in Chapter 8. The algorithm arranges a stability diagram corresponding to the load. For illustration, stability diagrams were created for feeds of 0.1 and 0.05 mm/rev. However, it is possible to create any feed corresponding to a linearised range. The resulting diagram is then unique for every feed and cutting force.

Figure 12.3 shows an illustrative stability chatter diagram for feeds of 0.1 mm/rev and 0.05 mm/rev, respectively, given a specific cutting force of Ks = 2500 MPa. For a feed of 0.1 mm/rev, the lobe diagram has noticeable regions corresponding to a loss of contact at B_2 and D_1 are observed, resulting in notches in the range of 10000-12000 RPM at loads of 218 N and 375 N. The loss of contact in B_2 also affects the speed range of 3500-5000 RPM causes; with increasing load, the first mode becomes significant and reduces the stable

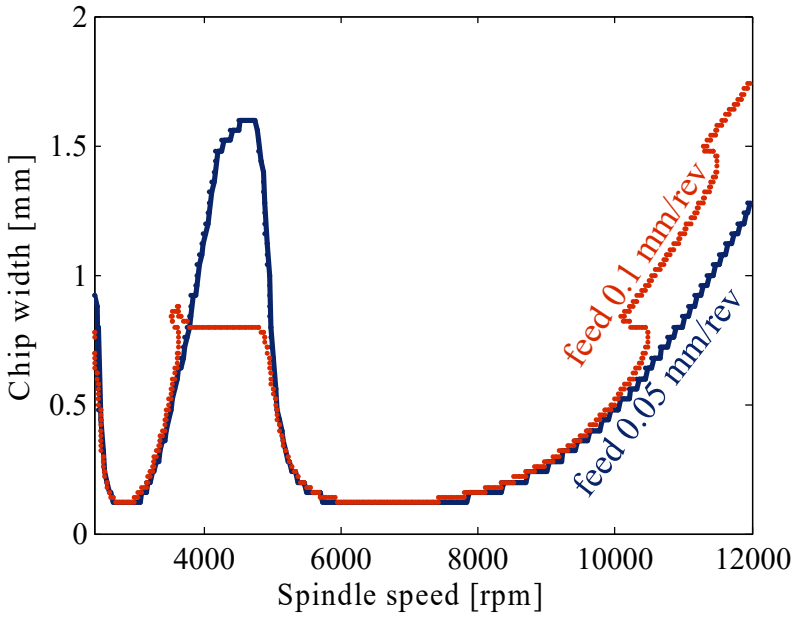

Figure 12.3: Stability chatter diagram compiled by synthesis of linearisation in operating points

area. For a lower feed of 0.05 mm/rev, the system behaves more like a linear system. In particular, the changes in the lobe diagram shape are less significant since due to lower load the more considerable changes shift to a higher chip width. In fact, the only change observed is a slight deformation of the connection of the lobes at 4500 RPM.

The stepped effect in the chatter stability diagram is given by the linearisation interval used for the nonlinear static analysis of the contacts in the bonds. Overall, the results presented in Fig. 12.3 show that the required fineness of linearisation increases with a reducing feed. Thus, when using consistent linearisation, this effect of linearisation intervals is more pronounced in the case of slower feeds. Part of the chatter stability prediction is also the frequency response analysis. Applying the linearised solution to Eq. (4.3) yields the predicted chatter frequency for specific cutting conditions. By monitoring the frequency response, the influence of both structural damping and process damping can be eliminated, thereby allowing the effects of stiffness nonlinearities to be reduced.

13
Experimental Setup

13.1 Comparison of Simulated Impulse with Impulse Hammer Measurements

The cosimulation model enables time-domain simulation. It is thus feasible to simulate the structure response for a particular impact and compare the results with the corresponding experimental observations and linearised solutions. In the present study, the simulation input was taken as the force signals acquired in real-world impulse hammer tests. The hammer impact points and sensor locations used in the experimental and simulation processes are shown in Fig. 13.1.

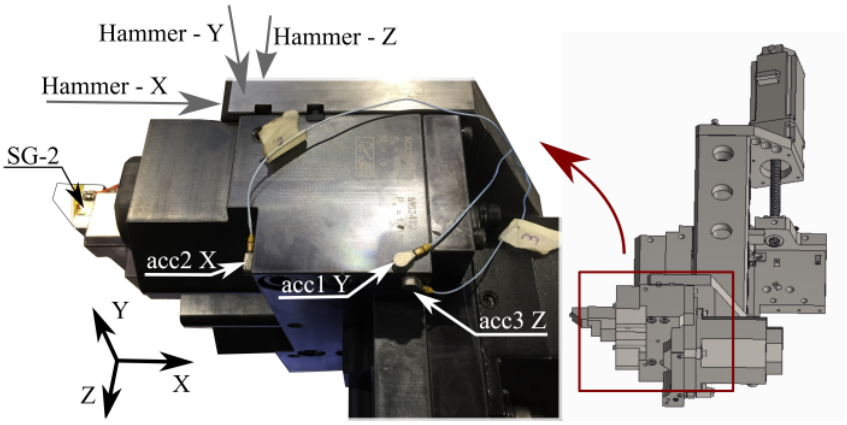

Figure 13.1: Positions of impact points and accelerometers in experimental and simulation processes.

Figure 13.2 shows dynamic compliance at the measurement points; the result of the measurement proves the previous findings, the dominant first two-mode shapes, the first bending mode dominant at the YZ plane on 60 Hz, and the second one rotational dominant in the XZ plane on 81 Hz. This corresponds to the modal analysis results on Fig. 10.4 for the unloaded analysis as well as for the following unloaded analysis. The higher modes have lower amplitudes, so their contribution to chatter vibration stability is a neglectable; however, it also contains information about the structure behaviour. The second significant antiresonance frequency as well as the third natural mode peak drifts to lower frequency in comparison with X and Y signals; this could be a sign of nonlinear behaviour, that the dominant mode changes its frequency according to the force input orientation. The interesting thing is that the X and Y responses follow a similar pattern in contrast to the Z signal.

Figure 13.3 compares the experimental and simulation results for the dynamic compliance of the test structure under the effects of a 160 g impulse. It is observed that the

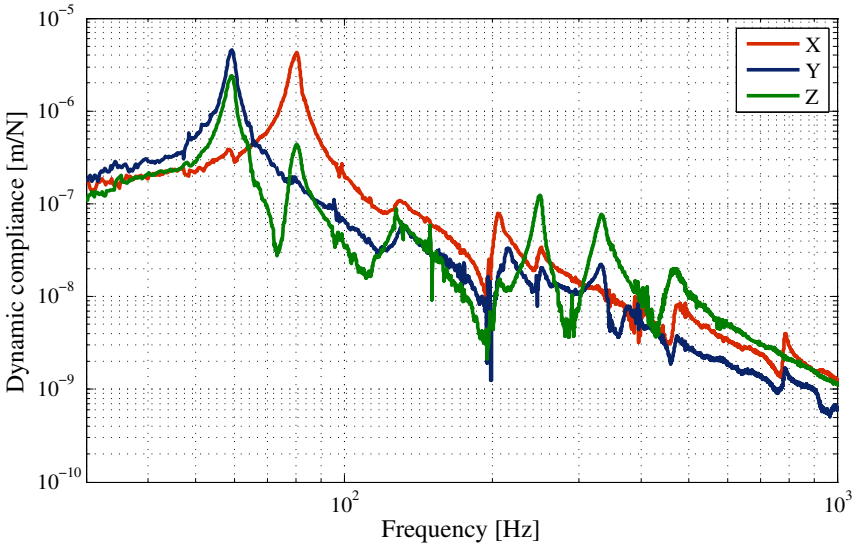

Figure 13.2: Dynamic compliance at measuring points

measurement results correspond to the modelled values. In general, the results show that the second mode has the lowest dynamic stiffness in the x-direction. In addition, the simulation results for the third mode frequency are around 30 Hz higher than the measured data. The higher modes in comparison then approximately correspond in frequency position but differ in peak size.

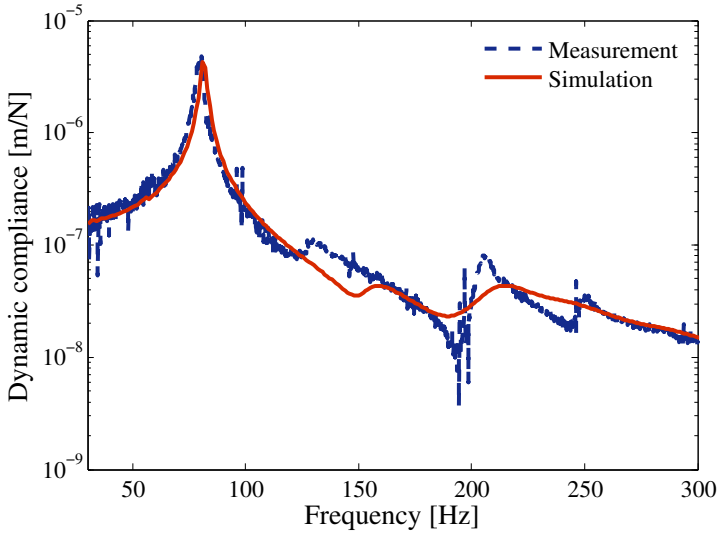

Figure 13.3: Comparison of simulated and measured dynamic compliance of test structure in x-axis direction given impulse force of 160 g

The model assumes a constant damping parameter, and higher frequencies are thus attenuated compared to the experimental results. However, the stability of the considered system depends mainly on the frequency shifts which occur at low frequencies (i.e., the first two modes), and hence discrepancies between the measurement and model are insignificant. In addition, its significance is enhanced by the logarithmic scale of Fig. 13.3.

Figure 13.4 presents a comparison between the measured signal and the simulation of (a) real and (b) imaginary components on the linear scale. The dominance of 80 Hz mode is evident, also, that the role of higher frequency components on chatter frequency are negligible. The negative real part of the measured signals is more disproportional than the simulated one. The imaginary measured part has a lower peak which leads to lower damping. Despite these deviations, this model can be considered an acceptable representation of the system, mainly because the model's goal is not to accurately copy reality, but to capture major trends.

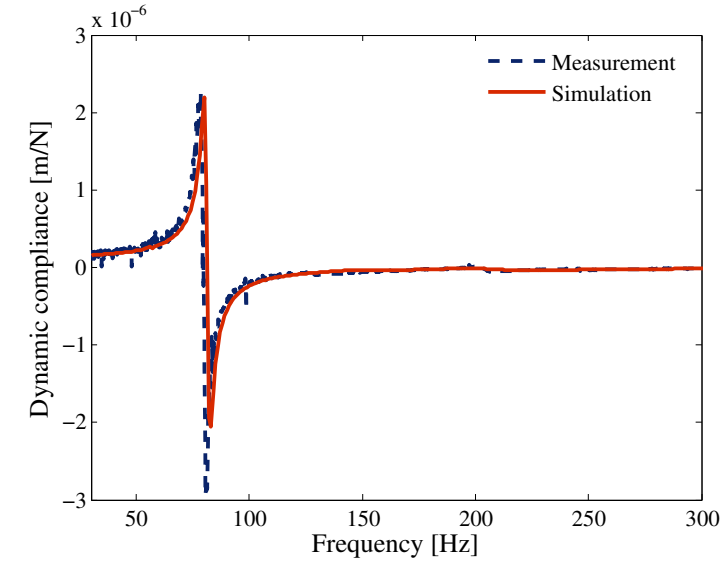

(a) Real component

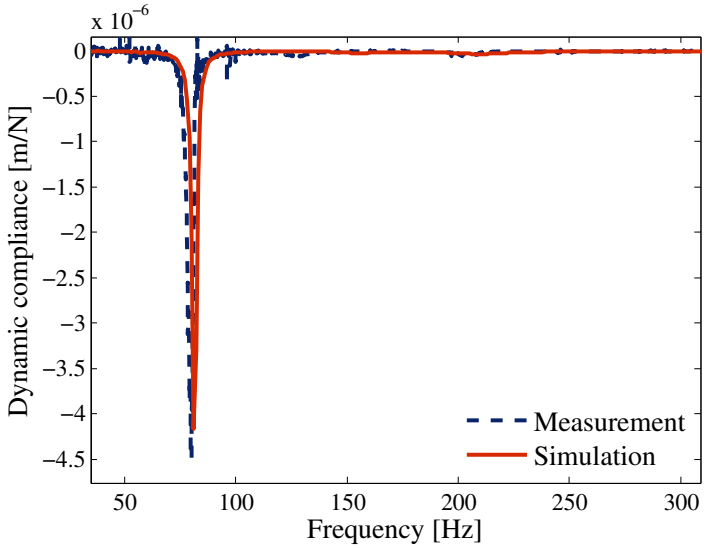

(b) Imaginar component

Figure 13.4: Comparison of simulated and measured dynamic compliance of test structure in x-axis direction given impulse force of 160 g

13.2 Strain Gauge Layout and Force Estimation

The FEM analysis was used to estimate the force and its component in different axes. Based on the strain measured on two stain gauges applied to the tool holder. The reason is that the direction has a mainly non-trivial character of direction with no simple relation between strain and force. Figure 13.5 shows the tool holder with the strain gauges. FEM

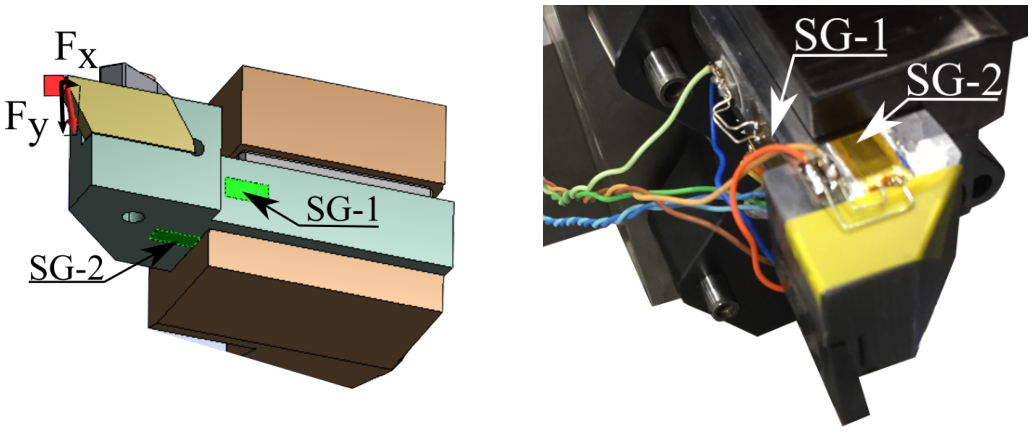

(a) FEM model main layout (b) Applied sensors on the structure

Figure 13.5: Position of the strain gauges on the structure

analysis of the behaviour of the structure was used to choose the place of the strain gauges at the location and reconstruct the force from the measured strain. The main parameter of the FEM analysis was loading the structure by force with different combinations of X and Y compounds, then the strain in the places where the strain gauge is observed. The static analysis for different combinations of input forces in the X and Y directions create detection data in both paces of the model.

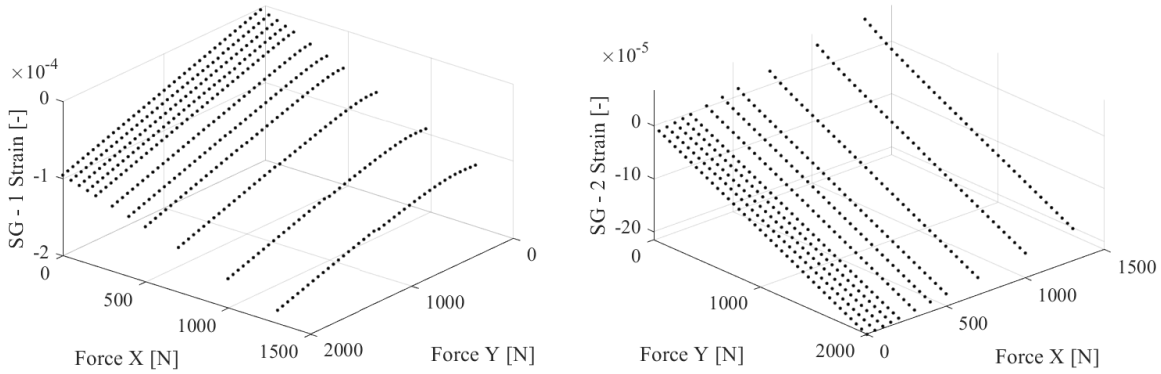

(a) Strain gauge 1 (b) Strain gauge 2

Figure 13.6: Results of FEM analysis of strain dependency on force components

Figure 13.6 shows that the strain gauge 2 deformation characteristic creates a plane, the strain gauge 1 surface is mostly plane too, but it bands for cases where the force in the X direction is higher than in Y. However, this situation would not occur in the grooving process and would mean a cutting disorder. Therefore, these data could be neglected.

Neglecting these system data can be represented by two linear equations:

$$F_x = C_{x1} \cdot \varepsilon_{SG1} + C_{x2} \cdot \varepsilon_{SG2} \tag{13.1}$$

$$F_y = C_{y1} \cdot \varepsilon_{SG1} + C_{y2} \cdot \varepsilon_{SG2}. \tag{13.2}$$

The coefficients of the models are obtained using linear regression (see Table 13.1).

Table 13.1: Parameters of linear regression for force estimation

F_x		F_y	
C_{x1}	C_{x2}	C_{y1}	C_{y2}
-1.125e+07	4.951e+06	-4.797e+06	-7.212e+06
R-square:			
0.9994		0.9999	
RMSE:			
8.653		6.254	

Questionable could be the usage of static dependency for measuring the dynamic process. The assumption is that the dominant frequencies are below 500 Hz; the first natural frequency of the holder is on 3970 Hz, so far higher than these dominant frequencies. Thus, even for the range 0–500 Hz the behaviour of the holder would be quasi-static. According to this assumption, we can compile a function that transforms the measured stress into a force. Linear regression can be used to approximate the dependence because, as we have already mentioned, the relationship between force and deformation is linear in an important area.

13.3 Experimental Machining Trials for Chatter Behaviour Verification

In practise, experimental verification of the chatter behaviour faces several key challenges, including the low stability of the system itself and the fact that there is no stable area between the lobes in the stability diagram at lower speeds, the area practically filled with harmonic lobes without any windows of higher chip width stability.

Due to the dimensions of the tested structure and the requirements for independent movement, the verification trials were performed on a large horizontal milling machine (TOS WHN 13 A), which allowed both the spindle function and table movement to change the chip width and ensure feed in the cut. The milling machine provided several advantages for the verification process, including most notably its large dimensions and sliding guide mounting, which allowed its dynamics to be isolated from those of the tested LBG system. However, the machine offered only a very limited choice of spindle speeds for the cutting process (i.e., 430, 465, 600, and 765 RPM). Consequently, the acquisition of an experimental lobe diagram was almost impossible, and hence the only feasible option for evaluating the chatter behaviour of the guideway was to verify the frequency response under unstable machining conditions.

Figure 13.3 presents a photograph of the experimental setup. As shown, the guideway was mounted on a milling machine table. Strain gauges were attached to the tool holder

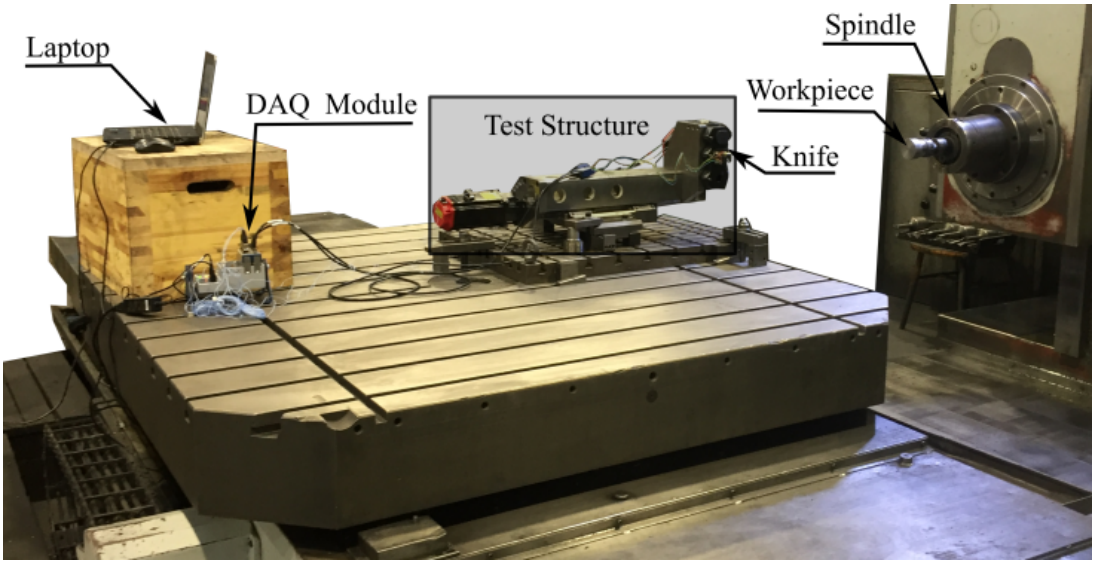

Figure 13.7: Photograph of experimental setup used to verify chatter behaviour of LBG.

to reconstruct the force load, and accelerometers were applied to the body of the system to measure vibration in different directions during the machining (Fig. 13.1). The signals generated by the strain gauges and accelerometers were collected by a DAQ module and interfaced to a PC for subsequent processing. The workpiece was a steel cylinder (C45) with a diameter of 70 mm, it was mounted on the spindle of the horizontal milling machine. In the machining trials, grooves were cut into the end face of the workpiece with a grooving width in the range of 1 to 4.5 mm with increments of 0.5 mm (see Fig. 13.8). As the width was increased, the depth was gradually reduced from 3 mm to 1.4 mm in

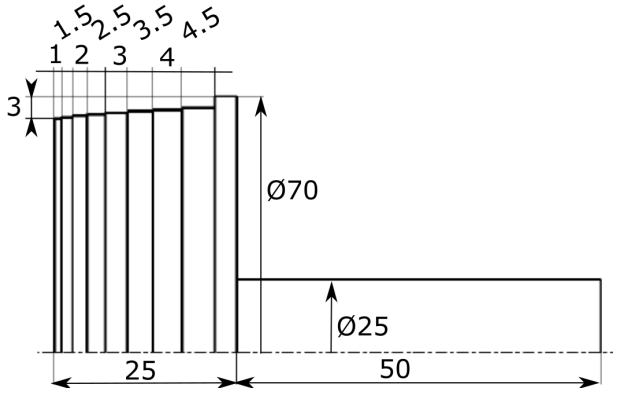

Figure 13.8: Scheme of the workpiece after the machining test with stepped grooves

steps of 0.2 mm. For each machining condition (i.e., groove width and depth), two trials were performed in order to ensure the reliability of the measurement results. The signals acquired from the strain gauges and accelerometers were used to construct a corresponding power spectral density (PSD) diagram from which the frequency response of the system was then determined.

14
Results and Discussion

The example of two measurement power spectral density PSD Fig. 14.1a and 14.1b show the spectrum of each channel. The difference is obvious the 1 mm chip data have more significant frequency peaks in accelerometer data and the first mode peak on 60 Hz in the Y and Z data and 80 Hz of the second mode responsible for the chatter vibration; This is

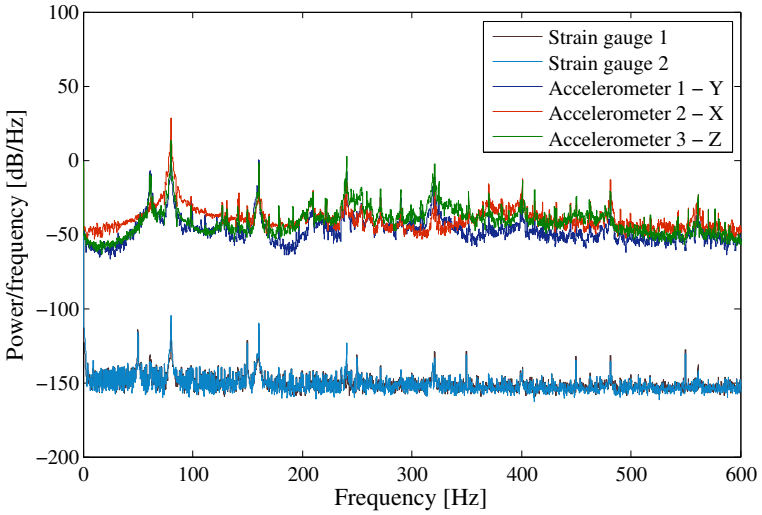

(a) Chip width 1 mm

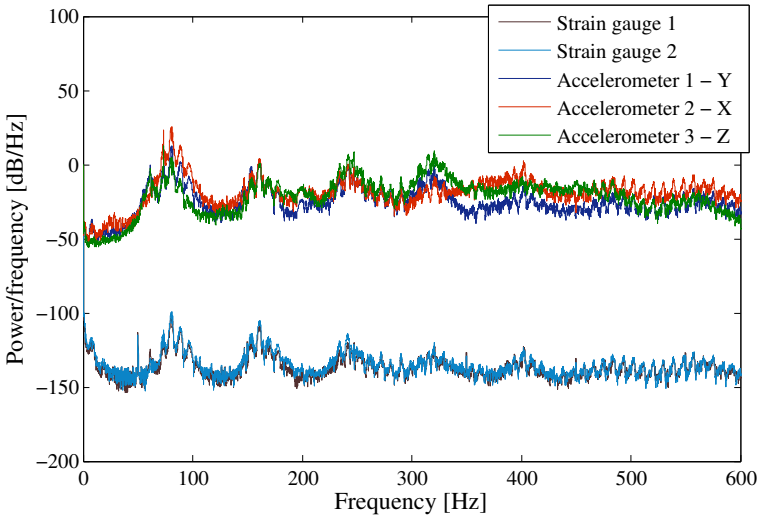

(b) Chip width 4.5 mm

Figure 14.1: Power spectral density of all measured channels for spindle speed 430 rpm

also noticeable from the deflection data, where this peak is noticeable. In contrast, during the 4.5 mm chip width machining, the main peaks are compounds of several subpeaks

that are most noticeable in chatter frequency where the dominant 80 Hz frequency is replaced by four dominant frequencies 73, 80, 89, and 96 Hz – which are also projected through their harmonics to higher frequency spectra.

It must be considered that the signals of all measurements are processed; the important pieces of information are mainly in the frequency spectrum. The accelerometer signals are stronger than the deflection signal; this is caused by the low values of deflection on the workpiece. However, after transforming the deflection signal into force, the force data will have a higher value. All data have a significant amount of frequency noise; this is an effect of the production facility where the experiment takes place; the nose is caused by other machine tools, crane and another production rush. In the deflection data there is a noticeable 50 Hz frequency noise peak caused by the electric voltage frequency.

PSD maps in Figs. 14.2 (a) (d) show the dependence of the response frequency of the experimental structure in the x-axis direction on the width of the chip at spindle speeds of 430, 465, 600, and 765 RPM, respectively. The most significant spectral changes are observed at a spindle speed of 765 RPM, for which a frequency component of 74 Hz, which is not predicted by linear theory, is detected at machining depths greater than 4 mm. (A similar phenomenon also occurred at the other spindle speeds; however, the signal strength was much weaker and thus is not easily seen in the corresponding PSDs. For spindle speeds of 430 RPM and 465 RPM, the PSD changes in the area above 3 mm, multiple new spectra occur, and the original peaks are expanding. The least noticeable is the spectral change in PSD at 600 RPM where these changes in PSD are the weakest and when there are small changes for data above 4 mm. These changes can also be observed at higher harmonic frequencies.

The spectral changes observed in the PSDs can be attributed most feasibly to the nonlinearity of the system. The nonlinear model presented in Section 4.2 accurately depicts the behaviour of the system and the aforementioned spectra, whereas a simple linear approach cannot. Figures 14.3 (a) and (b) compare the chatter frequencies predicted by the nonlinear model and a linear model for chip widths of 1 mm and 4.5 mm, respectively. It will be recalled that the linear model does not consider the change in system stiffness caused by the load and represents the results obtained in impulse hammer measurements. For reference purposes, the estimated spectra are compared with the experimental data acquired by the strain gauges, which more accurately describe the self-excited frequency responses and eliminate the surrounding influences of random excitation. The size of the plotted points corresponds to the signal strength of the corresponding PSD and hence provides an indication of the measured instability. In other words, the points indicate the most dominant chatter frequencies.

It should be noted that the results correspond to unstable cutting conditions. Although the chatter has an impulse character, during its initialisation, the static component of the cutting force is dominant, and the force oscillates around the value of the static force. Therefore, the static force component is expected to load the LBGs, resulting in initialising the corresponding chatter frequency. Consequently, the linearised estimates for frequency prediction are not as accurate as those for the machining process performed at the edge of stability, since, during unstable cutting, the tool passes through many different stiffness states.

Nevertheless, despite this limitation, the estimates obtained using the cosimulation model are in good qualitative agreement with the measurements results for the self-excited vibrations. In most cases, the estimates deviate from the measured frequencies by no more than 2 Hz. However, more significant deviations are observed for the largest chip width of 4.5 mm and lower spindle speeds (430 465 RPM). For example, an estimation error of

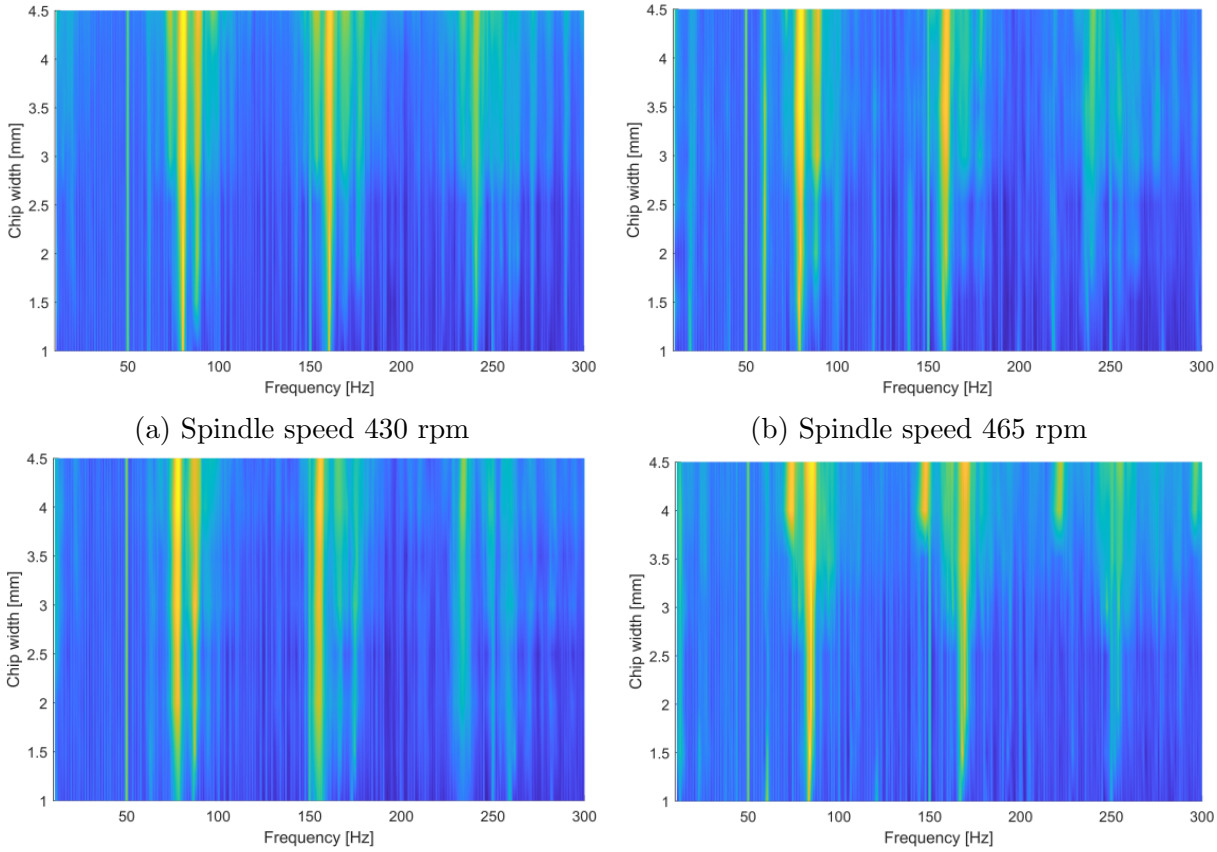

(a) Spindle speed 430 rpm

(b) Spindle speed 465 rpm

(c) Spindle speed 600 rpm

(d) Spindle speed 765 rpm

Figure 14.2: Experimental results obtained for frequency response of experimental structure in x-axis direction given different chip widths and spindle speeds (430, 465, 600, and 765 rpm).

5 Hz occurs at 465 RPM, while an error of 3 Hz occurs at 430 RPM. In particular, these findings confirm the nonlinear behaviour of the system, since, according to linear theory and impulse hammer measurements, no vibration should occur in the spectrum band of 70 80 Hz.

Overall, the results confirm that the nonlinearity of the LBG structure must be taken into account, especially when the external load causes preload loss. Furthermore, the measurements obtained by a modal hammer for such structures provide only limited information about the structure response. In future work, the linearisation method applied in the present study for stability estimation will be integrated with a process damping model to better describe the system response in the low-speed region. Furthermore, the estimation performance will be enhanced by applying the stochastic approach to the dispersion of the specific cutting force and the definition of the probability band of the stability lobe diagram.

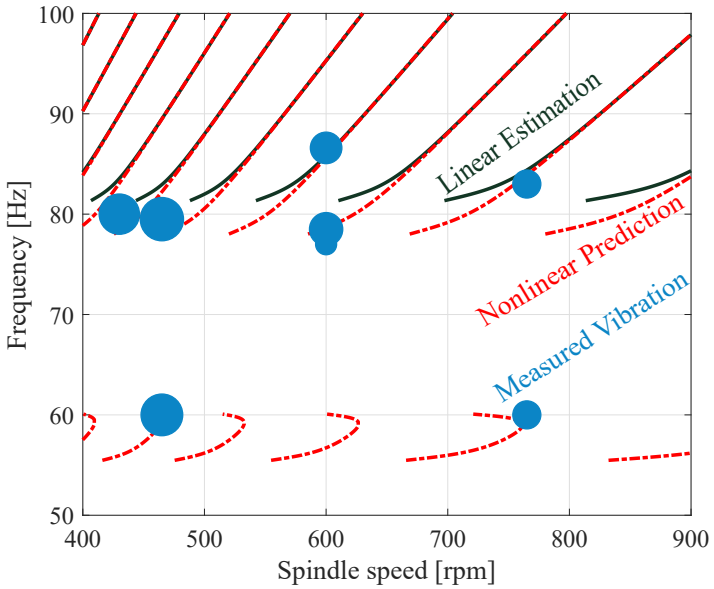

(a) Chip width 1 mm

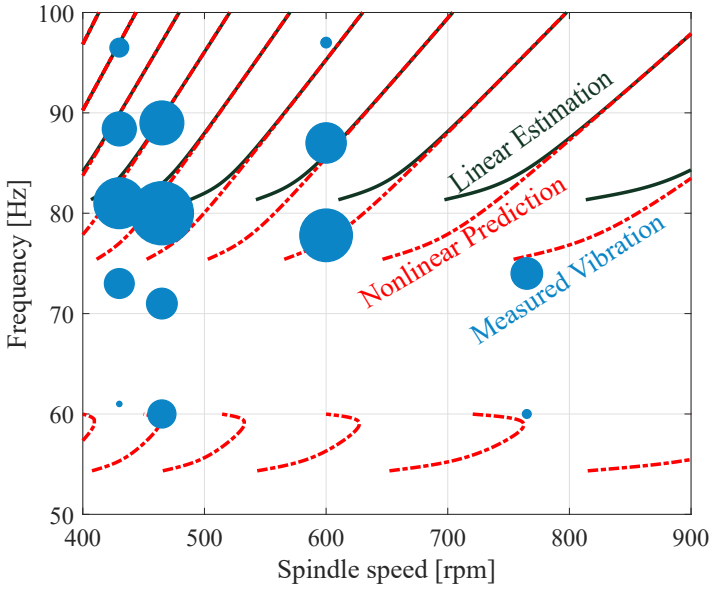

(b) Chip width 4.5 mm

Figure 14.3: Comparison of estimated frequencies of chatter vibration and scaled measured response obtained in experimental trials for chip widths of: (a) 1 mm and (b) 4.5 mm.

15

Proposed Methodology of Machine-Tool Design

Like many natural processes, a logistical function can also describe technical development. In many cases, it seems that the current types have reached the top and therefore that further efforts to improve will not lead to a better product, especially in terms of the layout of the machine structure. As was evident in the previous chapters, the influence of nonlinear bounds on the overall machine behaviour is underestimated during the machine's design and operation. Therefore, it is necessary to reconsider the methodology of structural design. The design should focus on the whole system and the optimisation of the partial structures considering the load flow in the structure, leading to an iterative process, where the first part focusses on the appropriate distribution of links. The creation of dynamic substructures decomposes the overall assembly into substructures, so it is possible to solve separate tasks in parallel; then it is necessary to verify the overall machine behaviour.

It is often very difficult to apply loads from the cutting process, as they are very variable and depend on the type of technology, and even different batches of the same material can fundamentally change the behaviour of the cutting process. Therefore, it is necessary to approach the problem stochastically and not just choose deterministic conditions. Here, it is necessary to emphasise the effect of nonlinearities when even a small change in conditions results in a significant deviation of the change in result; as shown in the example presented, the load was able to reduce the natural frequencies of the system by ten percent and thus seemingly reduce system's stiffness 100 times. Knowledge of the behaviour of nonlinear bonds enables the improvement of the machine tool structure. For instance, the property of a linear ball guideway enables the use of both hardening and softening regions with the right design. Based on these assumptions, we can propose a development methodology. The scheme of the proposed methodology is shown in Fig. 15.1. Each machine design should begin by defining a basic machine concept and analysis of the expected load. In the first step, that is necessary to define the layout of the bonds between each piece of the structure. Optimizing layout and number and position is crucial for the whole structure-property.

In the first step, it is necessary to define the layout of the bonds between each piece of the structure. Optimising layout and number and position is crucial for the whole structure-property. In this, a very vague first draught of the structure is necessary to estimate the load of each bond and optimise the layout using knowledge of the nonlinear behaviour of the bonds. The next step is to use substructuring and split the whole machine into single structures, which could be optimised independently, knowing the load in the connections between them. All the parts should be of more detailed design. Furthermore, the structure should be simulated again as a whole, and if the load distribution changes significantly, the process should return to the point of individual substructures and re-optimise them based on new knowledge. As soon as the input and output simulations

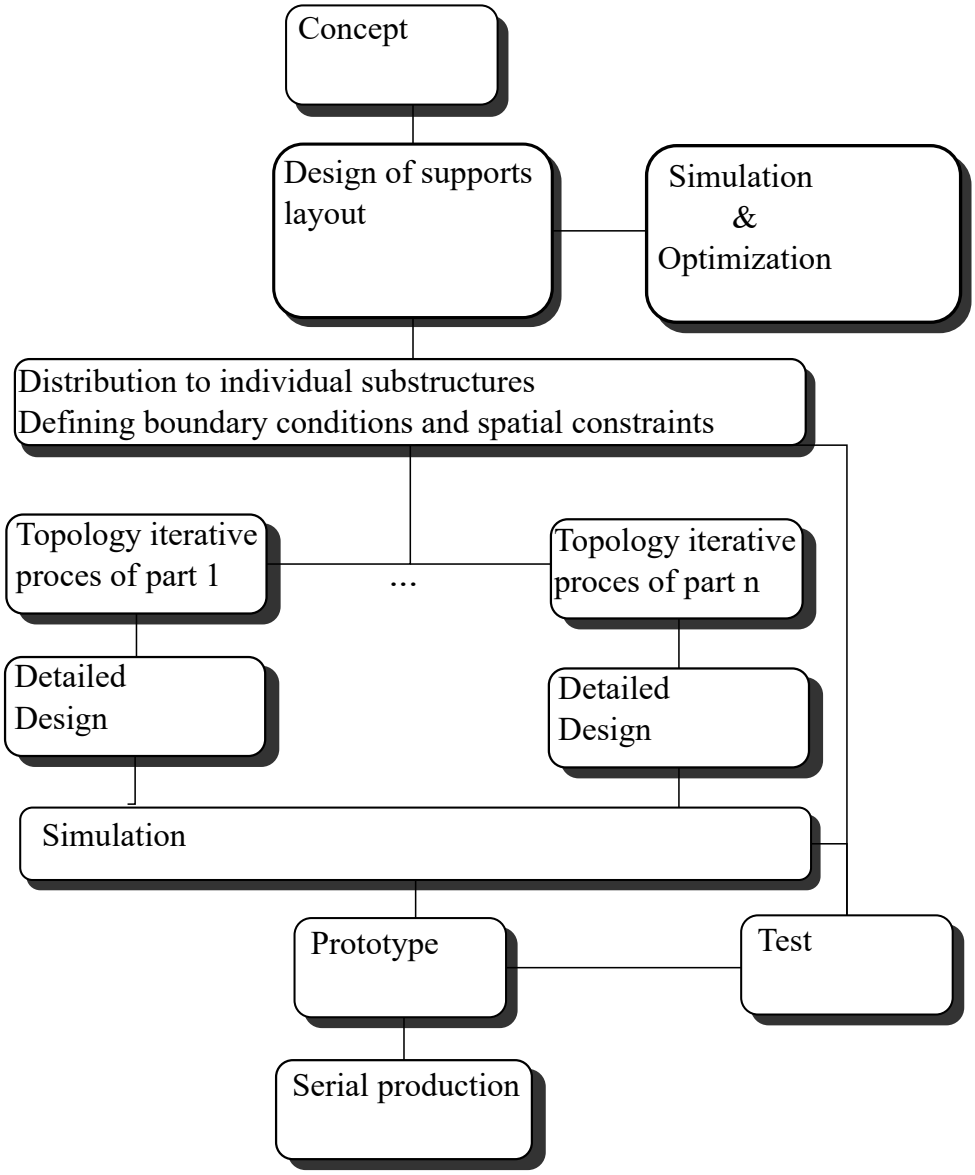

Figure 15.1: Scheme of development of new machine tools

differ minimally, it is possible to proceed to the production of a prototype. The prototype test verifies the behaviour of the machine tool behaviour and verifies the simulation model. If the prototype test satisfies the entering requirements, then serial production could start. However, if the requirements are not satisfied, then it is necessary to analyse the problem, namely redesigning the structure. The test data are also valuable for the verification of the simulation model and for its improvement.

16
Summary of Work Benefits

This work deals with the case of nonlinear behaviour due to nonlinear stiffness, the nonlinearities are commonly underestimated in machine design and regularly presented as unsolvable problems which over complicated the analysis and does not provide enough additional benefits to deal with them.

This work not only proves the importance of considering nonlinearities that can have a crucial effect on machine tool performance but also provides the effective way to deal with these cases. As the experimental data prove, the method enables providing more valid information than the simple linearisation in the unloaded stage, which is usually the only method used for evaluating the behaviour of the machine tool. This work also highlights that linear ball guideway deformation and stiffness cannot be considered as directionally independent and gravity must be considered as the important parameter influencing the system dynamic behaviour.

The better understanding of the nonlinear behaviour of the components and proper analysis improve the prediction of dynamic behaviour and, therefore, enable better machine tool design. Following the provided methodology, better chatter stability should be achieved. Better knowledge of machine tool dynamics enables better productivity by using a larger area of stability.

The scientific benefits of this work are as follows:

- Time domain cosimulation of nonlinear stiffnes model with modal reduced submodels,
- Proposal of an effective method for estimation stability lobe diagram based on synthesis of local linearisation – SLOP algorithm,
- Concept of machine tool design methodology using nonlinear bond analysis and substructure optimisation.

The application benefits of this work are:

- The presented methods enables design bounds layouts design and analyse force distribution in the structure in early stages of machine tool development,
- Improvement of machine tool chatter stability simulation and optimisation of machining process.

17
Conclusion

Machine tool analysis without considering nonlinearities could lead to wrong chatter stability assumptions. Therefore, nonlinear operation of a real machine cannot be simply estimated and analysed by a linear system. Neglecting nonlinearities could lead to an incorrect estimation of vibration stability. It may seem clear that linear analysis cannot simply represent nonlinear systems; still, nonlinear analysis is rarely used for machine tool analysis and estimation of chatter stability prediction. Primarily for its simplicity, linear chatter estimation represents most of all analyses, regardless of the nonlinearity of the contact bonds.

This work presents an example of a machine tool with nonlinear stiffness that has a critical influence on its chatter behaviour. Step-by-step analysis uncovers the cause of this behaviour of nonlinearities and describes the phenomenon of linear ball guideways in the early stages; the analysis focusses on the time-domain simulation of the machining process, which in later stages become too computationally demanding. To effectively predict the system chatter stability lobe, the linearisation method was presented. This method was compared with the simulation of the simplified structures; because of promising results, the method was applied to the experimental structure. Two methods of nonlinear static analysis were applied in the experimental structure, the first was the simplified analysis based on contact reactions, and the second used dynamic substrusturing and cosimulation to estimate contact load in the nonlinear bounds. The first method represents the basic analysis, which could be used as the first draught of the behaviour; however, more precise results were obtained by the cosimulation method. Using the linearisation scheme and cosimulation mode, the chatter frequencies and the stability lobe diagram were estimated. Experimental machining trials were compared with prediction and show good match, the biggest deviation was within the 3 Hz range.

The ‘mystery’ of the shifted chatter frequency problem was revealed. The nonlinearity plays a key role in machine tool systems and could cause a large change of dynamic behaviour. Therefore, this phenomenon is necessary during the design and operation. The experimental data prove that propose analysis could provide valid chatter prediction. Information about the behaviour of the boundaries should be considered during the first draught of the linear ball guideway layout to prevent the with minimal stiffness from operating machine in the limits. For this, the simplified static analysis provides enough information. The more complex cosimulation is more suitable for analysing structure during more advanced development stages and for analysing operating condition of machine tools. The analysis scheme could be applied to other types of nonlinear bounds which are crucial components defining the main machine tool property. Due to the non-intuitive character of the non-linear bound, ‘weird’ situations could occur where a lower number of linear ball guideways could provide a better dynamic property. Therefore, the layout considering bounds nonlinearity provides a better design of machine tools.

Nomenclature

β	Cuting force angle
μ	Contact shape function
ν	Poission ratio
Ω	Spindle speed frequency
φ_k	Angular deflection
A	Contact radius
B	Contact radius
B_{lim}	Limit chip width
e	Eccentricity of contact ellipse
E^*	Equivalent elastic modulus
E_n	Young's elastic modulus
F	Force
F_c	Cutting force
f_c	Chatter frequency
F_g	Weight
F_l	Force of preload lost
F_k	Force reaction
F_{pr}	Total preload force of lineat ball guideway
F_p	Preload force in single row
$Im[FRF]$	Imaginar part of frequency response
k_n	Nonlinear stiffness parameter
$k_{A...D}$	Nonlinear stiffness parameter of ball row
k_{beam}	Torsional stiffness
K_s	Specific cutting force
$l_{1,2...6}$	Lenght dimention
n_b	Number of balls under contact

R Contact radius

R_e Relative radius

$Re[FRF]$ Real part of frequency response

T_k Torsional reaction

x Deflection

x_p Deflection caused by preload

Bibliography

[1] L. Skyttner, "General systems theory: origin and hallmarks," *Kybernetes*, 1996.

[2] L. von Bertalanffy, *General System Theory: Foundations, Development, Applications*. International library of systems theory and philosophy, G. Braziller, 2003.

[3] G. J. Klir, *Facets of Systems Science*. IFSR International Series in Systems Science and Systems Engineering, Springer New York, NY, 1991.

[4] L. Skyttner, *General systems theory: ideas & applications*. World Scientific, 2001.

[5] R. L. Ackoff, "Creating the corporate future john wiley & sons," *New York*, 1981.

[6] W. Weaver, "Science and complexity," *American scientist*, vol. 36, no. 4, pp. 536–544, 1948.

[7] P. Janíček, *Systémová metodologie : brána do řešení problémů*. Brno: Akademické nakladatelství CERM, vyd. 1. ed., 2014.

[8] J. Tlustý, *Manufacturing Process and Equipment*. Upper Saddle River: Prentice Hall, 1. ed., 2000.

[9] B. Gegg, C. Suh, and A. Luo, *Machine Tool Vibrations and Cutting Dynamics*. SpringerLink : Bücher, Springer New York, 2011.

[10] S. Jiang, S. Yan, Y. Liu, C. Duan, J. Xu, and Y. Sun, "Analytical prediction of chatter stability in turning of low-stiffness pure iron parts by nosed tool," *The International Journal of Advanced Manufacturing Technology*, Nov 2018.

[11] Y. Altintas, "Modeling approaches and software for predicting the performance of milling operations at mal-ubc," *Machining Science and Technology - MACH SCI TECHNOL*, vol. 4, pp. 445–478, 11 2000.

[12] Y. Ayed, C. Robert, G. Germain, and A. Ammar, "Orthogonal micro-cutting modeling of the ti17 titanium alloy using the crystal plasticity theory," *Finite Elements in Analysis and Design*, vol. 137, pp. 43 – 55, 2017.

[13] E. Turkes, S. Orak, S. Neşeli, M. Sahin, and S. Selvi, "Modelling of dynamic cutting force coefficients and chatter stability dependent on shear angle oscillation," *The International Journal of Advanced Manufacturing Technology*, vol. 91, pp. 679–686, Jul 2017.

[14] Z. Fu, X. Zhang, X. Wang, and W. Yang, "Analytical modeling of chatter vibration in orthogonal cutting using a predictive force model," *International Journal of Mechanical Sciences*, vol. 88, pp. 145 – 153, 2014.

[15] M. Eynian, H. Onozuka, and Y. Altintas, "Chatter in turning with process damping," *Proceedings of the 22nd Annual ASPE Meeting, ASPE 2007*, 01 2007.

[16] Y. Altintas, M. Eynian, and H. Onozuka, "Identification of dynamic cutting force coefficients and chatter stability with process damping," *CIRP Annals*, vol. 57, no. 1, pp. 371 – 374, 2008.

[17] M. A. Rubeo and T. L. Schmitz, "Global stability predictions for flexible workpiece milling using time domain simulation," *Journal of Manufacturing Systems*, vol. 40, pp. 8 – 14, 2016. SI:Challenges in Smart Manufacturing.

[18] L. Zhu and C. Liu, "Recent progress of chatter prediction, detection and suppression in milling," *Mechanical Systems and Signal Processing*, vol. 143, p. 106840, 2020.

[19] L. Yuan, Z. Pan, D. Ding, S. Sun, and W. Li, "A review on chatter in robotic machining process regarding both regenerative and mode coupling mechanism," *IEEE/ASME Transactions on Mechatronics*, vol. PP, pp. 1–1, 08 2018.

[20] K. Hassan, A. Kang, and G. Singh, "Metamorphic developmental possibilities related to boring operation in the near future," in *AIP Conference Proceedings*, vol. 2281, p. 020030, American Institute of Physics Inc., 10 2020.

[21] M. Ashby, "Multi-objective optimization in material design and selection," *Acta Materialia*, vol. 48, p. 359–369, 01 2000.

[22] H.-C. Moehring, C. Brecher, E. Abele, J. Fleischer, and F. Bleicher, "Materials in machine tool structures," *CIRP Annals - Manufacturing Technology*, vol. 64, 06 2015.

[23] B. Li, J. Hong, S. Yan, and Z. Liu, "Multidiscipline topology optimization of stiffened plate/shell structures inspired by growth mechanisms of leaf veins in nature," *Mathematical Problems in Engineering*, vol. 2013, 01 2013.

[24] L. Shen, X. Ding, T. Li, X. Kong, and X. Dong, "Structural dynamic design optimization and experimental verification of a machine tool," *The International Journal of Advanced Manufacturing Technology*, vol. 104, 10 2019.

[25] H. Weule, J. Fleischer, W. Neithardt, D. Emmrich, and D. Just, "Structural optimization of machine tools including the static and dynamic workspace behavior," in *The 36th cirp-international seminar on manufacturing systems*, vol. 12, pp. 56–60, Citeseer, 2003.

[26] L. Shen, X. Ding, T. Hu, H. Zhang, and S. Xu, "Simultaneous optimization of stiffener layout of 3d box structure together with attached tuned mass dampers under harmonic excitations," *Structural and Multidisciplinary Optimization*, vol. 64, pp. 1–17, 08 2021.

[27] S. Elias and V. Matsagar, "Research developments in vibration control of structures using passive tuned mass dampers," *Annual Reviews in Control*, vol. 44, pp. 129 – 156, 2017.

[28] Y. Yang, J. Muñoa, and Y. Altintas, "Optimization of multiple tuned mass dampers to suppress machine tool chatter," *International Journal of Machine Tools and Manufacture*, vol. 50, no. 9, pp. 834 – 842, 2010.

[29] J. Saffury, "Chatter suppression of external grooving tools," *Procedia CIRP*, vol. 58, pp. 216 – 221, 2017. 16th CIRP Conference on Modelling of Machining Operations (16th CIRP CMMO).

[30] W. Ma, J. Yu, Y. Yang, and Y. Wang, "Optimization and tuning of passive tuned mass damper embedded in milling tool for chatter mitigation," *Journal of Manufacturing and Materials Processing*, vol. 5, p. 2, 12 2020.

[31] B. Yao, Q. Chen, H. Xiang, and X. Gao, "Experimental and theoretical investigation on dynamic properties of tuned particle damper," *International Journal of Mechanical Sciences*, vol. 80, pp. 122–130, 2014.

[32] K. Zhang, T. Chen, X. Wang, and J. Fang, "A model of tuned particle damper," in *Proceedings of the 22nd International Congress on Sound and Vibration, Florence, Italy*, pp. 12–16, 08 2015.

[33] S. Simonian, "New particle damping applications," in *45th AIAA/ASME/ASCE/AHS/ASC Structures, Structural Dynamics & Materials Conference*, vol. 6, 04 2004.

[34] Y. Yang, D. Xu, and Q. Liu, "Milling vibration attenuation by eddy current damping," *The International Journal of Advanced Manufacturing Technology*, vol. 81, 05 2015.

[35] U. Zuperl, F. Cus, and M. Reibenschuh, "Modeling and adaptive force control of milling by using artificial techniques," *Journal of Intelligent Manufacturing - J INTELL MANUF*, vol. 23, 10 2010.

[36] G. Urbikain, D. Olvera, L. L. de Lacalle, and A. Elías-Zúñiga, "Spindle speed variation technique in turning operations: Modeling and real implementation," *Journal of Sound and Vibration*, vol. 383, pp. 384 – 396, 2016.

[37] T. Insperger and G. Stepan, "Stability analysis of turning with periodic spindle speed modulation via semidiscretization," *Modal Analysis*, vol. 10, no. 12, pp. 1835–1855, 2004.

[38] G. Jin, H. Qi, Z. Li, and J. Han, "Dynamic modeling and stability analysis for the combined milling system with variable pitch cutter and spindle speed variation," *Communications in Nonlinear Science and Numerical Simulation*, vol. 63, pp. 38 – 56, 2018.

[39] S. Yamato, T. Ito, H. Matsuzaki, and Y. Kakinuma, "Programmable optimal design of sinusoidal spindle speed variation for regenerative chatter suppression," *Procedia Manufacturing*, vol. 18, pp. 152 – 160, 2018. 18th Machining Innovations Conference for Aerospace Industry, MIC 2018, 28-29 December 2018, Garbsen Germany.

[40] C. Wang, X. Zhang, R. Yan, X. Chen, and H. Cao, "Multi harmonic spindle speed variation for milling chatter suppression and parameters optimization," *Precision Engineering*, vol. 55, pp. 268 – 274, 2019.

[41] F. Kšica and Z. Hadaš, "Position-dependent response simulation of machine tool using state-space models," *MM Science Journal*, no. 1, pp. 2120–2127, 2017.

[42] F. Kšica and Z. Hadaš, "Prediction of position-dependent stability lobes based on reduced virtual model," in *14th International Conference on Vibration Engineering and Technology of Machinery, VETOMAC 2018 Proceedings*, vol. 211, (EDP Sciences), pp. 1–6, EDP Sciences, october 2018.

[43] F. Beards, "Damping in structural joints," *The Shock and Vibration Digest*, vol. 11, pp. 35–41, 09 1979.

[44] M. Weck and K. Teipel, *Dynamisches Verhalten spanender Werkzeugmaschinen*. Berlin: Springer-Verlag Berlin Heidelberg, 1. ed., 1977.

[45] W. Wang, C. Li, Y. Zhou, H. Wang, and Y. Zhang, "Nonlinear dynamic analysis for machine tool table system mounted on linear guides," *Nonlinear Dynamics*, vol. 94, pp. 2033–2045, Nov 2018.

[46] G. Zhang, Y. Huang, W. Shi, and W. Fu, "Predicting dynamic behaviours of a whole machine tool structure based on computer-aided engineering," *International Journal of Machine Tools and Manufacture*, vol. 43, no. 7, pp. 699 – 706, 2003.

[47] J. Větiška, *Analýza stability řezného procesu obráběcího stroje vzhledem k samobuzenému kmitání*. PhD thesis, Vysoké učení technické v Brně, Brno, 5 2012.

[48] R. J. Guyan, "Reduction of stiffness and mass matrices," *AIAA journal*, vol. 3, no. 2, pp. 380–380, 1965.

[49] R. R. Craig Jr and M. C. Bampton, "Coupling of substructures for dynamic analyses.," *AIAA journal*, vol. 6, no. 7, pp. 1313–1319, 1968.

[50] S. Gordon, "Femci book - the craig-bampton method."

[51] W. Sun, X. Kong, and B. Wang, "Precise finite element modeling and analysis of dynamics of linear rolling guideway on supporting direction," *Journal of Vibroengineering*, vol. 15, no. 3, pp. 1330–1340, 2013.

[52] W. Sun, X. Kong, B. Wang, and X. Li, "Statics modeling and analysis of linear rolling guideway considering rolling balls contact," *Proceedings of the Institution of Mechanical Engineers, Part C: Journal of Mechanical Engineering Science*, vol. 229, no. 1, pp. 168–179, 2015.

[53] X. Kong, W. Sun, B. Wang, and B. Wen, "Dynamic and stability analysis of the linear guide with time-varying, piecewise-nonlinear stiffness by multi-term incremental harmonic balance method," *Journal of Sound and Vibration*, vol. 346, pp. 265 – 283, 2015.

[54] K. Johnson, *Contact Mechanics*. Cambridge University Press, 1987.

[55] D. Krampert, M. Ziegler, S. Unsleber, L. Reindl, and S. J. Rupitsch, "On the stiffness hysteresis of profiled rail guides," *Tribology International*, vol. 160, p. 107019, 2021.

List of Figures

List of Tables

List of Author's Publications Related to Thesis

[A1] Hadraba, P. and Wang, J.J. and Hadas, Z.: *Effects of Nonlinear Behaviour of Linear Ball Guideway on Chatter Frequency of Lathe Machine Tool*. The International Journal of Advanced Manufacturing Technology, 2023.

[A2] Hadraba, P., Wang, J., Lin, H. and Hadas, Z.: *Theoretical Study of Nonlinear Chatter Stability Analysis Based on Synthesis of Linearizations in Operating Points for Different Turning Conditions*. MM Science Journal, 2022.

[A3] Hadraba, P. and Hadas, Z.: *Time-domain regenerative chatter analysis of nonlinear stiffness system*. Advances in Intelligent Systems and Computing , 2020.

[A4] Hadraba, P. and Svobodova, M. and Lin, H. and Hadas, Z.: *Time-Domain Simulations of Grooving Process with Stiffness Uncertantities*. Engineering Mechanics 2020 (IM2020), 2020, ISBN 978-80-214-5896-3.

[A5] Hadraba, P. and Hadas, Z.: *Virtual Twin of the Multi-spindle Lathe for the Chatter Time-domain Analysis*. Proceedings of the 2018 18th International Conference on Mechatronics - Mechatronika, ME 2018,2019.

[A6] Hadraba, P. and Hadas, Z.: *Multi Body Vibration Analysis of a Three-Axis Slide for Mass Damper Design*. Engineering Mechanics 2018 , VOL 24, 2018.

[A7] Hadraba, P. and Hadas, Z.: *Dynamic analysis of multispindle lathe*. Advances in Intelligent Systems and Computing, VOL 644, 2018.